

# Oxidative and Initiated Chemical Vapor Deposition for application to Organic Electronics

by

Sung Gap Im

Master of Science, Chemical Engineering  
Seoul National University, Seoul, Republic of Korea, 1999

Bachelor of Science, Chemical Engineering  
Seoul National University, Seoul, Republic of Korea, 1997

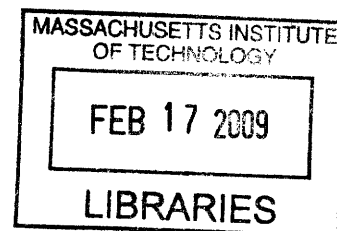
Submitted to the Department of Chemical Engineering  
in Partial Fulfillment of the Requirements for the Degree of

DOCTOR OF PHILOSOPHY IN CHEMICAL ENGINEERING

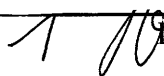
at the

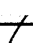
MASSACHUSETTS INSTITUTE OF TECHNOLOGY

January 2009



© 2009 Massachusetts Institute of Technology. All rights reserved.

Signature of Author: \_\_\_\_\_  
 Department of Chemical Engineering  
January 12, 2009

Certified by: \_\_\_\_\_  
 Karen K Gleason  
Professor of Chemical Engineering  
Thesis Advisor

Accepted by: \_\_\_\_\_  
\_\_\_\_\_ William M. Deen  
Professor of Chemical Engineering  
Chairman, Committee for Graduate Students

ARCHIVES

# Oxidative and Initiated Chemical Vapor Deposition for application to Organic Electronics

by

Sung Gap Im

Submitted to the Department of Chemical Engineering  
on January 12, 2009 in Partial Fulfillment  
of the Requirements for the Degree of  
Doctor of Philosophy in Chemical Engineering

## Abstract

Since the first discovery of polymeric conductors in 1977, the research area of “organic electronics” has grown dramatically. However, methods for forming thin films comprised solely of conductive polymers are limited by the rigid nature of the conjugated backbone. Neither spin casting from solution nor melt processing can be used.

To answer to this challenge, a solvent-free method of oxidative chemical vapor deposition (oCVD) to synthesize conductive poly (3, 4-ethylenedioxythiophene) (PEDOT) films was demonstrated. The substrate temperature systemically controls the conjugation length, resulting in films with conductivity of  $9.1 \times 10^{-4}$  to 348 S/cm. The highest conductivity was about 1000 S/cm. The doping level could also be tuned with substrate temperature. Consequently, the work function was varied from 5.1 to 5.4 eV. The polymerization rate could be modulated with various oxidants, which significantly affects the surface morphology of PEDOT film. With milder oxidant, the surface morphology was highly nano-porous. Conformal coverage of PEDOT was also observed on trench structures and paper mats. Furthermore, with this one-step method, PEDOT film could be grafted on various kinds of organic substrates. Huge increase in adhesion strength was consistently observed. With this grafting technique, nanometer-scale PEDOT pattern was firstly obtained on flexible substrates down to 60 nm.

A click chemistry functionalizable poly (propargyl methacrylate) (PPMA) films also were prepared via initiated chemical vapor deposition (iCVD). PPMA itself exhibits e-beam sensitivity and hence can be directly patterned via electron beam (e-beam) lithography without requiring a conventional resist layer. With this PPMA layer, a nanopatterned multi-functional surface was also fabricated and we demonstrated the covalent functionalization of two independent components in a one-pot, self-sorted area-selective process, performed in an aqueous solution at room temperature, having conditions which are bio-compatible. Finally, we report a novel nano-adhesive layer deposited by the iCVD process. An epoxy-containing polymer, poly (glycidyl methacrylate) (PGMA) was used as a nano-adhesive layer. No leakage was observed up to the test pressure of 50 psia from the resulting microfluidic devices.

Thesis Supervisors: Karen K Gleason  
Title: Professor Chemical Engineering

To Junsoo, Minsoo, and Kyung Eun

## Acknowledgments

This thesis and my doctoral degree at MIT could not be achieved without the support of advisors, mentors and colleagues, friends, and family. It will never be possible for me to thank enough all of them but I would like to send my deepest gratitude for all the help, comments, and considerations.

First of all, I would like to thank Professor Karen K. Gleason, a truly honorable educator, great mentor, and brilliant scientist. She offered me the maximum of freedom and borderless opportunities in my research. With her full support, I could delve deep into various research topics. At the same time, she patiently waited for me, encouraged me when my research did not go well as expected.

Professors Paula T. Hammond and Vladimir Bulović were my thesis committee members. I thank them for their valuable comments, encouragement, and time. They also generously supported me for co-operations and it was literally a great success! In addition, I would like to thank Professor Patrick S. Doyle for all his support and valuable comments.

I believe I have had a dreamlike time with Gleason lab – energetic, highly stimulating, and considerate. I would like to send my appreciation and I would happily observe their groundbreaking success in the future as an ex-group member. In addition to Gleason lab, my research was soundly nourished with collaboration with many other research lab in MIT and I thank for their support to Pil J. Yoo and Byeong-Su Kim in Hammond lab, John Kymissis, Kevin Ryu, John C. Ho, and Tim Osedach in Bulović lab, Elsa A. Olivetti in Mayes lab, Wonjae Choi in McKinley lab, Ki Wan Bong in Doyle lab and David Kusters in van de Sanden lab at Eindhoven University. I also thank to supporting staff in the department including Craig Abernethy, Suzanne Easterly, and Stephen Wetzel.

In addition to the research in MIT, the four-and-half-year Doctoral course was a precious part of my life. I would like to thank all of my friends in MIT for enriching my life. Especially, I would like to thank all members in Korean Graduate Students Association in Chemical

Engineering, who helped me to settle down at MIT when I first arrived here and encouraged me when I was in trouble.

I also really appreciate my parents who were always worried about me and prayed for my success. Their existence itself was a big driving force and a strong support for my stay in a foreign country. I especially send my deepest appreciation to my father, who put his son's affair as his first priority.

During my stay in MIT, I have seen my son, Junsoo become a proud kindergartener, and I first met my second son, Minsoo. My wife gave a birth and resumed her career. The growth and progress of family was an irreplaceable joy and inexhaustible source of energy and the reason of my life.

Finally, I dedicate this thesis to my mother in Heaven.

## TABLE OF CONTENTS

<b>Abstract</b>	<b>2</b>
<b>Dedication</b>	<b>3</b>
<b>Acknowledgments</b>	<b>4</b>
<b>List of Figures</b>	<b>11</b>
<b>List of Tables</b>	<b>17</b>
<b>List of Schemes</b>	<b>18</b>
<b>List of Notations</b>	<b>19</b>

### **CHAPTER ONE** \_\_\_\_\_ **23**

#### **Introduction**

1.1 Motivation	24
1.1.1 Oxidative Chemical Vapor Deposition of Conducting Polymer Films	24
1.1.2 Initiated Chemical Vapor Deposition of Biofunctionalizable Polymer Films	25
1.2 Conducting Polymer of Interest: PEDOT	26
1.3 Biofunctionalizable Surfaces	26
1.4 Outlook	28
1.4.1 Oxidative Chemical Vapor Deposition of Conducting Polymer Films	28
1.4.2 Initiated Chemical Vapor Deposition of Biofunctionalizable Polymer Films	29
1.5 Thesis Framework	29
References	33

### **CHAPTER TWO** \_\_\_\_\_ **39**

#### **Systematic Control of the Electrical Conductivity of Poly (3, 4-ethylenedioxythiophene) via Oxidative Chemical Vapor Deposition (oCVD)**

Abstract	40
2.1 Introduction	41
2.2 Experimental	46
2.3 Results and Discussion	48
2.3.1 UV-Visible Absorption Spectroscopy	48
2.3.2 Raman Spectroscopy	50
2.3.3 Fourier Transform Infra-red (FTIR) Spectroscopy	52
2.3.4 Conductivity	53
2.4 Conclusion and outlook	56
References	57

## **CHAPTER THREE** \_\_\_\_\_ **64**

### **Doping Level and Work Function Control in Oxidative Chemical Vapor Deposited (oCVD) Poly (3, 4-ethylenedioxythiophene)**

Abstract	65
3.1 Introduction	66
3.2 Experimental	67
3.3 Results and Discussion	68
3.4 Conclusion and outlook	72
References	73

## **CHAPTER FOUR** \_\_\_\_\_ **77**

### **Grafted Conducting Polymer Films for Nano-patterning onto Various Organic and Inorganic Substrates by Oxidative Chemical Vapor Deposition**

Abstract	78
4.1 Introduction	79
4.2 Experimental	81
4.2.1 Deposition of PEDOT	81
4.2.2 Attaching the silane coupling agent for inorganic substrates	82
4.2.3 Buckling	82
4.2.4 Photolithography	82
4.2.5 Capillary force lithography	83
4.2.6 e-beam lithography	83
4.2.7 Analysis	84
4.3 Results and Discussion	84
4.4 Conclusion	93
References	94

## **CHAPTER FIVE** \_\_\_\_\_ **98**

### **Conformal Coverage of Poly (3,4-ethylenedioxythiophene) films with tunable nanoporosity via Oxidative Chemical Vapor Deposition (oCVD)**

Abstract	99
5.1 Introduction	100
5.2 Experiment	102
5.3 Results and Discussion	103
5.3.1 FTIR Spectra	104
5.3.2 Surface Morphology	105
5.3.3 Conformal Coverage on Complex Geometries	111
5.3.4 Superhydrophobicity and Oil Repellency	114
5.4 Conclusion and outlook	120

References	121
------------	-----

## **CHAPTER SIX** \_\_\_\_\_ **125**

### **Oxidative Chemical Vapor Deposited Poly (3,4-ethylenedioxythiophene) Films for Organic Photovoltaic Cell Application**

Abstract	126
6.1 Introduction	127
6.2 Experimental	129
6.2.1 ITO/glass substrate cleaning	129
6.2.2 ITO surface modification	130
6.2.3 oCVD of PEDOT film	130
6.2.4 PEDOT:PSS spin-coating	131
6.2.5 oPV cell fabrication	131
6.2.6 Characterization	132
6.3 Results and Discussion	132
6.3.1 ITO surface modification	132
6.3.2 oPV Cell Performance	135
6.4 Conclusion	142
References	143

## **CHAPTER SEVEN** \_\_\_\_\_ **148**

### **A Directly Patternable, Click-Active Polymer Film via Initiated Chemical Vapor**

#### **Deposition (iCVD)**

Abstract	149
7.1 Introduction	150
7.2 Experimental	152
7.2.1 iCVD	152
7.2.2 Plasma polymerization	152
7.2.3 Surface grafting	153
7.2.4 Click chemistry	153
7.2.5 Photolithography	154
7.2.6 e-beam lithography	154
7.2.7 Measurement	154
7.3 Results and Discussion	155
7.4 Conclusion	164
References	165

## **CHAPTER EIGHT** \_\_\_\_\_ **169**

### **Patterning Nanodomains with Orthogonal Functionalities: Solventless Synthesis of Self-Sorting Surfaces**



Abstract	170
8.1 Introduction	171
8.2 Experimental	173
8.2.1 Plasma polymerization of poly allylamine (PAAm)	173
8.2.2 Initiated Chemical Vapor Deposition (iCVD) of PPMA	173
8.2.3 Silane treatment for surface grafting of inorganic substrates	174
8.2.4 Capillary force lithography	174
8.2.5 Surface Functionalization	175
8.2.6 Microscopy	175
8.3 Results and Discussion	176
8.4 Conclusion	180
References	181

## **CHAPTER NINE** \_\_\_\_\_ **184**

### **A Conformal Nano-adhesive via Initiated Chemical Vapor Deposition for Microfluidic**

#### **Devices**

Abstract	185
9.1 Introduction	186
9.2 Experimental	189
9.2.1 Plasma polymerization of PAAm	189
9.2.2 iCVD of PGMA	190
9.2.3 Silane treatment for surface grafting of inorganic substrates	190
9.2.4 Curing nano-adhesive layers	191
9.2.5 Fabrication of test microfluidic devices and leakage test	191
9.2.6 Microscopy	192
9.3 Results and Discussion	192
9.3.1 Adhesive Bonding	192
9.3.2 Conformal coverage and fabrication of nano-channel	197
9.3.3 Bond strength of sealed microfluidic devices	197
9.4 Conclusion	199
References	200

## **CHAPTER TEN** \_\_\_\_\_ **205**

#### **Conclusions and Future Works**

10.1 Conclusions	206
1.1.1 Oxidative Chemical Vapor Deposition of Conducting Polymer Films	206
1.1.2 Initiated Chemical Vapor Deposition of Biofunctionalizable Polymer Films	208
1.4 Future Works	209
1.4.1 Oxidative Chemical Vapor Deposition of Conducting Polymer Films	209
1.4.2 Initiated Chemical Vapor Deposition of Biofunctionalizable Polymer Films	212

## **APPENDIX A** \_\_\_\_\_ **215**

## **New iCVD/oCVD System Integrated into a Organic Electronic Device Fabrication Line**

A.1	Motivation	216
A.2	Design	216
A.2.1	Location	216
A.2.2	Chamber configuration	217
A.2.2.1	Introduction of Reactants into the iCVD/oCVD system	217
A.2.2.2	Chamber configuration of iCVD/oCVD system	217
A.2.2.3	Transfer line and sample holder-stage alignment	221
A.2.2.4	Pumping system in iCVD/oCVD system	222
A.2.2.5	iCVD process in iCVD/oCVD system	223
A.2.2.6	oCVD process in iCVD/oCVD system	224

## List of Figures

### CHAPTER TWO

---

- Figure 2-1: Proposed polymerization mechanism for oxidative polymerization of PEDOT; (1) oxidation of EDOT to form cation radical; (2) dimerization of cation radical; (3) deprotonation to form conjugation; (4) further polymerization from n-mer to (n+1)-mer; (5) doping process of PEDOT.
- Figure 2-2: **B** benzoid; **Q** quinoid type of PEDOT.
- Figure 2-3: Schematic figure of modified oCVD process chamber.
- Figure 2-4: UV-Vis optical spectra of CVD polymerized PEDOT with various substrate temperature ( $T_{\text{sub}}$ ); (a)  $T_{\text{sub}} = 100\text{ }^{\circ}\text{C}$ ; (b)  $T_{\text{sub}} = 85\text{ }^{\circ}\text{C}$ ; (c)  $T_{\text{sub}} = 71\text{ }^{\circ}\text{C}$ ; (d)  $T_{\text{sub}} = 47\text{ }^{\circ}\text{C}$ ; (e)  $T_{\text{sub}} = 15\text{ }^{\circ}\text{C}$ . **A** represents the bathochromic shift of polaronic energy state with the increase of substrate temperature. **B** represents the bathochromic peak shift and intensity decrease of the  $\pi$  to  $\pi^*$  transition energy state with the increase of substrate temperature.
- Figure 2-5: Overlapped Raman spectra of CVD polymerized PEDOT with various substrate temperature ( $T_{\text{sub}}$ ); (a)  $T_{\text{sub}} = 100\text{ }^{\circ}\text{C}$ ; (b)  $T_{\text{sub}} = 85\text{ }^{\circ}\text{C}$ ; (c)  $T_{\text{sub}} = 71\text{ }^{\circ}\text{C}$ ; (d)  $T_{\text{sub}} = 47\text{ }^{\circ}\text{C}$ ; (e)  $T_{\text{sub}} = 15\text{ }^{\circ}\text{C}$ . Peak shift indicated by the arrow represents that the C=C conjugation is shifted from undoped benzoidal type ( $1444\text{ cm}^{-1}$ ) to doped quinoidal type ( $1428\text{ cm}^{-1}$ ).
- Figure 2-6: FT-IR spectra of PEDOT with various substrate temperature ( $T_{\text{sub}}$ ); (a)  $T_{\text{sub}} = 100\text{ }^{\circ}\text{C}$ ; (b)  $T_{\text{sub}} = 85\text{ }^{\circ}\text{C}$ ; (c)  $T_{\text{sub}} = 71\text{ }^{\circ}\text{C}$ ; (d)  $T_{\text{sub}} = 47\text{ }^{\circ}\text{C}$ ; (e)  $T_{\text{sub}} = 15\text{ }^{\circ}\text{C}$ . Arrow represents the C=C stretch peak at  $1520\text{ cm}^{-1}$ .
- Figure 2-7: Arrhenius plot of substrate temperature vs. conductivity.

### CHAPTER THREE

---

- Figure 3-1: (a) XPS survey scan of oCVD PEDOT deposited at a substrate temperature of  $15\text{ }^{\circ}\text{C}$ ; (b) high resolution XPS spectrum of (b) O 1s; (c) S 2p; and (d) Cl 2p.
- Figure 3-2: (a) STEM cross-sectional image of oCVD PEDOT. I corresponds to epoxy, II corresponds PEDOT layer, and III represents polymer substrate; (b) EDX scan data according to the red line.

Figure 3-3: Effect of the oCVD PEDOT deposition temperature on (a) doping level and (b) work function.

## CHAPTER FOUR

---

Figure 4-1: A schematic representation of the reaction mechanism involved in grafting PEDOT films onto aromatic polymeric substrates.

Figure 4-2: FT-IR spectra of (a) standard PS (200 nm, MW = 250K); (b) oCVD PEDOT (60 nm); (c) ungrafted PS-on-PEDOT; (d) grafted PEDOT-on-PS; (e) ungrafted PS-on-PEDOT after 5 s of rinsing with THF; (f) grafted PEDOT-on-PS after one hour of soaking in THF.

Figure 4-3: (a) PEDOT grafted on PET (left) and PEDOT on PP, ungrafted (right) after tape testing; (b) PEDOT grafted (left) and ungrafted (right) on glass after the ultrasonication for 5 min.; (c) Conventional lift-off photolithography pattern on Si wafers with ungrafted PEDOT (left) and with grafted PEDOT (right). The scale bars represent a length of 50  $\mu\text{m}$ .

Figure 4-4: Atomic force microscope (AFM) of PEDOT films on PS after treatment with THF vapors for (a) 5 s and (b) 15 s. Rings appearing in the corresponding fast Fourier transforms (insets) indicates that the patterns of surface wrinkles are isotropic and of single length-scale<sup>1</sup> of  $2.1 \pm 0.3 \text{ } \mu\text{m}$  and  $3.9 \pm 0.9 \text{ } \mu\text{m}$  for (a) and (b), respectively. This uniform wrinkling confirms the strong adhesion of grafted PEDOT on PS. Uniform surface wrinkling is absent in the optical microscope images of the PEDOT films on PEO after treatment with water vapor for (c) 15 min, and (d) 30 min., consistent with the lack of PEDOT grafting to the non-aromatic PEO layer.

Figure 4-5: PEDOT pattern on flexible PET substrate by capillary force lithography; (a) image of patterned PEDOT film on flexible PET substrate; (b) 120 nm line pattern; (c) complex pattern; (d) 60 nm line pattern of PEDOT film grafted on flexible PET substrate by e-beam lithography.

## CHAPTER FIVE

---

Figure 5-1: FTIR spectra of PEDOT films via oCVD process with (a-c)  $\text{CuCl}_2$  or (d)  $\text{FeCl}_3$  as an oxidant; (a)  $T_{\text{sub}} = 20 \text{ } ^\circ\text{C}$ , conductivity was 0.22 S/cm; (b)  $T_{\text{sub}} = 50 \text{ } ^\circ\text{C}$ , conductivity was 3.3 S/cm; (c)  $T_{\text{sub}} = 80 \text{ } ^\circ\text{C}$ , conductivity was 11.3 S/cm; (d)  $T_{\text{sub}} = 55 \text{ } ^\circ\text{C}$ , conductivity was 11.2 S/cm. The rectangle highlights an absorption region associated with conjugation in the oCVD PEDOT.

- Figure 5-2: SEM images of (a-c) C-PEDOT and (d) F-PEDOT, respectively; (a)  $T_{\text{sub}} = 20\text{ }^{\circ}\text{C}$ ; (b)  $T_{\text{sub}} = 50\text{ }^{\circ}\text{C}$ ; (c)  $T_{\text{sub}} = 80\text{ }^{\circ}\text{C}$ ; (d)  $T_{\text{sub}} = 55\text{ }^{\circ}\text{C}$ . Each scale bars represents 500 nm. Scale bar in the inset of (a) represents 5  $\mu\text{m}$ . Inset of (b) is the digital camera image of basalt. Copyright (2008) by Andrew Alden, geology.about.com, reproduced under educational fair use.
- Figure 5-3: Size distribution of diameter of (a) nodules of C-PEDOT at  $T_{\text{sub}}=20\text{ }^{\circ}\text{C}$  and fibrils of C-PEDOT at (b) at  $T_{\text{sub}}=50\text{ }^{\circ}\text{C}$  and (c) at  $T_{\text{sub}}=80\text{ }^{\circ}\text{C}$ , respectively. Arrows denoted in (a) represent the peak position of merged nodules.
- Figure 5-4: Cross-sectional SEM images of (a) C-PEDOT and (b) F-PEDOT deposited on trenches and (c) EDOT and  $\text{FeCl}_3$  mixture solution was spin-cast to form highly anisotropic PEDOT on trench. Each scale bars represents 2  $\mu\text{m}$ . Black line in the right side of (a) and white line in the left side of (b) and (c) show the borders between Si trench and C-PEDOT film. SEM images of conformally coated C-PEDOT film on paper mat (d) before and (e) after the deposition of C-PEDOT film. Each scale bars represents 10  $\mu\text{m}$ .
- Figure 5-5: Water droplet contact angle variations of PEDOT film according to the surface roughness; (a) F-PEDOT, RMS roughness = 3.7 nm,  $\theta = 84^{\circ}$ ; (b) C-PEDOT, RMS roughness = 22.7 nm,  $\theta = 37^{\circ}$ ; (c) C-PEDOT, RMS roughness = 43.0 nm,  $\theta = 10^{\circ}$  respectively. Contact angle variations of PFA-modified PEDOT film; (d) F-PEDOT,  $\theta = 120^{\circ}$ ; (b) C-PEDOT,  $\theta = 150^{\circ}$ . (f) digital camera image of PFA-modified C-PEDOT coated paper mat. A series of picture captured from CCD camera for advancing and receding water droplet on (g) PFA-modified paper mat and (h) PFA-modified C-PEDOT coated paper mat, respectively. Each scale bar represents 1 mm.
- Figure 5-6: Ethanol droplet contact angles on (a) PFA-modified C-PEDOT film on Si wafer ( $\theta = 88^{\circ}$ ) and (b) PFA-modified C-PEDOT coated paper mat ( $\theta = 113^{\circ}$ ), respectively. Each scale bar represents 1 mm.

## CHAPTER SIX

---

- Figure 6-1: (a) Equivalent circuit for oPV cells.  $J_{\text{ph}}$  is photo-generated current density,  $J_{\text{D}}$  is reverse saturation current,  $R_{\text{sh}}$  is shunt resistance, and  $R_{\text{s}}$  is series resistance. (b) Schematic of current-voltage characteristics of oPV cells under dark (black) and light (red) illumination.  $J_{\text{sc}}$  is short-circuit current,  $V_{\text{oc}}$  is open-circuit voltage, and FF is the fill factor that maximizes the power output from the cell.

- Figure 6-2: (a) Schematic structure of P3HT:PCBM BHJ oPV cell. (b) Band structure diagram that shows the HOMO and LUMO energy levels of P3HT, PCBM, ITO, PEDOT, and Mg:Ag/Ag. The energy difference between the HOMO of donor and LUMO of acceptor is the theoretical maximum  $V_{oc}$ .
- Figure 6-3: J-V curves of ITO/PEDOT/P3HT:PCBM/Mg:Ag/Ag bulk heterojunction (BHJ) device (a) linear scale, (b) logarithmic scale. PEDOT was either PEDOT:PSS or oCVD PEDOT.
- Figure 5-4: AFM image of (a) PEDOT:PSS film and (b) oCVD PEDOT film coated on Si wafer. The scanned area was  $2 \times 2 \text{ } \mu\text{m}^2$  and height scale is 100 nm. The calculated root-mean squared roughness of PEDOT:PSS and oCVD PEDOT was 0.34 nm and 5.4 nm, respectively.

## CHAPTER SEVEN

---

- Figure 7-1: FTIR spectra of (a) PMA monomer, (b) iCVD PPMA, and (c) plasma polymerized PPMA. Rectangular regions represent C-H stretch peak in alkyne group (around  $3200 \text{ cm}^{-1}$ ) and  $\text{C}\equiv\text{C}$  stretch peak in alkyne group (around  $2100 \text{ cm}^{-1}$ ). The arrow represents  $\text{C}=\text{C}$  stretch peak in the monomer (a) (around  $1600 \text{ cm}^{-1}$ ) which, due to vinyl polymerization, is absent in the iCVD film (b). The iCVD film (b) clearly returns clickable alkyne group while this functionality is destroyed by plasma polymerization (c).
- Figure 7-2: XPS high resolution spectra of PPMA; (a) C 1s and (b) O 1s, respectively. The chemical structure is labeled with numbers, providing the assignment for (a), and capital letters, which correspond to the assignment for (b).
- Figure 7-3: XPS (a) Survey scan of PPMA (bottom) and  $\text{N}_3$ -coumarin functionalized PPMA films (top) and (b) high resolution N 1s scan data of  $\text{N}_3$ -coumarin functionalized PPMA films via click reaction, respectively. Dotted circles in (a) highlight the newly formed N 1s peak by click addition reaction. Inset in (b) represents a fluorescence microscope image of patterned PPMA film click-functionalized with  $\text{N}_3$ -coumarin. Scale bar in the inset represents  $20 \text{ } \mu\text{m}$ . Each superscripted numbers in chemical formula of click functionalized PPMA in (a) corresponds to peaks assigned in XPS N 1s spectrum in (b).
- Figure 7-4: (a) Schematic patterning procedure of standard e-beam lithography (A) and direct e-beam patterning with e-beam sensitive PPMA film (B) and (b) AFM image of e-beam patterned iCVD PPMA. (c) Schematic procedure of QD-streptavidin immobilization onto the patterned polymer film by biotin-streptavidin binding via click reaction. (d) fluorescence

microscope image and (e) Enlarged 3-D AFM image of e-beam patterned PPMA film conjugated with QD particles via click chemistry, respectively.

## CHAPTER EIGHT

---

Figure 8-1: (A) Schematic procedure of nano-pattern fabrication: (a) PECVD of PAAm; (b) iCVD of PPMA; (c) apply CFL mold to induce capillary rise; (d) remove CFL mold to complete the nano-pattern. (B) FTIR spectra of (a) iCVD PPMA and (b) PECVD PAAm.

Figure 8-2: Scanning electron microscope (SEM) and atomic images of nano-patterned platform of iCVD PPMA on PECVD PAAm background film via CFL; (a) 500 nm, (b) 110 nm stripe pattern, and (c) 800 nm, (d) 500 nm dot patterns, and atomic force microscope (AFM) image of (e) 110 nm and (f) 500 nm line pattern AFM image clear demonstrates the pattern fidelity and exposure of PAAm of the structure.

Figure 5-3: (A) Schematic procedure of one-pot functionalization; (B) Fluorescence microscope image of (a) click functionalized red dye excited at 545 nm, (b) NHS functionalized green dye excited at 491 nm, and (c) overlapped image of (a) and (b). Each scale bars represents 30  $\mu\text{m}$ .

## CHAPTER NINE

---

Figure 9-1: Schematic of process for nano-adhesive bonding. Deposition of the (a) iCVD of PGMA onto a pre-patterned substrate and of the (b) plasma polymerized PAAm onto flat substrate, followed by curing at 70 °C to complete the bonding of two substrates (c). Note that the final adhesive bonding step produces no gaseous by-products and so avoids any potential issues arising due to outgassing.

Figure 9-2: Pre-patterned PU substrate bonded with PC film (a) and compressive (b) and tensile (c) stresses were applied to a test microfluidic device composed of pre-patterned PDMS substrate bonded with PET film.

Figure 9-3: Cross sectional SEM images of (a) a 318 nm thick PGMA film deposited conformally on standard trench (2  $\mu\text{m}$   $\times$  8  $\mu\text{m}$ ) and (b) the thickness variation of PGMA film with respect to the trench position in (a). Each numbers in x-axis corresponds to the numbers in (a). (c, d) a cured iCVD PGMA film on pre-patterned PDMS with a flat PET film coated with PAAm with different magnification. The cross sectional SEM image of (c) and (d) clearly shows that 200 nm-channels at the interface between PDMS and PU film are retained.

## APPENDIX A

---

- Figure A-1: Location of iCVD/oCVD system in organic electronic device fabrication line.
- Figure A-2: Schematic diagram of iCVD/oCVD system in organic electronic device fabrication line.
- Figure A-3: Digital camera images of (a) reactants introduction line configuration, (b) power supply of heating tape, and (c) MFC controller and heating tape temperature controller in electrical rack.
- Figure A-4: (a) Schematic drawing and (b) digital camera image of iCVD/oCVD system.
- Figure A-5: Schematic drawing of (a) base, (b) stage, (c) cross-section of iCVD/oCVD system. A z-stage motor is attached at the bottom flange of iCVD/oCVD system.
- Figure A-6: Schematic drawing of sample holder alignment onto the stage: (a) upper part and (b) bottom part of iCVD/oCVD system.
- Figure A-7: Digital camera image of (a) vacuum gauges for high vacuum (red circle at bottom left) and low vacuum (red circle at upper right), (b) turbomolecular pump, PID controllable butterfly valve, and gate valve for turbomolecular pump connection, and (c) PID controllable butterfly valve control readout in electrical rack.
- Figure A-8: Digital camera images of (a) upper part of iCVD/oCVD system for iCVD process and (b) source jar setup. Schematic diagram of (c) top view of iCVD/oCVD system for iCVD process and (d) filament chuck configuration.
- Figure A-9: Digital camera images of (a) bottom part of iCVD/oCVD system for iCVD process and (b) source jar setup. z-stage motor, thickness monitor, and resistive heating unit for oxidant evaporation is shown in (a).



## List of Tables

### CHAPTER TWO

---

Table 2-1: Summary of selected properties of oCVD deposited PEDOT film

### CHAPTER SIX

---

Table 6-1: Summary of device performance of P3HT:PCBM BHJ oPV cells with different anode buffer layers.  $R_s$  and  $R_{sh}$  were estimated as an inverse slope in the J-V curve at  $V=1.2V$  and  $0V$ , respectively.

### CHAPTER NINE

---

Table 9-1: Summary of leakage test of microfluidic devices with PDMS and various kinds of substrate materials at the channel pressure of 50 psia

## List of Schemes

### CHAPTER SIX

---

Scheme 6-1: Schematic procedure of grafting oCVD PEDOT on ITO surface using redox-active coupling agent: (a) surface treatment of oxygen-plasma cleaned ITO surface with 2-TAA for 2 hours in ethanol; (b) subsequent oCVD PEDOT deposition in which the  $\text{FeCl}_3$  oxidant can activate both EDOT monomer and the thiophene ring at the surface of ITO to covalently attach PEDOT

### CHAPTER SEVEN

---

Scheme 7-1: Click reaction between iCVD pPA and azido functionalized fluorescent dye,  $\text{N}_3$ -coumarin.

## List of Acronyms, Abbreviations, and Symbols

### Roman Acronyms and Abbreviations

2-TAA	2-thiophene acetic acid
3-D	Three Dimensional
ABS	poly(acrylonitrile-butadiene-styrene)
AFM	Atomic force microscopy
ATRP	atom transfer radical polymerization
BAYTRON C	Bayer Chemicals Product (Catalyst)
BAYTRON M	Bayer Chemicals Product (Monomer)
BAYTRON P	Bayer Chemicals Product (Polymer)
BHJ	bulk-heterojunction
C-PEDOT	PEDOT films grown with the CuCl <sub>2</sub> oxidant
CA	Contact Angle
CFL	Capillary force lithography
COC	cyclo-olefin copolymers
CVD	Chemical Vapor Deposition
DI	deionized
DMF	<i>N,N'</i> -dimethylformamide
DMSO	Dimethyl sulfoxide
DNA	Deoxyribonucleic acid
E <sub>a</sub>	activation energy
e-beam	Electron Beam
EDOT	3,4-ethylenedioxythiophene
EDX	energy dispersive X-ray analysis
EG	ethylene glycol
eV	Electron Volt
F-PEDOT	PEDOT with FeCl <sub>3</sub> as an oxidizing agent
FETs	field-effect transistors
FF	Fill Factor
FTIR	Fourier Transform Infrared Spectroscopy
GMA	glycidyl methacrylate
GPC	Gel-Permeation Chromatography
HIL	hole injecting layer
HOMO	Highest Occupied Molecular Orbital
HPLC	High performance liquid chromatography
iCVD	Initiated Chemical Vapor Deposition/Deposited
IR	Infrared
ITO	Indium Tin Oxide
J	Current Density
J <sub>D</sub>	dark current Density
J <sub>ph</sub>	photo-generated Current Density
J <sub>sc</sub>	short circuit current density
LUMO	Lowest Unoccupied Molecular Orbital

MEMS	Micro Electro Mechanical Systems
MFC	Mass Flow Controller
NHS	N-hydroxysuccinimide
NPB	<i>N,N'</i> -(di- <i>n</i> -naphthalene-1-yl)- <i>N,N'</i> -diphenyl-benzidine
oCVD	Oxidative Chemical Vapor Deposition/Deposited
oLEDs	Organic Light-Emitting Diodes
oPV	organic photovoltaic
oTFTs	organic thin film transistors
P3HT	poly(3-hexylthiophene)
PAAm	poly allylamine
PANI	Polyaniline
PC	polycarbonate
PCBM	[6,6]-phenyl C <sub>61</sub> butyric acid methyl ester
PCE	power conversion efficiency
PDMS	Poly-dimethylsilane
PE	polyethylene
PECVD	Plasma-Enhanced Chemical Vapor Deposition
PEDOT	Poly-3,4-ethylenedioxythiophene
PEG	poly (ethylene glycol)
PEN	polyethylenenaphthalate
PEO	polyethyleneoxide
PES	photoelectron spectroscopy
PET	polyethyleneterephthalate
PFA	poly(perfluorodecyl acrylate)
PGMA	poly (glycidyl methacrylate)
PID	Proportional, Integral, Derivative
PL	photolithography
PMA	Propargyl methacrlate
PMMA	poly (methyl methacrylate)
PP	polypropylene
PPMA	poly (propargyl methacrylate)
PR	photoresist
PS	polystyrene
PSS	Poly-styrene Sulfonic Acid
PTCS	phenyltrichlorosilane
PTFE	polytetrafluoroethylene
PU	poly urethane
PUA	poly (urethaneacrylate)
PVA	poly vinylalcohol
QCM	Quartz Crystal Monitor
QDs	Quantum Dots
R	Organic Sidegroup Constituent (ie Methyl, Phenyl, etc)
R <sub>s</sub>	series resistance
R <sub>sh</sub>	shunt resistance
<i>r</i>	ratio of true surface area to the projected surface area
RF	Radio Frequency

RMS	Root Mean Squared
ROM	Read-Only Memory
S/cm	Siemens/cm (Units of Bulk Conductivity)
SAM	self-assembled monolayer
sccm	Standard Cubic Centimeters per Minute
SEM	Scanning electron microscopy
SMU	Source-Measure Unit
STEM	scanning transmission electron microscopy
TBPO	tert-butyl peroxide
TCPS	tissue culture polystyrene
TCVS	trichlorovinyl silane
THF	Tetrahydrofuran
$T_{bp}$	Boiling Point Temperature
$T_g$	Glass Transition Temperature
$T_{mp}$	Melting Point Temperature
$T_{sub}$	substrate temperature
TCO	Transparent conducting oxides
UV	Ultraviolet Light
UV/Vis	Ultraviolet and Visible Light
V	Voltage
$V_{oc}$	open circuit voltage
XPS	X-ray photoelectron spectroscopy

## Greek Symbols

$\gamma_{SV}$	solid-vapor interfacial tension
$\gamma_{SL}$	solid-liquid interfacial tension
$\gamma_{LV}$	liquid-vapor interfacial tension
$\theta$	Contact Angle
$\theta^{app}$	Apparent Contact Angle
$\lambda_{abs}$	Peak maximum wavelength in absorption spectroscopy
$\lambda_{em}$	Peak maximum wavelength in photoluminescence spectroscopy
$\phi_s$	the fraction of solid-liquid contact area
$\pi$	Pi Bond
$\pi^*$	Anti Pi Bond

# **Chapter One**

## INTRODUCTION

## **1.1 Motivation**

Chemical vapor deposition (CVD) process is a versatile, solventless process which can offer a variety of advantages including the tunability of properties, high purity and uniformity. Moreover, the CVD films are generally conformal to the surface topology and free of damage to the substrate underneath. For these reasons, CVD process is highly suitable for high-end applications such as electronics and biological devices. In this thesis, we utilized CVD process of polymer films for electronic and biological device applications.

### **1.1.1 Oxidative Chemical Vapor Deposition of Conducting Polymer Films**

Since the first discovery of polymeric conductors in 1977, the research area of “organic electronics” has grown dramatically. Current development in this area showed that the performance of electronic devices made of organic electronic materials is almost comparable with that of conventional inorganic semiconductor devices,<sup>1</sup> which has greatly stimulated both academic and industrial interest. Since the electronic properties of organic materials can be easily tuned by use of well-established tools of organic chemistry,<sup>1</sup> a variety of organic electronic devices have been enabled and demonstrated such as organic thin film transistors (oTFTs),<sup>2</sup> organic light-emitting diodes (oLEDs),<sup>3</sup> organic photovoltaic (oPV) cells<sup>4</sup> for cheap solar energy source, and organic memory devices<sup>5</sup> using different kinds of organic materials with the properties that each electronic devices requires. Polymeric conductors have also been utilized for various kinds of applications such as Li-



ion battery electrodes,<sup>6</sup> chemical and biochemical sensors,<sup>7</sup> capacitors,<sup>8</sup> and electrochromic devices.<sup>6,9</sup> Combined with the highly promising electronic properties, the extremely low price of organic electronic materials compared with the inorganic semiconductors, and the compatibility with various substrates including papers, fabrics, and foils envision the future flexible, transparent electronics embedded into our environments.

### **1.1.2 Initiated Chemical Vapor Deposition of Biofunctionalizable Polymer Films**

Another important issue dealt with in this thesis is bio-functionalizable surfaces. Since the bio-system is a grand mixture of thousands of bioactive components including hormones, enzymes, proteins, ions, and nutrients, selective recognition with high sensitivity is highly desirable. Therefore, designed bio-active patterned functional surfaces can offer advantageous properties such as controlled adsorption and site-specific affinity.<sup>10, 11</sup> In particular, area-selective functionalization of multiple components onto a pre-designed surface<sup>11-15</sup> is highly desirable. Such a system can be utilized to detect and identify more than one analyte in biosensor applications, which enables fabrication of more effective bio-devices.<sup>12</sup> Moreover, the multi-functional surface can be used as a template to monitor the interaction among the adsorbed components from a complex mixture, such as an extracellular environment. For these reasons, nanopatterned functional surfaces are regarded as excellent vehicles for exploring the interfacial interactions of biological components and can be utilized for applications including controlled drug release, biosensors, and artificial skin.

## 1.2 Conducting Polymer of Interest: PEDOT

One of the most promising conducting polymers is poly 3, 4 ethylenedioxythiophene (PEDOT)<sup>6, 8, 16</sup>, in which the 3 and 4 positions of the thiophene ring are blocked by oxygen, minimizing unwanted polymerization at these two  $\beta$ -carbon sites. Moreover, the oxygen acts as an electron donating group, increasing the electron density of the thiophene ring. Therefore, the conjugated polythiophene ring can easily be positively charged by the anion dopants. The opposite side of oxygen atoms is capped by an ethylene moiety to form a stable six-membered ring. This backbonded ring minimizes the unwanted polymerization reaction branched from 3 and/or 4 position.

The methods for forming thin films comprised solely of a conductive polymer, such as PEDOT, are limited by the rigid nature of the conjugated backbone.<sup>17</sup> Neither spin casting from solution nor melt processing can be used. High conductivity ( $\sim 300$  S/cm) PEDOT thin films have been synthesized by electropolymerization<sup>9, 18</sup> but a conductive substrate is required. Oxidative polymerization can also yield PEDOT thin film<sup>19, 20</sup>, but it is not trivial to reproducibly obtain highly conductive films.<sup>21</sup> An alternate approach to create PEDOT films is the use of “flexible polymer dopants” to make the solution process of conjugated polymers possible. One of the most successful combinations is PEDOT doped with polystyrene sulfonic acid (PSS) water emulsion developed by scientists at Bayer AG (commercial name of Baytron P<sup>TM</sup>)<sup>16, 22, 23</sup>.

## 1.3 Biofunctionalizable Surfaces

Selective bio-functionalizable surfaces with high sensitivity require high selectivity and strong binding of biological components onto the synthetic surface. A number of immobilization schemes have been suggested including silane and thiol chemistry<sup>24</sup> and biotin-streptavidin binding.<sup>25</sup> Conversely, physisorption of biomaterials to the surface is undesirable because it is generally nonspecific to the binding site.<sup>25</sup> Therefore, a high contrast for adhesion strength and site-selectivity is of great importance. Currently, immobilization schemes combined with micropatterning techniques<sup>26</sup> provides a variety of opportunities of investigation into how the specifically immobilized biological components interact with their environment.<sup>27</sup>

Currently, a new organic synthesis method termed “click” chemistry has attracted many researchers’ interest. “Click” chemistry quickly and selectively creates covalent linkages between molecular building blocks. One of the most efficient and versatile click reactions is the Huisgen 1,3-dipolar cycloaddition introduced by Sharpless and co-workers<sup>28</sup> in which the reaction of azides and terminal acetylene groups are catalyzed by Cu(I). The Sharpless-type click reactions are known to be i) highly efficient with fast reaction rate when the reaction is catalyzed by Cu(I), ii) highly regioselective without any side products and tolerant to various other functionalities, iii) biologically friendly, because the reaction can be performed in various solvents, including water at mild temperature (25 – 70 °C).<sup>29</sup>

Click active surfaces have been synthesized via multistep processing comprised of either i) forming a protected functional surface followed by conversion of the protected surface functional groups to reactive azides/acetylenes or ii) synthesis of azide/acetylene terminated monomer and polymerizing the monomer to form functionalized coatings.<sup>30, 31</sup>

For example, D. Rozkiewicz et al prepared a click-active surface by generating a bromo-terminated self-assembled monolayer (SAM) and converting the bromo-termination to an azido-terminated functionality afterward.<sup>32</sup> On the other hand, H. Nandivada et al first synthesized acetyl-functionalized paracyclophane monomers, and then applied a chemical vapor deposition (CVD) process to obtain clickable surface.<sup>31</sup> Similarly, B. Sumerlin et al also synthesized an azido-functionalized methacrylate and applied atom transfer radical polymerization (ATRP) process with this clickable monomer.<sup>33</sup> These approaches are necessary because of the chemically vulnerable characteristics of azides/acetylenes and/or the lack of commercially available monomers able to form stable coatings in which the azides/acetylene functionalities are maintained.<sup>33</sup>

## **1.4 Outlook**

### **1.4.1 Oxidative Chemical Vapor Deposition of Conducting Polymer Films**

Even though the solution-processible conjugated PEDOT film can be made with PEDOT:PSS emulsion, the conductivity is inherently low (less than 10 S/cm). In addition, a complicated additional hydrophilic substrate treatment such as oxygen plasma treatment or UV-ozone treatment must be applied to achieve a uniform polymer film.<sup>34</sup> Chemical vapor deposition (CVD) of PEDOT films has several potential benefits. Substrates which are not electrically conductive or which can be degraded by solvent can also be used, including paper, fabric, glass, wafer, and metal oxide.<sup>35</sup> Using the same feed gases, the CVD process conditions, such as temperature, pressure, and flow rates, can be varied to adjust the

properties required for successful integration of the film into organic devices such as oLEDs and oTFTs.

#### **1.4.2 Initiated Chemical Vapor Deposition of Biofunctionalizable Polymer Films**

For bio-functionalizable surfaces, we introduce a click chemistry active polymer coating prepared by the simple one-step synthetic process of initiative chemical vapor deposition (iCVD) using the commercially available monomer propargyl metacrylate (PMA). The iCVD process can offer a variety of advantages<sup>36</sup> including highly conformal coverage on the substrates with complex geometries such as electrospun fiber mats,<sup>37</sup> and carbon nanotubes,<sup>38, 39</sup> and trenches. Vapor deposition process are favored over solution processes when insoluble surface coatings are desired.<sup>35, 40, 41</sup> The hot filament temperature is generally less than 300 °C which generally does not thermally damage the monomers introduced to the iCVD process. Consequently, reactive functional groups in the monomer are easily retained in the polymer film forming on the surface. The heated filaments selectively result in the decomposition of the initiator species which then reacts with tens or hundreds of intact monomer units, making the iCVD process a highly power-efficient and mild process compared with plasma CVD process.<sup>38, 42, 43</sup>

### **1.5 Thesis Framework**

This thesis consists of two main issues: the oxidative chemical vapor deposition (oCVD) and their device application of PEDOT films and the iCVD and functionalization of propargyl methacrylate (PPMA).

In CHAPTER TWO, the oCVD process was tuned for maximum conductivity and reproducibility. The oCVD process provides systematic control over the final electrical conductivity of the films. Rigorous characterization methods were exploited including four-point probe measurements, profilometer, UV-visible absorption spectroscopy, Fourier Transform Infrared spectroscopy (FTIR), and Raman spectroscopy.

In CHAPTER THREE, X-ray photoelectron spectroscopy (XPS), scanning transmission electron microscopy (STEM) with energy dispersive X-ray analysis (EDX), and photoelectron spectroscopy (PES) were used to determine the chemical and electrical properties of a series PEDOT films systematically prepared by varying only the substrate temperature of the oCVD process.

CHAPTER FOUR demonstrates a one-step process for directly grafting conducting polymers onto flexible polymer substrates which contain aromatic groups. This process of oCVD does not employ a linker, such as silane or thiol compounds, but relies on covalent bonding directly between the conducting polymer film and aromatic moiety in these polymeric substrates. The inherently grafted PEDOT displays greatly enhanced adhesion, thus enabling patterning down to 60 nm features on flexible polymeric substrates.

In CHAPTER FIVE, we describe a new synthetic scheme to fabricate nano-porous, basalt-like PEDOT films by introducing a new oxidant,  $\text{CuCl}_2$ , to the oCVD process. The surface morphology and nanostructure of the resultant films could be systematically

controlled by changing substrate temperature during the oCVD process. The nanostructured PEDOT could also be conformally coated on various geometries, including trenches with high aspect ratio and complex, fragile surfaces without damaging the subtle surface structure. Water and ethanol droplet contact angles on these nano-porous PEDOT films showed that the contact angle was highly affected by the surface morphology. Superhydrobicity and oleophobicity was also readily obtained via vapor phase, initiative chemical vapor deposition (iCVD) of fluorinated polymer film on nanostructured oCVD PEDOT.

In CHAPTER SIX, oCVD PEDOT was used as a buffer layer in oPV cell which showed high power conversion efficiency (PCE) and large short circuit current ( $J_{sc}$ ) and the performance is almost similar with that of fully optimized oPV device with PEDOT:PSS.

In CHAPTER SEVEN, PPMA films were successfully prepared via iCVD, and further functionalization using click chemistry was also successfully applied on the terminal acetylene functionality in PPMA. Alternatively, iCVD PPMA itself exhibits e-beam sensitivity and hence can be directly patterned via electron beam (e-beam) lithography without requiring a conventional resist layer. Thus, iCVD PPMA exhibits the dual functions of the “clickable” e-beam sensitive material.

In CHAPTER EIGHT, we propose a facile solventless method for synthesizing nanopatterned multi-functional surfaces. One nanodomain contains an acetylene group which can be functionalized via click chemistry. The other nanodomain contains surface amine groups which can be functionalized by carbodiimide chemistry with *N*-hydroxysuccinimide (NHS).<sup>13, 29</sup> The click and NHS-reactions are highly orthogonal to

each other so that non-specific immobilization can be minimized. With these functionalities, we demonstrated the covalent functionalization of two independent components in a one-pot, self-sorted area-selective process, performed in an aqueous solution at room temperature, having conditions which are bio-compatible.

In CHAPTER NINE, we report a novel nano-adhesive layer deposited by the iCVD process. An epoxy-containing polymer, poly (glycidyl methacrylate) (PGMA) was used as a nano-adhesive layer. The PGMA coated substrate was brought into contact with the substrates covered with plasma polymerized poly (allylamine) (PAAm), and the ring-opening curing reaction of PGMA layer with conjugate PAAm layer was performed at the temperature of 70 °C to form a strong covalent bond between the two substrates. No leakage was observed up to the test pressure of 50 psia from the resulting microfluidic devices.

APPENDIX A provides a comprehensive illustration of newly installed CVD polymerization chamber. The system is designed for both iCVD and oCVD in one system. The system is integrated into the organic electronic device fabrication line and the substrates can be transferred without breaking the vacuum to minimize the potential defects from ambient.

Each of the chapters has been formatted as a technical journal paper, so that it can be read independently. After eight chapters, the thesis is concluded with summary and future applications based upon this work is presented.



## References

1. Forrest, S.R. The path to ubiquitous and low-cost organic electronic appliances on plastic. *Nature* **2004** *428*, 911-918.
2. Newman, C.R.; Frisbie, C.D.; da Silva, D.A.; Bredas, J.L.; Ewbank, P.C.; Mann, K.R. Introduction to organic thin film transistors and design of n-channel organic semiconductors. *Chemistry of Materials* **2004** *16*, 4436-4451.
3. Chen, C.T. Evolution of red organic light-emitting diodes: Materials and devices. *Chemistry of Materials* **2004** *16*, 4389-4400.
4. Thompson, B.C.; Frechet, J.M.J. Organic photovoltaics - Polymer-fullerene composite solar cells. *Angewandte Chemie-International Edition* **2008** *47*, 58-77.
5. Moller, S.; Perlov, C.; Jackson, W.; Taussig, C.; Forrest, S.R. A polymer/semiconductor write-once read-many-times memory. *Nature* **2003** *426*, 166-169.
6. Kirchmeyer, S.; Reuter, K. Scientific importance, properties and growing applications of poly(3,4-ethylenedioxythiophene). *J Mater Chem* **2005** *15*, 2077-2088.
7. Sotzing, G.A.; Briglin, S.M.; Grubbs, R.H.; Lewis, N.S. Preparation and properties of vapor detector arrays formed from poly(3,4 ethylenedioxy)thiophene-poly(styrene sulfonate)/insulating polymer composites. *Analytical Chemistry* **2000** *72*, 3181-3190.

8. Groenendaal, B.L.; Jonas, F.; Freitag, D.; Pielartzik, H.; Reynolds, J.R. Poly(3,4-ethylenedioxythiophene) and its derivatives: Past, present, and future. *Advanced Materials* **2000** *12*, 481-494.
9. Groenendaal, L.; Zotti, G.; Aubert, P.H.; Waybright, S.M.; Reynolds, J.R. Electrochemistry of poly(3,4-alkylenedioxythiophene) derivatives. *Advanced Materials* **2003** *15*, 855-879.
10. Nie, Z.; Kumacheva, E. Patterning Surfaces with Functional Polymers. *Nature Materials* **2008** *7*, 277-290.
11. Xu, H.; Hong, R.; Lu, T.X.; Uzun, O.; Rotello, V.M. Recognition-directed orthogonal self-assembly of polymers and nanoparticles on patterned surfaces. *Journal of the American Chemical Society* **2006** *128*, 3162-3163.
12. Katz, J.S.; Doh, J.; Irvine, D.J. Composition-tunable properties of amphiphilic comb copolymers containing protected methacrylic acid groups for multicomponent protein patterning. *Langmuir* **2006** *22*, 353-359.
13. Malkoch, M.; Thibault, R.J.; Drockenmuller, E.; Messerschmidt, M.; Voit, B.; Russell, T.P.; Hawker, C.J. Orthogonal approaches to the simultaneous and cascade functionalization of macromolecules using click chemistry. *Journal of the American Chemical Society* **2005** *127*, 14942-14949.
14. Slocik, J.M.; Beckel, E.R.; Jiang, H.; Enlow, J.O.; Zabinski, J.S.; Bunning, T.J.; Naik, R.R. Site-specific patterning of biomolecules and quantum dots on functionalized surfaces generated by plasma-enhanced chemical vapor deposition. *Advanced Materials* **2006** *18*, 2095-+.

15. Zhou, F.; Zheng, Z.J.; Yu, B.; Liu, W.M.; Huck, W.T.S. Multicomponent polymer brushes. *Journal of the American Chemical Society* **2006** *128*, 16253-16258.
16. Jonas, F.; Morrison, J.T. 3,4-polyethylenedioxythiophene (PEDT): Conductive coatings technical applications and properties. *Synthetic Metals* **1997** *85*, 1397-1398.
17. Bredas, J.L.; Silbey, R.J. Conjugated Polymers: The novel science and technology of highly conducting and nonlinear optically active materials; Kluwer Academic Publishers: Dordrecht ; Boston, 1991;xviii, 624 p.
18. Yamato, H.; Kai, K.; Ohwa, M.; Asakura, T.; Koshiba, T.; Wernet, W. Synthesis of free-standing poly(3,4-ethylenedioxythiophene) conducting polymer films on a pilot scale. *Synthetic Metals* **1996** *83*, 125-130.
19. Kim, J.; Kim, E.; Won, Y.; Lee, H.; Suh, K. The preparation and characteristics of conductive poly(3,4-ethylenedioxythiophene) thin film by vapor-phase polymerization. *Synthetic Metals* **2003** *139*, 485-489.
20. Ha, Y.H.; Nikolov, N.; Pollack, S.K.; Mastrangelo, J.; Martin, B.D.; Shashidhar, R. Towards a transparent, highly conductive poly(3,4-ethylenedioxythiophene). *Advanced Functional Materials* **2004** *14*, 615-622.
21. Winther-Jensen, B.; Breiby, D.W.; West, K. Base inhibited oxidative polymerization of 3,4-ethylenedioxythiophene with iron(III)tosylate. *Synthetic Metals* **2005** *152*, 1-4.
22. Jonas, F.; Heywang, G. Technical Applications for Conductive Polymers. *Electrochimica Acta* **1994** *39*, 1345-1347.

23. Jonas, F.; Krafft, W.; Muys, B. Poly(3,4-Ethylenedioxythiophene) - Conductive Coatings, Technical Applications and Properties. *Macromolecular Symposia* **1995** *100*, 169-173.
24. Wink, T.; vanZuilen, S.J.; Bult, A.; vanBennekom, W.P. Self-assembled monolayers for biosensors. *Analyst* **1997** *122*, R43-R50.
25. Raiteri, R.; Grattarola, M.; Butt, H.J.; Skladal, P. Micromechanical cantilever-based biosensors. *Sensors and Actuators B-Chemical* **2001** *79*, 115-126.
26. Senaratne, W.; Andruzzi, L.; Ober, C.K. Self-assembled monolayers and polymer brushes in biotechnology: Current applications and future perspectives. *Biomacromolecules* **2005** *6*, 2427-2448.
27. Falconnet, D.; Csucs, G.; Grandin, H.M.; Textor, M. Surface engineering approaches to micropattern surfaces for cell-based assays. *Biomaterials* **2006** *27*, 3044-3063.
28. Kolb, H.C.; Finn, M.G.; Sharpless, K.B. Click chemistry: Diverse chemical function from a few good reactions. *Angewandte Chemie-International Edition* **2001** *40*, 2004-+.
29. Lutz, J.F. 1,3-dipolar cycloadditions of azides and alkynes: A universal ligation tool in polymer and materials science. *Angewandte Chemie-International Edition* **2007** *46*, 1018-1025.
30. Binder, W.H.; Sachsenhofer, R. 'Click' chemistry in polymer and materials science. *Macromolecular Rapid Communications* **2007** *28*, 15-54.

31. Nandivada, H.; Chen, H.Y.; Bondarenko, L.; Lahann, J. Reactive polymer coatings that "click". *Angewandte Chemie-International Edition* **2006** *45*, 3360-3363.
32. Rozkiewicz, D.I.; Janczewski, D.; Verboom, W.; Ravoo, B.J.; Reinhoudt, D.N. "Click" chemistry by microcontact printing. *Angewandte Chemie-International Edition* **2006** *45*, 5292-5296.
33. Sumerlin, B.S.; Tsarevsky, N.V.; Louche, G.; Lee, R.Y.; Matyjaszewski, K. Highly efficient "click" functionalization of poly(3-azidopropyl methacrylate) prepared by ATRP. *Macromolecules* **2005** *38*, 7540-7545.
34. Kobayashi, H.; Kanbe, S.; Seki, S.; Kiguchi, H.; Kimura, M.; Yudasaka, I.; Miyashita, S.; Shimoda, T.; Towns, C.R.; Burroughes, J.H. et al. A novel RGB multicolor light-emitting polymer display. *Synthetic Metals* **2000** *111*, 125-128.
35. Lock, J.P.; Im, S.G.; Gleason, K.K. Oxidative chemical vapor deposition of electrically conducting poly(3,4-ethylenedioxythiophene) films. *Macromolecules* **2006** *39*, 5326-5329.
36. Tenhaeff, W.T.; Gleason, K.K. Initiated and Oxidative Chemical Vapor Deposition of Polymeric Thin Films: iCVD and oCVD *Advanced Functional Materials* **2008** *18*, 969-1140.
37. Ma, M.L.; Mao, Y.; Gupta, M.; Gleason, K.K.; Rutledge, G.C. Superhydrophobic fabrics produced by electrospinning and chemical vapor deposition. *Macromolecules* **2005** *38*, 9742-9748.
38. Lau, K.K.S.; Gleason, K.K. Particle surface design using an all-dry encapsulation method. *Advanced Materials* **2006** *18*, 1972-+.

39. Lau, K.K.S.; Bico, J.; Teo, K.B.K.; Chhowalla, M.; Amaratunga, G.A.J.; Milne, W.I.; McKinley, G.H.; Gleason, K.K. Superhydrophobic carbon nanotube forests. *Nano Letters* **2003** *3*, 1701-1705.
40. Chan, K.; Gleason, K.K. Air-gap fabrication using a sacrificial polymeric thin film synthesized via initiated chemical vapor deposition. *Journal of the Electrochemical Society* **2006** *153*, C223-C228.
41. Lin, J.; Murthy, S.K.; Olsen, B.D.; Gleason, K.K.; Klivanov, A.M. Making thin polymeric materials, including fabrics, microbicidal and also water-repellent. *Biotechnology Letters* **2003** *25*, 1661-1665.
42. Lau, K.K.S.; Gleason, K.K. All-dry synthesis and coating of methacrylic acid copolymers for controlled release. *Macromolecular Bioscience* **2007** *7*, 429-434.
43. Mao, Y.; Felix, N.M.; Nguyen, P.T.; Ober, C.K.; Gleason, K.K. Towards all-dry lithography: Electron-beam patternable poly(glycidyl methacrylate) thin films from hot filament chemical vapor deposition. *Journal of Vacuum Science & Technology B* **2004** *22*, 2473-2478.

## **Chapter Two**

### **SYSTEMATIC CONTROL OF THE ELECTRICAL CONDUCTIVITY OF POLY (3, 4- ETHYLENEDIOXYTHIOPHENE) VIA OXIDATIVE CHEMICAL VAPOR DEPOSITION (oCVD)**

**Sung Gap Im** and Karen K. Gleason, 'Systematic Control of the Electrical Conductivity of Poly(3,4-ethylenedioxythiophene) via Oxidative Chemical Vapor Deposition', *Macromolecules*, 40 (2007) 6552 -6556

## **Abstract**

Systematic variation in the electrical conductivity of poly (3,4 ethylenedioxythiophene) (PEDOT) was achieved by oxidative chemical vapor deposition (oCVD). For oCVD, both the oxidant, Fe(III)Cl<sub>3</sub>, and 3,4 ethylenedioxythiophene (EDOT) monomer are introduced in the vapor phase. A heated crucible allows for sublimation of the oxidant directly into the reactor chamber operating at 150 mTorr. Spontaneous reaction of the oxidant with the monomer introduced through a feedback controlled mass flow system, results in the rapid (> 200 nm thick film in 30 min) formation of  $\pi$ -conjugated PEDOT thin films directly onto a temperature controlled substrate. As the substrate temperature is increased from 15 °C to 110 °C, increasing conjugation length, doping level, and electrical conductivity of the PEDOT chains are observed by UV-visible absorption spectroscopy (UV-Vis), Fourier transform infrared spectroscopy (FTIR), and Raman spectroscopy. Concomitantly, the measured electrical conductivity of the PEDOT films increases systematically with an apparent activation energy of  $28.2 \pm 1.1$  kcal/mol.

**Key words:** oxidative chemical vapor deposition (oCVD), poly 3,4 ethylenedioxythiophene (PEDOT), substrate temperature, electrical conductivity,  $\pi$ -conjugation, doping level.



## 2.1 Introduction

Conjugated polymers offer the advantages of high flexibility as compared to conventional electrically conductive inorganic materials.<sup>1, 2</sup> One of the most promising conducting polymers is poly 3, 4 ethylenedioxythiophene (PEDOT)<sup>1-3</sup>, in which the 3 and 4 positions of the thiophene ring are blocked by oxygen, minimizing unwanted polymerization at these two  $\beta$ -carbon sites. Moreover, the oxygen acts as an electron donating group, increasing the electron density of the thiophene ring. Therefore, the conjugated polythiophene ring can easily be positively charged by the anion dopants. The opposite side of oxygen atoms is capped by an ethylene moiety to form a stable six-membered ring. This backbonded ring minimizes the unwanted polymerization reaction branched from 3 and/or 4 position.

The methods for forming thin films comprised solely of a conductive polymer, such as PEDOT, are limited by the rigid nature of the conjugated backbone.<sup>4</sup> Neither spin casting from solution nor melt processing can be used. High conductivity ( $\sim 300$  S/cm) PEDOT thin films have been synthesized by electropolymerization<sup>5, 6</sup> but a conductive substrate is required. Oxidative polymerization can also yield PEDOT thin film<sup>7, 8</sup>, but it is not trivial to reproducibly obtain highly conductive films.<sup>9</sup>

An alternate approach to create PEDOT films is the use of “flexible polymer dopants” to make the solution process of conjugated polymers possible. One of the most successful combinations is PEDOT doped with polystyrene sulfonic acid (PSS) water emulsion developed by scientists at Bayer AG (commercial name of Baytron P<sup>TM</sup>)<sup>3, 10, 11</sup>. Even though the conjugated PEDOT film can be made with this emulsion, the conductivity

is inherently low (less than 10 S/cm). In addition, a complicated additional hydrophilic substrate treatment such as oxygen plasma treatment or UV-ozone treatment must be applied to achieve a uniform polymer film.<sup>12</sup>

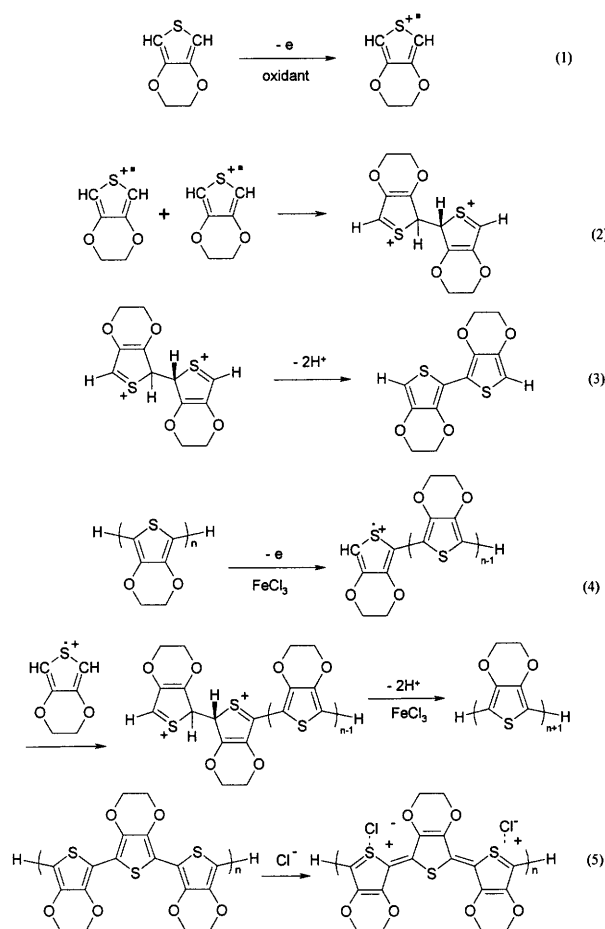


**Figure 2-1** Proposed polymerization mechanism for oxidative polymerization of PEDOT; (1) oxidation of EDOT to form cation radical; (2) dimerization of cation radical; (3) deprotonation to form conjugation; (4) further polymerization from n-mer to (n+1)-mer; (5) doping process of PEDOT.

Chemical vapor deposition (CVD) of PEDOT films has several potential benefits. Substrates which are not electrically conductive or which can be degraded by solvent can also be used, including paper, fabric, glass, wafer, and metal oxide.<sup>13</sup> Using the same feed gases, the CVD process conditions, such as temperature, pressure, and flow rates, can be varied to adjust the properties required for successful integration of the film into an organic devices such as organic light-emitting diodes (oLEDs) and organic thin film transistors (oTFTs).

Recently Winther-Jensen reported PEDOT thin film deposition in which the EDOT monomer was introduced in the vapor phase resulting in reported conductivities as high as of 1000 S/cm.<sup>14</sup> This method used spin-coating of the oxidizing agent of iron toluenesulfonate. H. Meng also introduced a CVD process using chlorinated EDOT for PEDOT<sup>15</sup>. Building on the idea of introducing the EDOT from the vapor phase, J. Lock developed an oxidative chemical vapor deposition (oCVD) method which employs the sublimation of oxidizing agent of iron(III) chloride obtaining a maximum conductivity of 105 S/cm<sup>13</sup>.

Various schemes are suggested to control the conductivity of PEDOT:PSS. By diluting the conducting polymer with non-conductive host polymer such as poly (methyl methacrylate) or poly (vinylpyrrolidone), the conductivity of PEDOT:PSS was increased by the factor of ten<sup>1, 16</sup>. By adding ethylene glycol (EG) or *meso*-erythritol into PEDOT:PSS film, the conductivity was increased from 0.4 S/cm to 200 S/cm<sup>17-19</sup>. By changing chemical species of dopants in electrochemically prepared PEDOT film, L Groenendaal *et. al.* could obtain various range of conductivity from 50 to 650 S/cm<sup>6, 20</sup>. By adding base materials

such as imidazole or pyridine in the course of liquid phase or vapor phase oxidative polymerization<sup>8, 9, 14</sup>, enormous conductivity increase – up to more than 1000 S/cm<sup>14</sup> – was obtained. The most successful way of systematically controlling the conductivity to date is doping level control by electrochemistry<sup>6, 20-22</sup>. T. Johansson *et. al.* observed the conductivity variation from  $6 \times 10^{-5}$  to 16 S/cm by electrochemical doping – dedoping process, but due to the extremely unstable nature of dedoped PEDOT film, low conductivity of  $6 \times 10^{-5}$  S/cm cannot be maintained in ambient condition and spontaneous doping process was occurred<sup>22</sup>. The first report of PEDOT films prepared by oCVD process displayed an amazingly wide span of conductivity<sup>13, 23</sup>.

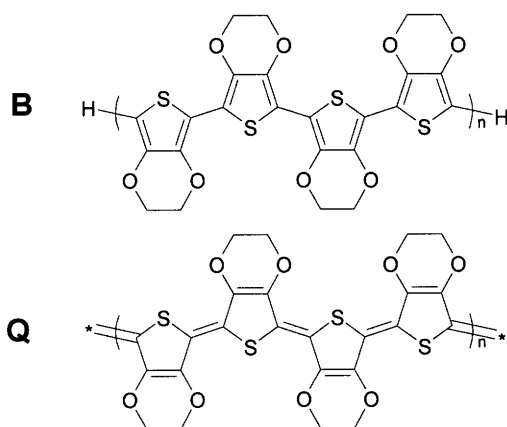


**Figure 2-2** B benzoid; Q quinoid type of PEDOT.

It is important to consider that the oCVD method may have many similarities to the stepwise reaction mechanism that is widely accepted for PEDOT oxidative polymerization<sup>2, 8, 13, 24</sup>, which is schematically shown in Fig. 2-1. Stoichiometric amounts of oxidizing agent react with the EDOT monomer to generate cation radicals. (Fig. 2-1-(1)) Pairs of cation

radicals dimerize (Fig. 2-1-(2)) and the anions of oxidizing agent scavenge two protons to stabilize the dimer. (Fig. 2-1-(3)) The oxidizing agent then acts on the dimer and again. (Fig. 2-1-(4)) These stepwise reactions are repeated continuously to form the PEDOT polymer. Some of the positively charged thiophene rings are stabilized by the counter ion in the polymer, which is referred as a dopant. (Fig. 2-1-(5)) The doping process results in charges along the conjugated backbone of the conducting polymer which enable the flow of current. Therefore, the amount of dopant is directly related with the conductivity of conjugated polymer<sup>6,22</sup>. As shown in Fig. 2-2, the type of conjugation may be distorted in the course of doping process. The two possible type of conjugation was shown in **B** and **Q** in Fig. 2-1<sup>18, 25</sup>. Form **B** is often referred as benzoid and form **Q** as quinoid. The transition energy between two type is called distortion energy which is a function of conjugation length<sup>26-28</sup>.

In this work, the oCVD process was tuned for maximum conductivity and reproducibility. The oCVD process provides systematic control over the final electrical conductivity of the films. Rigorous characterization methods were exploited including four-point probe measurements, profilometer, UV-visible absorption spectroscopy, Fourier Transform Infrared spectroscopy (FTIR), and Raman spectroscopy.

## 2.2 Experimental

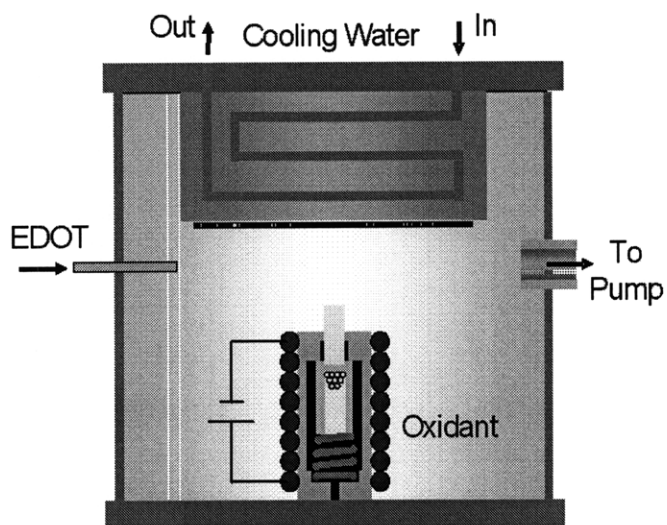


**Figure 2-3** Schematic figure of modified oCVD process chamber.

Previously, highly conductive PEDOT films (up to 105 S/cm) were obtained via oCVD and this conductivity could be modulated by controlling substrate temperature and by introducing basic pyridine vapor<sup>13</sup>. In the current work, two important hardware changes were made in order to improve the uniformity of oxidant delivery: the chamber was inverted so that the substrate faces down to oxidant source and the distance between the oxidant crucible and the substrate was increased to 20 cm to minimize the heating effect from the oxidant cell to the substrates. The schematic figure of newly modified oCVD process chamber is shown in Fig. 2-3. The process conditions of the current work are similar to the previous work, but some adjustments have been made to optimize deposition for the new hardware configuration. For example the current work uses a pressure of 150 mtorr instead of the previous value of 300 mtorr. Glass slides and silicon wafers were used

for substrates. The substrate temperature was controlled with cooling water and PID controlled substrate heater. The chamber pressure was controlled by a butterfly valve and was maintained at about 150 mTorr. Additional argon (Grade 5.0, BOC Gases) was introduced into the crucible to maintain the process pressure of oCVD. Fe(III)Cl<sub>3</sub> (97%, Aldrich) was used as the oxidant without further purification. The oxidant is loaded in a porous crucible placed above the stage. The crucible was heated to a temperature of about 320 °C where sublimation of the oxidant set on. At the same time, vapor phase EDOT monomer (3,4-ethylenedioxythiophene, Aldrich) was delivered into the reactor. The EDOT flow rate was set at 3 sccm. The process time was 30 minutes for all of the films. All the chemicals used in the experiments are used without any further purification. Substrate temperature was varied from 15 °C to 110 °C with other process parameters fixed. After the CVD process, the films are dried for at least 2 hours in a vacuum oven heated to 70 °C at a gauge pressure of -15 in. Hg. After drying deposited films were rinsed in methanol (HPLC Grade, J.T. Baker). The rinse step is intended to remove any unreacted monomer or oxidant in the films as well as short oligomers and reacted oxidant in the form of Fe(II)Cl<sub>2</sub>.

The thicknesses of the films deposited on glass are measured on a Tencor P-10 profilometer. Conductivity measurements are done with a four point probe (Model MWP-6, Jandel Engineering, Ltd) with Keithley 236 Source-Measure Unit. Constant source current of 0.001 to 1 mA is applied and the voltage is monitored. Sheet resistivity is calibrated by ITO coated glass and copper coated wafer. All the conductivity values are calculated using the sheet resistivity measured by four – point probe and thickness measured by profilometer. Films on silicon substrates were measured with FTIR (Nexus 870, Thermo Electron

Corporation) and Raman spectroscopy (Kaiser Hololab, 5000R, spectra obtained with an excitation wavelength of 785 nm) for information of chemical composition. UV-Visible absorption spectroscopy (Cary 5E) was also performed to monitor the energy levels of the conjugated polymer film. As the resultant PEDOT films have different film thickness, every UV-Vis spectrum was normalized with respect to the peaks in 1.3 – 1.5 eV.

## 2.3 Results and Discussion

### 2.3.1 UV-Visible Absorption Spectroscopy

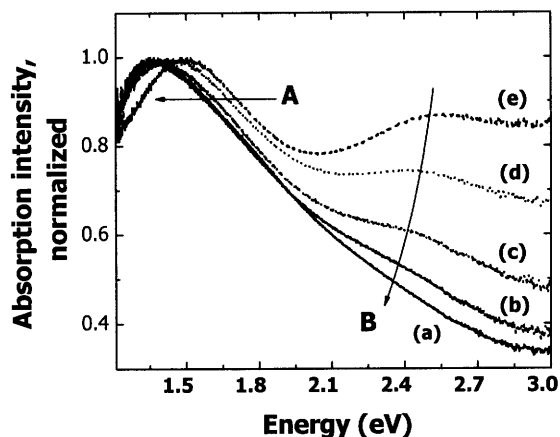


**Figure 2-4** UV-Vis optical spectra of CVD polymerized PEDOT with various substrate temperature ( $T_{\text{sub}}$ ); (a)  $T_{\text{sub}} = 100\text{ }^{\circ}\text{C}$ ; (b)  $T_{\text{sub}} = 85\text{ }^{\circ}\text{C}$ ; (c)  $T_{\text{sub}} = 71\text{ }^{\circ}\text{C}$ ; (d)  $T_{\text{sub}} = 47\text{ }^{\circ}\text{C}$ ; (e)  $T_{\text{sub}} = 15\text{ }^{\circ}\text{C}$ . **A** represents the bathochromic shift of polaronic energy state with the increase of substrate temperature. **B** represents the bathochromic peak shift and intensity decrease of the  $\pi$  to  $\pi^*$  transition energy state with the increase of substrate temperature.



Fig. 2-4 represents the UV-Vis absorption spectra of the oCVD PEDOT films deposited at the substrate temperature from 15°C to 100 °C. In undoped PEDOT films of sufficient conjugation length, the  $\pi$  to  $\pi^*$  transition is observed in the range of 580 to 600 nm. (2.0 ~ 2.2 eV).<sup>18, 21, 25</sup> In oligomeric PEDOT, the  $\pi$  to  $\pi^*$  transition occurs at higher energy and shifts to lower energy as the conjugation length increases<sup>29-31</sup>. In the series of oCVD deposited PEDOT film, the  $\pi$  to  $\pi^*$  transition has a maximum energy of 2.5 eV (sample (e) in Fig. 2-4) and this energy decreases as the substrate temperature increases. This observation strongly infers that the conjugation length of oCVD deposited PEDOT increases systemically as the substrate temperature increases.

The doping level change of oCVD deposited PEDOT was also observed. Dopants introduce polaron and bipolaron states having energy gaps at ~1.4 eV and ~1.1 eV, respectively for PEDOT<sup>21</sup>. As the doping level increases the  $\pi$  to  $\pi^*$  transition energy state shifts to the lower polaronic energy state.<sup>21</sup> As a result, the relative intensity of the  $\pi$  to  $\pi^*$  transition peak decreases as the doping level increases. In Fig. 2-2, the relative intensity of the  $\pi$  to  $\pi^*$  transition peak (around 2.1 to 2.5 eV) decreases with increasing electrical conductivity of PEDOT. The absorption spectrum of PEDOT deposited at the highest substrate temperature (sample (a) in Fig. 2-4) displays that the  $\pi$  to  $\pi^*$  transition peak is completely overlapped by the polaronic peak, whose spectrum is very similar with that of fully doped PEDOT film in the literature.<sup>6</sup> The observed absorption spectrum indicates that the doping level of PEDOT can be tuned by changing the substrate temperature in the oCVD process. Similar trend was observed in the peaks of polaronic energy state. With

increasing doping levels, the polaronic gap shifts to lower energy<sup>17, 18, 21</sup>. Thus, the observed shift of the polaronic energy peak maximum in Fig. 2-4 from 1.5 eV to 1.35 eV corresponds to increased doping levels for the series of films with increasing conductivity.

The observed shifts to lower energy of both the  $\pi$  to  $\pi^*$  transition peak and polaronic peak, and the relative reduction of  $\pi$  to  $\pi^*$  transition peak demonstrate that higher doping levels are achievable in oCVD PEDOT films deposited at high substrate temperature. Several previous reports have shown that longer conjugation length facilitates doping by lowering the required distortion energy required<sup>26, 27, 32</sup>. Thus, increasing conjugation length with increasing deposition temperature is a straightforward hypothesis which accounts for all the trends in the UV-Vis absorption data (Fig. 2-4) which will be tested by additional characterization methods reported in the following sections.

### 2.3.2 Raman Spectroscopy

Raman spectra of the series of oCVD PEDOT films were collected and compared with that of the monomer (Fig. 2-5). The obtained Raman spectra are similar to one another have the same primary features as that of electrochemically grown PEDOT<sup>17, 18, 25, 33</sup>. Characteristic peaks of well-defined PEDOT, such as symmetric  $C_{\alpha}=C_{\beta}$  symmetric stretching peak at 1444 and 1428  $\text{cm}^{-1}$ ,<sup>17, 18, 33</sup> and  $C_{\beta}=C_{\beta}$  stretching peak at 1368  $\text{cm}^{-1}$  are clearly observed<sup>25, 33</sup>.

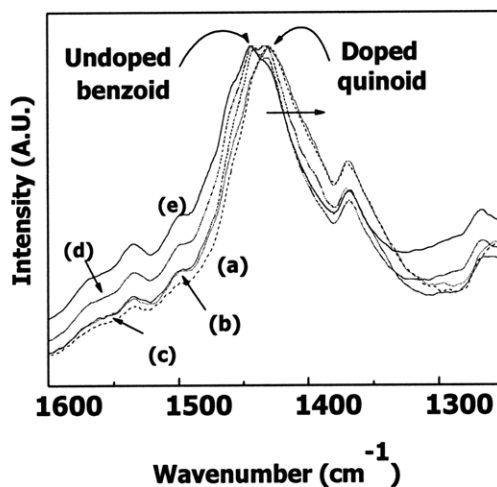
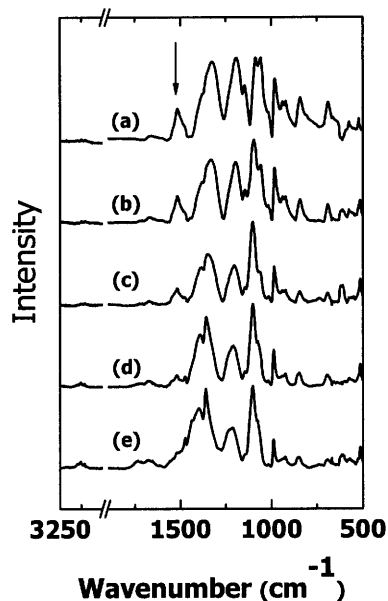


**Figure 2-5** Overlapped Raman spectra of CVD polymerized PEDOT with various substrate temperature ( $T_{\text{sub}}$ ); (a)  $T_{\text{sub}} = 100\text{ }^{\circ}\text{C}$ ; (b)  $T_{\text{sub}} = 85\text{ }^{\circ}\text{C}$ ; (c)  $T_{\text{sub}} = 71\text{ }^{\circ}\text{C}$ ; (d)  $T_{\text{sub}} = 47\text{ }^{\circ}\text{C}$ ; (e)  $T_{\text{sub}} = 15\text{ }^{\circ}\text{C}$ . Peak shift indicated by the arrow represents that the C=C conjugation is shifted from undoped benzoidal type ( $1444\text{ cm}^{-1}$ ) to doped quinoidal type ( $1428\text{ cm}^{-1}$ ).

Variation in the doping level variation was observed in Raman spectrum. In PEDOT deposited at the lowest substrate temperature (sample (e) in Fig. 2-5), the peak at  $1444\text{ cm}^{-1}$  is dominant and a small shoulder of  $1428\text{ cm}^{-1}$  peak is observed. For samples deposited at higher substrate temperature, the symmetric  $C_{\alpha}=C_{\beta}$  symmetric stretching peak maximum shifts gradually from  $1444\text{ cm}^{-1}$  to  $1428\text{ cm}^{-1}$ . In PEDOT deposited at the highest substrate temperature (sample (a) in Fig. 2-5), the peak at  $1428\text{ cm}^{-1}$  is dominant and a trace shoulder of  $1444\text{ cm}^{-1}$  was observed. Ouyang *et. al.* assigned these peaks as undoped benzoidal vibration for the peak at  $1444\text{ cm}^{-1}$  and doped quinoidal vibration for  $1428\text{ cm}^{-1}$  in the

PEDOT:PSS film<sup>17, 18</sup>. They also observed that the conductivity of PEDOT:PSS film was increased as the Raman peak was shifted from benzoid to quinoid.<sup>17, 18</sup> Thus, the shift from  $1444\text{ cm}^{-1}$  to  $1428\text{ cm}^{-1}$  indicates that the nature of conjugation shifts from undoped benzoid to doped quinoid and is completely consistent with the UV-Vis results (Fig. 2-4).

### 2.3.3 Fourier Transform Infra-red (FTIR) Spectroscopy



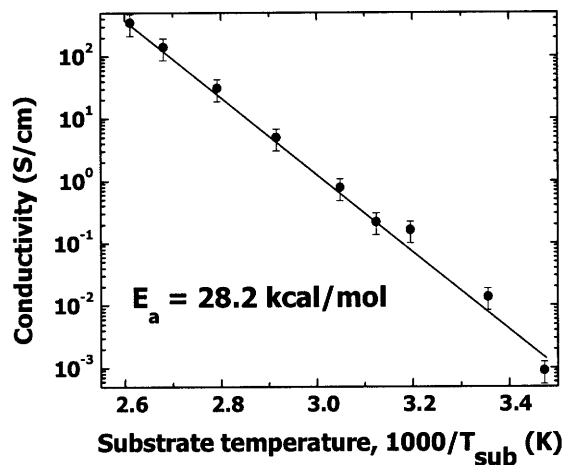
**Figure 2-6** FT-IR spectra of PEDOT with various substrate temperature ( $T_{\text{sub}}$ ); (a)  $T_{\text{sub}} = 100\text{ }^{\circ}\text{C}$ ; (b)  $T_{\text{sub}} = 85\text{ }^{\circ}\text{C}$ ; (c)  $T_{\text{sub}} = 71\text{ }^{\circ}\text{C}$ ; (d)  $T_{\text{sub}} = 47\text{ }^{\circ}\text{C}$ ; (e)  $T_{\text{sub}} = 15\text{ }^{\circ}\text{C}$ . Arrow represents the C=C stretch peak at  $1520\text{ cm}^{-1}$ .

Fig. 2-6 displays the FTIR spectra of the oCVD PEDOT films produced by variation in substrate temperature from  $15^{\circ}\text{C}$  to  $100^{\circ}\text{C}$ . Even though a quantitative analysis

of the FTIR spectra proved intractable due to the broadness and position shifts of the peaks from the conducting polymer films,<sup>32</sup> systematic changes are observed. As the substrate temperature decreases, the peak intensity of C=C stretch at  $1520\text{ cm}^{-1}$ <sup>33-35</sup> gradually decreases. In the spectra for PEDOT deposited at the lowest substrate temperature (sample (e) in Fig. 2-6), a considerable part of C=C stretch at  $1520\text{ cm}^{-1}$  is difficult to resolve. Similar spectral features are observed in undoped oligomeric PEDOT<sup>33, 34</sup>. Therefore, the decrease in C=C stretch at  $1520\text{ cm}^{-1}$  is a direct indication of short conjugation length. Thus, the FTIR results also support the hypothesis of higher substrate temperatures producing oCVD PEDOT films of longer conjugation length, as discussed in the previous UV-Vis and Raman sections.

#### 2.3.4 Conductivity

Fig. 2-7 demonstrates that oCVD is an excellent synthesis method for achieving systematic control of electrical conductivity over a wide range of values. The measured conductivity values of oCVD PEDOT polymer films grow dramatically as the substrate temperature increases  $15\text{ }^{\circ}\text{C}$  to  $110\text{ }^{\circ}\text{C}$ , the only processing parameter which was varied. The range of conductivity achieved was from a low of  $9.1 \times 10^{-4}\text{ S/cm}$  to a high of  $348\text{ S/cm}$ . Thus, by a simply varying substrate temperature, the conductivity of oCVD PEDOT can be systematically controlled over a range spanning more than five orders of magnitude.



**Figure 2-7** Arrhenius plot of substrate temperature vs. conductivity.

The Arrhenius plot of conductivity with the substrate temperature (Fig. 2-7) fits well to a single apparent activation energy of  $28.1 \pm 1.1$  kcal/mol. This linear relationship ( $R^2 > 99\%$ ) suggests that a fundamental link exists between electrical conductivity and a single thermally activated chemical reaction or diffusion step occurring at the substrate during oCVD growth<sup>36</sup>. Table 2-1 summarizes the the oCVD prepared and gives selected properties.

The observed conductivity data are completely consistent with the optical and chemical analysis performed above in that oCVD PEDOT with longer conjugation length and higher doping level has higher electrical conductivity. However, the extreme complexity of electrical conductivity of conducting polymer<sup>37, 38</sup> makes the true nature of conductivity unclear since the electrical conductivity is a collective function of not just the conjugation length and doping level, but also crystallinity<sup>38</sup>, interface with the substrate<sup>39, 40</sup>,

and the measurement conditions, such as frequency and temperature<sup>37</sup>. Nevertheless, the Arrhenius plot indicates that the conductivity has a close relationship with the substrate temperature of the oCVD process. Thus, we can reasonably postulate that the conductivity is intrinsically related with the polymerization reaction steps occurring at the surface of the substrate. At 25 °C, the EDOT monomer has limited volatility, with a vapor pressure of 0.278 torr. Even lower vapor pressures at 25 °C are associated with the dimers ( $1.57 \times 10^{-7}$  torr) and trimers ( $1.3 \times 10^{-13}$  torr)<sup>36</sup>. Higher order oligomers are anticipated to be essentially involatile at 25 °C and higher substrate temperature. Therefore, the oxidative polymerization reaction is confined at the surface of the substrate.

Substrate temperature, °C	15	47	71	85	100
Conductivity, S/cm	$9.1 \times 10^{-4}$	0.080	0.66	31	348
Thickness, nm	85	87	72	59	63
Position of C=C symmetric peak local maxima in Raman spectroscopy, $\text{cm}^{-1}$	1444.1	1431.3 1442.7	1431.9 1440.6	1430.9	1429.7
Polaronic energy peak maximum in UV-Vis spectroscopy, eV	1.50	1.44	1.38	1.36	1.35

**Table 2-1 Summary of selected properties of oCVD deposited PEDOT film**

Higher temperature for surface polymerization will increase cation radical reactivity and accelerates dimerization and polymerization reactions (Fig. 2-1-(a) to (c)) because the reaction rate constants will increase with higher temperature<sup>36</sup>. Thus, as reaction rates increase, monomer and oligomer cation radicals are more easily formed and then combine with each other to form stable high molecular weight chains until the high chain lengths lack the mobility limiting the mass transfer of radical cations. Chain mobility will also improve with increasing substrate temperature. In the same way, higher temperature can also promote deprotonation reaction to form conjugation due to increased reaction rate constant at higher temperature<sup>36</sup>. Therefore, the extent of the deprotonation reaction is directly related with the length of conjugation<sup>8, 13, 14</sup>. Then it follows that the conjugation length is governed by molecular weight of polymer and the degree of deprotonation of the polymer chain. Moreover, the scavenged protons are easily evaporated in the form of HCl<sup>41</sup>. Since the back-bonded dioxyethylene ring can be possibly destroyed by acid catalyzed reactions<sup>13, 14, 24</sup>, the rapid elimination of HCl is desirable to prevent formation of defects along the chain. Thus, high surface temperature promotes the formation of higher molecular weight chains and also decreases the density of defects along the chain caused by insufficient deprotonation or unwanted acid catalyzed side reactions. Therefore, the conjugation length will depend upon the completeness of each stepwise polymerization reaction.

## **2.4 Conclusion and outlook**



The substrate temperature of the oCVD process is a critical parameter which permits control over the conductivity of PEDOT films over a range of more than five orders of magnitude. From FTIR and Raman spectroscopy, the chemical nature giving rise to the systematic variation in the level conduction of the PEDOT film was elucidated. Specifically, the substrate temperature controls the conjugation length of the oCVD PEDOT. Additionally, the optical absorption spectra demonstrate that the combination of lack of doping and short conjugation length lead to low values of conductivity in films deposited at low substrate temperature. From the oCVD polymerization process, single apparent activation energy of  $28.1 \pm 1.1$  kcal/mol is observed for conductivity with respect to substrate temperature. Thus, oCVD process offers a straightforward means of controlling the conductivity of PEDOT to suit the various requirements of organic electronic devices, such as oLEDs<sup>42, 43</sup>, oTFTs<sup>44</sup>, and organic ROM-memory devices<sup>45</sup>. Therefore, its applications to the device can give opportunity of breakthrough for the organic electronics.

### **Acknowledgements**

This research was supported by, or supported in part by, the U.S. Army through the Institute for Soldier Nanotechnologies, under Contract DAAD-19-02-D-0002 with the U.S. Army Research Office. The authors thank Mr. Sunyoung Lee for the measurement of UV-Vis spectroscopy. The content does not necessarily reflect the position of the Government, and no official endorsement should be inferred.

### **References**

---

1. Groenendaal, B.L.; Jonas, F.; Freitag, D.; Pielartzik, H.; Reynolds, J.R. Poly(3,4-ethylenedioxythiophene) and its derivatives: Past, present, and future. *Advanced Materials* **2000** *12*, 481-494.
2. Kirchmeyer, S.; Reuter, K. Scientific importance, properties and growing applications of poly(3,4-ethylenedioxythiophene). *J Mater Chem* **2005** *15*, 2077-2088.
3. Jonas, F.; Morrison, J.T. 3,4-polyethylenedioxythiophene (PEDT): Conductive coatings technical applications and properties. *Synthetic Metals* **1997** *85*, 1397-1398.
4. Bredas, J.L.; Silbey, R.J. Conjugated Polymers: The novel science and technology of highly conducting and nonlinear optically active materials; Kluwer Academic Publishers: Dordrecht ; Boston, 1991;xviii, 624 p.
5. Yamato, H.; Kai, K.; Ohwa, M.; Asakura, T.; Koshiya, T.; Wernet, W. Synthesis of free-standing poly(3,4-ethylenedioxythiophene) conducting polymer films on a pilot scale. *Synthetic Metals* **1996** *83*, 125-130.
6. Groenendaal, L.; Zotti, G.; Aubert, P.H.; Waybright, S.M.; Reynolds, J.R. Electrochemistry of poly(3,4-alkylenedioxythiophene) derivatives. *Advanced Materials* **2003** *15*, 855-879.
7. Kim, J.; Kim, E.; Won, Y.; Lee, H.; Suh, K. The preparation and characteristics of conductive poly(3,4-ethylenedioxythiophene) thin film by vapor-phase polymerization. *Synthetic Metals* **2003** *139*, 485-489.

8. Ha, Y.H.; Nikolov, N.; Pollack, S.K.; Mastrangelo, J.; Martin, B.D.; Shashidhar, R. Towards a transparent, highly conductive poly(3,4-ethylenedioxythiophene). *Advanced Functional Materials* **2004** *14*, 615-622.
9. Winther-Jensen, B.; Breiby, D.W.; West, K. Base inhibited oxidative polymerization of 3,4-ethylenedioxythiophene with iron(III)tosylate. *Synthetic Metals* **2005** *152*, 1-4.
10. Jonas, F.; Heywang, G. Technical Applications for Conductive Polymers. *Electrochimica Acta* **1994** *39*, 1345-1347.
11. Jonas, F.; Krafft, W.; Muys, B. Poly(3,4-Ethylenedioxythiophene) - Conductive Coatings, Technical Applications and Properties. *Macromolecular Symposia* **1995** *100*, 169-173.
12. Kobayashi, H.; Kanbe, S.; Seki, S.; Kiguchi, H.; Kimura, M.; Yudasaka, I.; Miyashita, S.; Shimoda, T.; Towns, C.R.; Burroughes, J.H. et al. A novel RGB multicolor light-emitting polymer display. *Synthetic Metals* **2000** *111*, 125-128.
13. Lock, J.P.; Im, S.G.; Gleason, K.K. Oxidative chemical vapor deposition of electrically conducting poly(3,4-ethylenedioxythiophene) films. *Macromolecules* **2006** *39*, 5326-5329.
14. Winther-Jensen, B.; West, K. Vapor-phase polymerization of 3,4-ethylenedioxythiophene: A route to highly conducting polymer surface layers. *Macromolecules* **2004** *37*, 4538-4543.
15. Meng, H.; Perepichka, D.F.; Bendikov, M.; Wudl, F.; Pan, G.Z.; Yu, W.J.; Dong, W.J.; Brown, S. Solid-state synthesis of a conducting polythiophene via an

- unprecedented heterocyclic coupling reaction. *Journal of the American Chemical Society* **2003** *125*, 15151-15162.
16. Sotzing, G.A.; Briglin, S.M.; Grubbs, R.H.; Lewis, N.S. Preparation and properties of vapor detector arrays formed from poly(3,4 ethylenedioxy)thiophene-poly(styrene sulfonate)/insulating polymer composites. *Analytical Chemistry* **2000** *72*, 3181-3190.
  17. Ouyang, J.; Chu, C.W.; Chen, F.C.; Xu, Q.F.; Yang, Y. Polymer optoelectronic devices with high-conductivity poly(3,4-ethylenedioxythiophene) anodes. *Journal of Macromolecular Science-Pure and Applied Chemistry* **2004** *A41*, 1497-1511.
  18. Ouyang, J.; Xu, Q.F.; Chu, C.W.; Yang, Y.; Li, G.; Shinar, J. On the mechanism of conductivity enhancement in poly (3,4-ethylenedioxythiophene): poly(styrene sulfonate) film through solvent treatment. *Polymer* **2004** *45*, 8443-8450.
  19. Kim, J.Y.; Jung, J.H.; Lee, D.E.; Joo, J. Enhancement of electrical conductivity of poly(3,4-ethylenedioxythiophene)/poly(4-styrenesulfonate) by a change of solvents. *Synthetic Metals* **2002** *126*, 311-316.
  20. Groenendaal, L.; Zotti, G.; Jonas, F. Optical, conductive and magnetic properties of electrochemically prepared alkylated poly(3,4-ethylenedioxythiophene)s. *Synthetic Metals* **2001** *118*, 105-109.
  21. Zhang, F.; Petr, A.; Peisert, H.; Knupfer, M.; Dunsch, L. Electrochemical variation of the energy level of poly(3,4-ethylenedioxythiophene): poly(styrenesulfonate). *Journal of Physical Chemistry B* **2004** *108*, 17301-17305.

22. Johansson, T.; Pettersson, L.A.A.; Inganas, O. Conductivity of de-doped poly(3,4-ethylenedioxythiophene). *Synthetic Metals* **2002** *129*, 269-274.
23. Im, S.G.; Olivetti, E.A.; Gleason, K.K. Doping level and work function control in oxidative chemical vapor deposited poly (3,4-ethylenedioxythiophene). *Applied Physics Letters* **2007** *90*, 152112.
24. Sadki, S.; Schottland, P.; Brodie, N.; Sabouraud, G. The mechanisms of pyrrole electropolymerization. *Chemical Society Reviews* **2000** *29*, 283-293.
25. Garreau, S.; Louarn, G.; Buisson, J.P.; Froyer, G.; Lefrant, S. In situ spectroelectrochemical Raman studies of poly(3,4-ethylenedioxythiophene) (PEDT). *Macromolecules* **1999** *32*, 6807-6812.
26. Harima, Y.; Jiang, X.Q.; Kunugi, Y.; Yamashita, K.; Naka, A.; Lee, K.K.; Ishikawa, M. Influence of pi-conjugation length on mobilities of charge carriers in conducting polymers. *Journal of Materials Chemistry* **2003** *13*, 1298-1305.
27. Meisel, K.D.; Vocks, H.; Bobbert, P.A. Polarons in semiconducting polymers: Study within an extended Holstein model. *Physical Review B* **2005** *71*.
28. Chandrasekhar, P. Conducting polymers, fundamentals and applications : a practical approach; Kluwer Academic, 1999;Chapter 2, p23-41.
29. Apperloo, J.J.; Groenendaal, L.; Verheyen, H.; Jayakannan, M.; Janssen, R.A.J.; Dkhissi, A.; Beljonne, D.; Lazzaroni, R.; Bredas, J.L. Optical and redox properties of a series of 3,4-ethylenedioxythiophene oligomers. *Chemistry-a European Journal* **2002** *8*, 2384-2396.

30. Kiebooms, R.; Aleshin, A.; Hutchison, K.; Wudl, F. Thermal and electromagnetic behavior of doped poly(3,4-ethylenedioxythiophene) films. *Journal of Physical Chemistry B* **1997** *101*, 11037-11039.
31. Aleman, C.; Armelin, E.; Iribarren, J.I.; Liesa, F.; Laso, M.; Casanovas, J. Structural and electronic properties of 3,4-ethylenedioxythiophene, 3,4-ethylenedisulfanylfurane and thiophene oligomers: A theoretical investigation. *Synthetic Metals* **2005** *149*, 151-156.
32. Skotheim, T.A.; Elsenbaumer, R.L.; Reynolds, J.R. Handbook of conducting polymers; M. Dekker: New York, 1998;xiii, 1097 p.
33. Tran-Van, F.; Garreau, S.; Louarn, G.; Froyer, G.; Chevrot, C. Fully undoped and soluble oligo(3,4-ethylenedioxythiophene)s: spectroscopic study and electrochemical characterization. *Journal of Materials Chemistry* **2001** *11*, 1378-1382.
34. Yamamoto, T.; Abla, M. Synthesis of non-doped poly(3,4-ethylenedioxythiophene) and its spectroscopic data. *Synthetic Metals* **1999** *100*, 237-239.
35. Chiu, W.W.; Travas-Sejdic, J.; Cooney, R.P.; Bowmaker, G.A. Spectroscopic and conductivity studies of doping in chemically synthesized poly(3,4-ethylenedioxythiophene). *Synthetic Metals* **2005** *155*, 80-88.
36. Levenspiel, O. Chemical reaction engineering; New York : Wiley, 1999.
37. Lee, K.; Cho, S.; Park, S.H.; Heeger, A.J.; Lee, C.W.; Lee, S.H. Metallic transport in polyaniline. *Nature* **2006** *441*, 65-68.

38. Prigodin, V.N.; Epstein, A.J. Quantum hopping in metallic polymers. *Physica B-Condensed Matter* **2003** 338, 310-317.
39. Li, Z.F.; Ruckenstein, E. Patterned conductive polyaniline on Si(100) surface via self-assembly and graft polymerization. *Macromolecules* **2002** 35, 9506-9512.
40. Ruckenstein, E.; Li, Z.F. Surface modification and functionalization through the self-assembled monolayer and graft polymerization. *Advances in Colloid and Interface Science* **2005** 113, 43-63.
41. Moore, W.J. *Physical Chemistry*; McGraw-Hill: Boston, 1972.
42. Koch, N.; Elschner, A.; Schwartz, J.; Kahn, A. Organic molecular films on gold versus conducting polymer: Influence of injection barrier height and morphology on current-voltage characteristics. *Applied Physics Letters* **2003** 82, 2281-2283.
43. Koch, N.; Kahn, A.; Ghijsen, J.; Pireaux, J.J.; Schwartz, J.; Johnson, R.L.; Elschner, A. Conjugated organic molecules on metal versus polymer electrodes: Demonstration of a key energy level alignment mechanism. *Applied Physics Letters* **2003** 82, 70-72.
44. Lee, K.S.; Blanchet, G.B.; Gao, F.; Loo, Y.L. Direct patterning of conductive water-soluble polyaniline for thin-film organic electronics. *Applied Physics Letters* **2005** 86.
45. Moller, S.; Perlov, C.; Jackson, W.; Taussig, C.; Forrest, S.R. A polymer/semiconductor write-once read-many-times memory. *Nature* **2003** 426, 166-169.

# **Chapter Three**

## **DOPING LEVEL AND WORK FUNCTION CONTROL IN OXIDATIVE CHEMICAL VAPOR DEPOSITED (OCVD) POLY (3, 4- ETHYLENEDIOXYTHIOPHENE)**

**Sung Gap Im**, Karen K. Gleason, and Elsa A. Olivetti, 'Doping level and work function control in oxidative chemical vapor deposited poly (3,4-ethylenedioxythiophene)', *Applied Physics Letters* 90(2007) 152112



## **Abstract**

Control over doping level and work function is achieved for Poly(3,4-ethylenedioxythiophene) (PEDOT) films deposited by oxidative chemical vapor deposition (oCVD). Surface analysis reveals the equivalence of the surface and bulk compositions for the oCVD films. The oCVD PEDOT polymer chains doped solely with Cl<sup>-</sup> ions. By increasing the substrate temperature used for deposition, the doping level was monotonically increased from 17 to 33 at. %, resulting in a corresponding ability to tune the work function from 5.1 to 5.4 eV. The controllability of doping level and work function of oCVD PEDOT offers great potential advantages for organic devices.

**Key words:** oxidative chemical vapor deposition (oCVD), poly 3,4 ethylenedioxythiophene (PEDOT), X-ray photoelectron spectroscopy (XPS), scanning transmission electron microscopy (STEM), work function, substrate temperature, doping level.

### 3.1 Introduction

Poly(3,4-ethylenedioxythiophene) (PEDOT) is one of the most promising conjugated polymers, possessing high electrical conductivity, good optical transparency, and chemical stability<sup>1</sup>. PEDOT films can be applied by a variety of methods, and the aqueous suspension of PEDOT with poly(styrenesulfonate) (PSS) makes solution processing possible<sup>1</sup>. Indeed most organic device applications have been fabricated with PEDOT:PSS. Some limitations of the solution processing are that a) hydrophilic surface treatment of substrate is critical to obtain uniform films<sup>2</sup>, b) metallic ionic impurities are detrimental to device performance<sup>3</sup>, and c) the excess PSS in PEDOT:PSS system leads to corrosion<sup>4, 5</sup>. Indeed, XPS studies show that PSS segregates to the surface which may induce interfacial degradation in devices<sup>6</sup>. Low conductivity also limits the PEDOT:PSS film from practical applications, such as conducting electrodes<sup>7, 8</sup>. The conductivity of PEDOT:PSS film can be increased by treating with ethylene glycol or sorbitol but still the mechanism of conductivity enhancement is controversial<sup>7, 8</sup>.

PEDOT:PSS has been widely used as a hole injecting layer (HIL) in oLEDs<sup>3</sup>. The efficiency of hole injection depends critically upon the work function of the HIL layer<sup>9</sup>. Numerous empirical methods have been developed for altering work function. Electrochemical doping – dedoping treatments have achieved modulation of the work function in both PEDOT:PSS<sup>10</sup> and in electrochemically deposited PEDOT<sup>11</sup>. Chemical acid and/or base treatment also produce changes in the work function of PEDOT:PSS<sup>3</sup>. Metal ion concentration, pH<sup>12</sup>, and post heat-treatment<sup>9</sup> have also been shown to influence work function. Recently, the formation of PEDOT films via oxidative chemical vapor

deposition (oCVD) technology was reported. The oCVD vacuum process formed highly conductive and optically transparent PEDOT films<sup>13</sup>. The inherently conformal nature of coating makes oCVD PEDOT suitable for substrates with high surface area without damaging the substrate structure. Moreover, by controlling the substrate temperature of the oCVD process, the electrical conductivity and conjugation length of the resultant PEDOT film were systemically controlled with ease<sup>13</sup>. The systematic variation in chemical structure of the oCVD films presents an opportunity to perform research that will enhance the fundamental understanding of structure-property relationships in conducting polymers.

In this study, X-ray photoelectron spectroscopy (XPS), scanning transmission electron microscopy (STEM) with energy dispersive X-ray analysis (EDX), and photoelectron spectroscopy (PES) were used to determine the chemical and electrical properties of a series PEDOT films systematically prepared by varying only the substrate temperature of the oCVD process.

### **3.2 Experimental**

The oCVD reactor for PEDOT has been described in detail elsewhere<sup>13</sup>. All the chemicals were purchased from Sigma-Aldrich and used without further purification. To create a series of samples, the substrate temperature was systematically incremented over the range from 15 to 100 °C. For all depositions, the vacuum level was controlled at 150 mTorr and 3,4-ethylenedioxythiophene (EDOT) was introduced into the chamber at 3 sccm, sublimated Fe(III)Cl<sub>3</sub> was used as oxidizing agent, the process time was 30 minutes. The as-deposited film was subsequently annealed in dry oven at 70 °C for two hours and rinsed

with copious methanol to remove any unreacted oxidant and oxidation byproducts. XPS was done on a Kratos Axis Ultra spectrometer equipped with a monochromatized Al K $\alpha$  source. STEM (VGHB603 STEM) was performed on cryomicrotomed samples, using an Oxford EDX detector and Inca Vision software for elemental analysis. The work function of oCVD PEDOT was also monitored with a surface analyzer using Riken-Keiki AC-2<sup>14</sup>. The measurements were performed at room temperature with nitrogen purge. The measured work function was calibrated by measuring the ionization potential of *N,N'*-(di-naphthalene-1-yl)-*N,N'*-diphenyl-benzidine (NPB) and compared with the reference value of 5.4 eV<sup>15</sup>.

### 3.3 Results and Discussion

Fig. 3-1(a) shows the XPS survey scan of oCVD PEDOT deposited at substrate temperature of 15 °C. The C, O, and S are the characteristic elements of the PEDOT polymer while Cl represents the dopant ions. Significantly, Fe was not detected at the surface indicating that reaction byproducts from Fe(III)Cl<sub>3</sub> oxidant were completely removed by the rinsing step allowing a pure PEDOT:Cl surface to be obtained. XPS survey scans of the samples deposited at higher temperature (not shown) also detected only C, S, and O and no Fe. The XPS clearly shows that surface consists of pure, conductive PEDOT doped with Cl<sup>-</sup> ions without any phase segregation. In contrast, in PEDOT:PSS, the phase segregation occurs between and PEDOT and PSS phase and corrosive PSS-rich (78 atomic %) phase is dominant at the surface of PEDOT:PSS<sup>6</sup>.

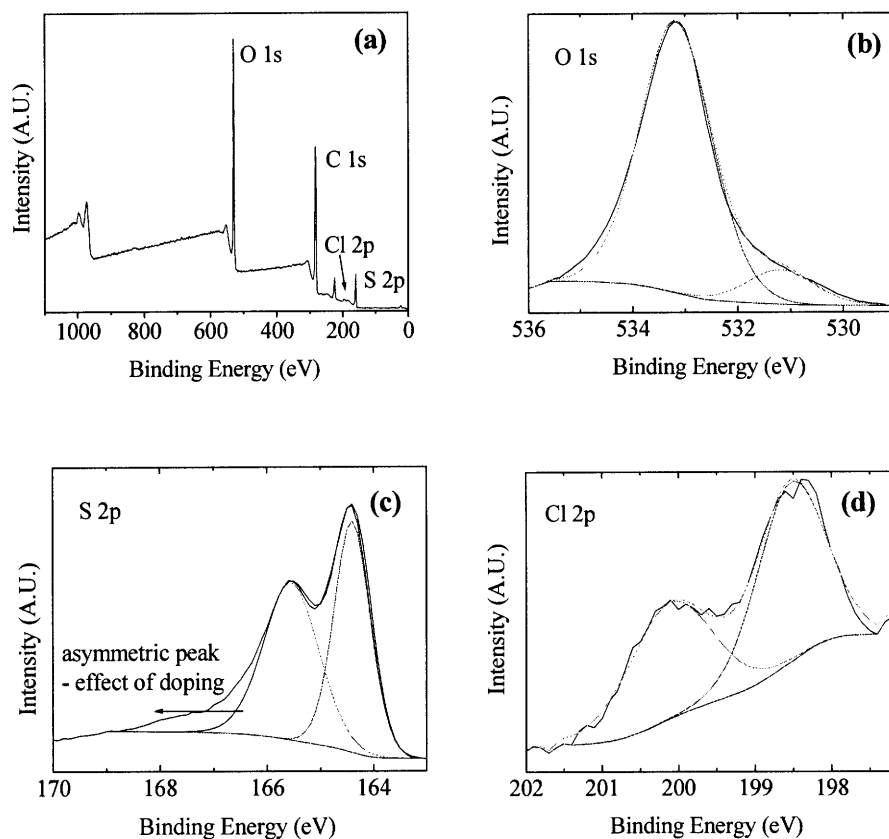


Figure 3-1 (a) XPS survey scan of oCVD PEDOT deposited at a substrate temperature of 15 °C; (b) high resolution XPS spectrum of (b) O 1s; (c) S 2p; and (d) Cl 2p.

The O 1s (b), S 2p (c), and Cl 2p (d) core-level high resolution XPS spectra of oCVD PEDOT deposited at the substrate temperature of 100 °C are also shown in Fig. 3-1. The XPS spectra of PEDOT deposited at the other substrate temperatures (not shown) showed all of the same major peaks. In O 1s core-level XPS spectrum (Fig. 3-1(b)), the dominant peak at 533.2 eV corresponds to the sole oxygen bonding environment in PEDOT while a small broad shoulder most likely results from residual rinsing solvent (methanol) or

moisture adsorption<sup>6</sup>. The S 2p core-level high resolution XPS spectrum (Fig. 3-1(c)) corresponds to single sulfur bonding environment in PEDOT with a spin-split doublet, S 2p<sub>1/2</sub> and S 2p<sub>3/2</sub> with an 1.18 eV energy splitting<sup>6, 16</sup>. The asymmetric tail to higher binding energy is related with the doping process<sup>6</sup>, in which the delocalized  $\pi$ -electrons in thiophene ring broaden the binding energy spectrum of the S atom. The Cl 2p core-level high resolution XPS spectrum (Fig. 3-1(d)) also reveals a single chemical species of Cl, which has a spin-split doublet, Cl 2p<sub>1/2</sub> and Cl 2p<sub>3/2</sub> having an 1.60 eV energy splitting<sup>16</sup>. Previous study of oxidatively synthesized PEDOT film with Fe(III)Cl<sub>3</sub> oxidizing agent has reported that the possible dopants of PEDOT is FeCl<sub>4</sub><sup>-</sup> or simple Cl<sup>-</sup> ion<sup>17</sup>. From both wide scan and Cl 2p core-level XPS spectrum, the possibility of FeCl<sub>4</sub><sup>-</sup> dopants can be clearly excluded. Therefore it can be concluded that the surface consist only of PEDOT chains doped solely with Cl<sup>-</sup> ion.

The cross-sectional STEM image in Fig. 3-2(a) shows a 200 nm thick oCVD PEDOT film (deposited on a rubbery block copolymer) having a conductivity of ~300 S/cm. An EDX scan of the red line in Fig. 3-2(a) is given as chemical profile information in Fig. 3-2(b). This line scan, performed after rinsing, shows a sharp decrease of S and Cl at the interface between the PEDOT film and polymer substrate. The observation of Cl in the post-rinsed films indicates that it is mostly likely present in the form of Cl<sup>-</sup> ions with strong electrostatic attraction to the PEDOT polymer. Additionally, the level of Fe detected in the PEDOT layer was negligible (< 4 counts) and indistinguishable from the level detected in the substrate, confirming that the majority of Fe from oxidizing agent is removed. Thus, the cross-sectional STEM analyses are fully consistent with the surface analysis observation.

From the combined result of STEM and XPS, we can conclude that the oCVD PEDOT film is uniform throughout its thickness and doped solely with Cl<sup>-</sup> ions.

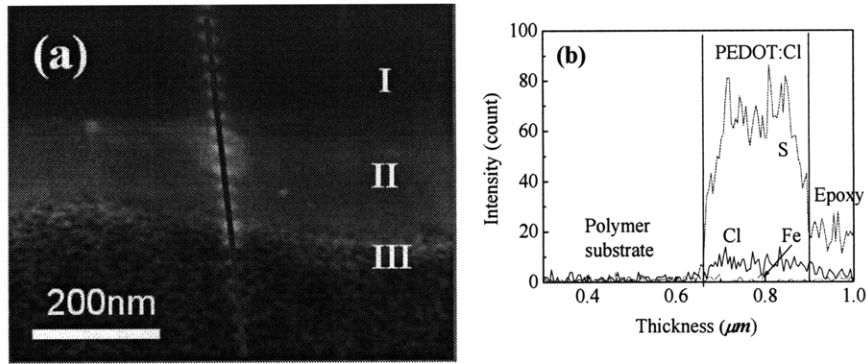


Figure 3-2 (a) STEM cross-sectional image of oCVD PEDOT. I corresponds to epoxy, II corresponds PEDOT layer, and III represents polymer substrate; (b) EDX scan data according to the red line.

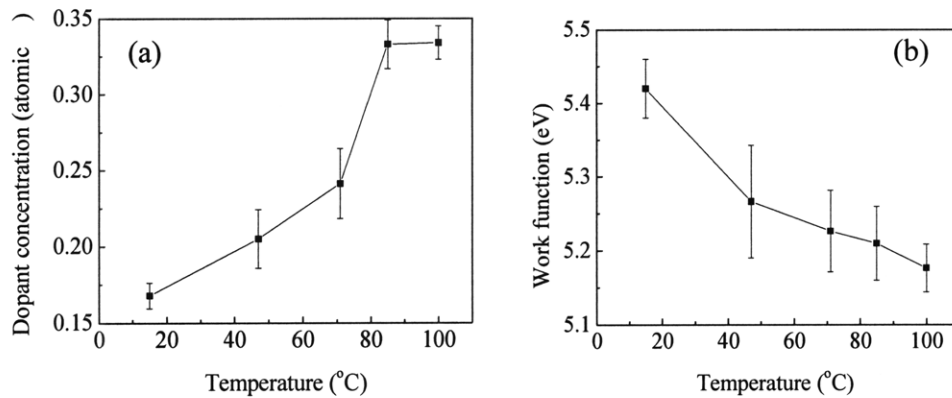


Figure 3-3. Effect of the oCVD PEDOT deposition temperature on (a) doping level and (b) work function.

The measured work function of oCVD PEDOT (Fig. 3-3(b)) decreases monotonically with increasing oCVD deposition temperature. Previously, increasing

substrate temperature was demonstrated to result in the longer conjugation length and higher dopant concentrations in oCVD PEDOT<sup>13</sup>. Fig. 3-3 demonstrates that higher dopant concentration produced at higher substrate temperatures introduce new electronic states in the otherwise forbidden energy gap which induce the movement of Fermi energy level<sup>19</sup>, leading to a decrease in work function. This observation is in good agreement with previous reports that increasing of doping level decreases work function<sup>3,9</sup>. From oCVD process, the systematic control over the work function is obtained without the need for post-processing. While doping by electrochemical and chemical methods is reversible<sup>10, 11</sup>, the control achieved by oCVD has a permanent upper bound imposed by the maximum achievable conjugation length. The ability to tune the work function of PEDOT over the range from 5.1 to 5.4 eV has technological importance for achieving balanced charge injection into organic devices<sup>3</sup>. In particular, the ionization potential of NPB is estimated to be 5.4 eV, and thus giving a very small barrier height between oCVD PEDOT and NPB which is desired for an ohmic contact.

### **3.4 Conclusion and outlook**

In summary, we have demonstrated with XPS that the surface of oCVD PEDOT consist purely of PEDOT doped with Cl<sup>-</sup> ions. Uniform composition was maintained uniformly throughout the entire thickness of bulk film and its surface. The EDX demonstrates that the oCVD film forms an abrupt interface with the substrate. Unlike PEDOT:PSS where excess dopant is observed to segregate to the surface, dopant segregation was not observed in the oCVD PEDOT films, creating an enormous potential



benefit for producing organic device with superior interfaces.. The elimination of the PSS dopant enhances conductivity. Indeed, the maximum conductivity for current series of oCVD was 348 S/cm. In addition, the dopant concentration of oCVD films can be systemically controlled from 16 atomic to 33 atomic by changing only substrate temperature employed for film growth, and thus the work function of the final material can also be precisely tuned over the range 5.1 eV to 5.4 eV. Tuning the work function over this range is anticipated to facilitate the formation of ohmic contacts in organic devices.

### **Acknowledgements**

This research was supported by, or supported in part by, the U.S. Army through the Institute for Soldier Nanotechnologies, under Contract DAAD-19-02-D-0002 with the U.S. Army Research Office. The authors thank Anthony Garrett-Reed for the STEM measurement. The authors thank LG Chemicals Ltd. for the measurement of work function.

### **References**

- 
1. Kirchmeyer, S.; Reuter, K. Scientific importance, properties and growing applications of poly(3,4-ethylenedioxythiophene). *J Mater Chem* **2005** *15*, 2077-2088.

2. Kawase, T.; Sirringhaus, H.; Friend, R.H.; Shimoda, T. Inkjet printed via-hole interconnections and resistors for all-polymer transistor circuits. *Advanced Materials* **2001** *13*, 1601-+.
3. Ho, P.K.H.; Kim, J.S.; Burroughes, J.H.; Becker, H.; Li, S.F.Y.; Brown, T.M.; Cacialli, F.; Friend, R.H. Molecular-scale interface engineering for polymer light-emitting diodes. *Nature* **2000** *404*, 481-484.
4. de Jong, M.P.; van Ijzendoorn, L.J.; de Voigt, M.J.A. Stability of the interface between indium-tin-oxide and poly(3,4-ethylenedioxythiophene)/poly(styrenesulfonate) in polymer light-emitting diodes. *Applied Physics Letters* **2000** *77*, 2255-2257.
5. Kim, W.H.; Makinen, A.J.; Nikolov, N.; Shashidhar, R.; Kim, H.; Kafafi, Z.H. Molecular organic light-emitting diodes using highly conducting polymers as anodes. *Applied Physics Letters* **2002** *80*, 3844-3846.
6. Greczynski, G.; Kugler, T.; Keil, M.; Osikowicz, W.; Fahlman, M.; Salaneck, W.R. Photoelectron spectroscopy of thin films of PEDOT-PSS conjugated polymer blend: A mini-review and some new results. *Journal of Electron Spectroscopy and Related Phenomena* **2001** *121*, 1-17.
7. Ouyang, J.; Xu, Q.F.; Chu, C.W.; Yang, Y.; Li, G.; Shinar, J. On the mechanism of conductivity enhancement in poly (3,4-ethylenedioxythiophene): poly(styrene sulfonate) film through solvent treatment. *Polymer* **2004** *45*, 8443-8450.

8. Kim, J.Y.; Jung, J.H.; Lee, D.E.; Joo, J. Enhancement of electrical conductivity of poly(3,4-ethylenedioxythiophene)/poly(4-styrenesulfonate) by a change of solvents. *Synthetic Metals* **2002** *126*, 311-316.
9. Huang, J.S.; Miller, P.F.; Wilson, J.S.; de Mello, A.J.; de Mello, J.C.; Bradley, D.D.C. Investigation of the effects of doping and post-deposition treatments on the conductivity, morphology, and work function of poly (3,4-ethylenedioxythiophene)/poly (styrene sulfonate) films. *Advanced Functional Materials* **2005** *15*, 290-296.
10. Zhang, F.; Petr, A.; Peisert, H.; Knupfer, M.; Dunsch, L. Electrochemical variation of the energy level of poly(3,4-ethylenedioxythiophene): poly(styrenesulfonate). *Journal of Physical Chemistry B* **2004** *108*, 17301-17305.
11. Frohne, H.; Shaheen, S.E.; Brabec, C.J.; Muller, D.C.; Sariciftci, N.S.; Meerholz, K. Influence of the anodic work function on the performance of organic solar cells. *Chemphyschem* **2002** *3*, 795-+.
12. de Kok, M.M.; Buechel, M.; Vulto, S.I.E.; van de Weijer, P.; Meulenkaamp, E.A.; de Winter, S.; Mank, A.J.G.; Vorstenbosch, H.J.M.; Weijtens, C.H.L.; van Elsbergen, V. Modification of PEDOT: PSS as hole injection layer in polymer LEDs. *Physica Status Solidi a-Applied Research* **2004** *201*, 1342-1359.
13. Lock, J.P.; Im, S.G.; Gleason, K.K. Oxidative chemical vapor deposition of electrically conducting poly(3,4-ethylenedioxythiophene) films. *Macromolecules* **2006** *39*, 5326-5329.

14. Hwang, D.H.; Lee, J.I.; Cho, N.S.; Shim, H.K. Light-emitting properties of a germlyl-substituted PPV derivative synthesized via a soluble precursor. *Journal of Materials Chemistry* **2004** *14*, 1026-1030.
15. Lee, S.T.; Wang, Y.M.; Hou, X.Y.; Tang, C.W. Interfacial electronic structures in an organic light-emitting diode. *Applied Physics Letters* **1999** *74*, 670-672.
16. Moulder, J.F.; Stickle, W.F.; Sobol, P.E.; Bomben, K.D. Handbook of X-ray Photoelectron Spectroscopy; Chastain, J. & Jr., R.C.K.: Eden Prairie, MN, 1995.
17. Yamamoto, T.; Abla, M. Synthesis of non-doped poly(3,4-ethylenedioxythiophene) and its spectroscopic data. *Synthetic Metals* **1999** *100*, 237-239.
18. Aleshin, A.; Kiebooms, R.; Menon, R.; Wudl, F.; Heeger, A.J. Metallic conductivity at low temperatures in poly(3,4-ethylenedioxythiophene) doped with PF6. *Physical Review B* **1997** *56*, 3659-3663.
19. Logdlund, M.; Lazzaroni, R.; Stafstrom, S.; Salaneck, W.R.; Bredas, J.L. Direct Observation of Charge-Induced Pi-Electronic Structural-Changes in a Conjugated Polymer. *Physical Review Letters* **1989** *63*, 1841-1844.

## **Chapter Four**

### **GRAFTED CONDUCTING POLYMER FILMS FOR NANO-PATTERNING ONTO VARIOUS ORGANIC AND INORGANIC SUBSTRATES BY OXIDATIVE CHEMICAL VAPOR DEPOSITION**

**Sung Gap Im**, Pil J. Yoo, Paula T. Hammond, and Karen K. Gleason, 'Grafted conducting polymer films for nano-patterning onto various organic and inorganic substrates by oxidative chemical vapor deposition', *Advanced Materials*, 19(2007) 2863-2867

## **Abstract**

Two methods are demonstrated for grafting conducting polymer film on various organic and inorganic substrates. Both methods provide an enormous increase in adhesion strength between the films and their substrates. While ungrafted conducting polymer films delaminate after only minutes of ultrasonic treatment, no delamination of the grafted films is observed even after three hours of ultrasonication. The first method requires only a single step and does not employ a separate linker molecule. Instead, the grafting occurs as an inherent feature of the oxidative chemical vapor deposition process, in which the propagation of the growing polymer chains proceeds directly from an activated surface site.. This one-step method allows grafting of conducting polymer films onto a host of flexible polymeric substrates in as-received form and offers the potential for low-cost mass-production. The second method extends the mechanistic concept of the first method to allow grafting of conducting polymer films onto other types of substrates, including silicon and metals. The adhesion provided by the grafting enables high resolution patterning of the conducting polymer layers by conventional subtractive pattern methods. Well defined patterns could only be formed in the grafted conducting polymer films. Features as small as 160 nm were achieved on flexible polyethyleneterephthalate (PET) while 80 nm features were demonstrated on silicon substrates. We utilized three different patterning processes of 1) conventional photolithography, 2) capillary force lithography, and 3) e-beam lithography.

This patterning capability made possible by grafting process can serve as an enabling technology for future integrated flexible circuitry.

**Key words:** oxidative chemical vapor deposition (oCVD), poly 3,4 ethylenedioxythiophene (PEDOT), grafting, Friedel-Craft Catalyst, patterning, silane treatment.

## 4.1 Introduction

Historically, integrated circuits have been flat and rigid, but the current development of “flexible electronics”<sup>1-5</sup> envisions rollable displays and wearable electronics, and will revolutionize our daily lives. Thanks to the explosive improvement in the performance of devices made from organic materials in recent years<sup>2, 6</sup>, the conjugated organic materials are regarded as one of the most promising candidates for commercializable flexible electronics. Current efforts are mainly focused on increasing the performance of devices and the density of integration of the devices for high-end electronic applications<sup>4</sup>. Patterning is essential for the fabrication of the integrated circuitry. Although current lithographic techniques for inorganic semiconductor chips produce features sizes as small as a few tens of nanometers, these techniques are incompatible with organic materials<sup>7</sup>. For example, organic substrates can be damaged by wet chemical treatments and are vulnerable to mechanical stress from the patterning process. These constraints demand either the modification of photolithography<sup>7</sup> or newly devised schemes applicable to organic

materials<sup>8</sup>. However, the performance of these circumvented strategies is still far from that of current photolithographic techniques in terms of minimum feature size, reliability, and throughput of patterning<sup>9</sup>. The ability to produce dense patterns of sub-micron features over the entire area of the substrate is limited by insufficient adhesion<sup>7</sup> which results in mechanical failures, such as cracks, displacements, and delaminations.

Moreover, for maximized durability and reliability of flexible electronic devices, mechanical robustness is extremely important, requiring excellent interfacial properties and adhesion between the conductive thin film and flexible polymeric substrates<sup>10</sup>. Transparent conducting oxides (TCO) such as indium tin oxide (ITO), usually used as anode materials in organic electronics, are inherently brittle, which limits their applications in flexible electronics<sup>11</sup>. Conducting polymer films regarded as alternatives to TCO are weakly physisorbed on substrates, and are also vulnerable to the delamination from the substrates with repeated flexing<sup>12</sup>. Covalent bonding of conducting polymer films to substrates can prevent delamination. In spite of its engineering significance, only few reports address grafting of conducting polymers<sup>13, 14</sup>. Well-defined, nano-scale patterning of conducting polymers over large areas on flexible organic substrates has also been an elusive goal.

The current work demonstrates a one-step process for directly grafting conducting polymers onto flexible polymer substrates which contain aromatic groups. This process, termed oxidative chemical vapor deposition (oCVD) does not employ a linker, such as silane or thiol compounds, but relies on covalent bonding directly between the conducting polymer film and aromatic moiety in these polymeric substrates. In this case, the only requirement is that the substrate should contain aromatic groups: no specific surface



treatment is needed. The grafting was successfully obtained on various, widely-used flexible substrates such as polystyrene (PS), polyethyleneterephthalate (PET), and polycarbonate (PC) in as-received form, which offers the possibility of mass-production of grafted flexible conducting layers at low cost. The inherently grafted poly (3,4-ethylenedioxythiophene) (PEDOT) displays greatly enhanced adhesion, thus enabling patterning down to 60 nm features on flexible PET substrates. Patterns were defined by a variety of methods including conventional photolithography, non-conventional physical molding (capillary force lithography)<sup>15</sup>, and e-beam lithography. Previously, oCVD films were demonstrated to provide conformal coverage and conductivities  $>700 \text{ S/cm}$ <sup>16-18</sup> were achieved. Obtaining high resolution features of highly, conformal, conducting polymer films on transparent plastic substrates serves as a potential breakthrough for fabrication of high-end flexible electronic devices.

## **4.2 Experiments and Characterization**

### **4.2.1 Deposition of PEDOT**

The detailed deposition procedure of oxidative chemical vapor deposition (oCVD) was published elsewhere<sup>18</sup>.  $\text{FeCl}_3$  is used as the oxidizing agent for polymerizing the monomer EDOT to obtain PEDOT. The process pressure was 150 mTorr, the substrate temperature was  $70 \sim 90 \text{ }^\circ\text{C}$  and EDOT flow rate was  $4 \pm 1 \text{ sccm}$ . After 30 minutes of oCVD process,  $30 \sim 100 \text{ nm}$  thick transparent PEDOT films were obtained on polymeric and Si wafer substrates. After the deposition, the film was rinsed with either copious water or methanol. Maintaining the same process conditions except for replacing the EDOT flow

with a 15 sccm of pyrrole or 20 sccm of aniline, resulted in oCVD polypyrrole and polyaniline, respectively. All the reagents were purchased from Aldrich and used without any further purification. For ungrafted PEDOT-PS layer in Figure 4-2c, additional 150 nm-thick PS layer was spun-cast onto oCVD PEDOT (60 nm) film on Si wafer.

#### **4.2.2 Attaching the silane coupling agent for inorganic substrates**

Substrates were cleaned by a 60 s exposure to oxygen plasma (100W/cm<sup>2</sup>, 100 mTorr). Then the substrates were placed in a vacuum chamber at a gauge pressure of -15 mmHg and exposed to PTCS (Aldrich, 98 %) vapor for 5 to 10 minutes at room temperature.

#### **4.2.3 Buckling**

PS (Number average molecular weight  $MW_n = 250,000$  from ACROS) was spun-cast onto Si wafers to form 200 – 300 nm thick films. Then, PEDOT was deposited by oCVD to form PEDOT/PS bilayers. The PEDOT/PS bilayers were attached to the lid of Petri dish and exposed to THF vapor for 5 – 60 s in room temperature. In analogous fashion PEDOT/PEO bilayers were formed by growing oCVD PEDOT on top of spun cast PEO ( $MW_n=200,000$  and from ACROS) and then exposed to water vapor for 15 – 60 min in room temperature.

#### **4.2.4 Photolithography**

The detailed procedures are described elsewhere<sup>19, 20</sup>. Firstly, the photoresist (PR) OCG 825 was spin coated onto a Si wafer to form 1  $\mu\text{m}$  thick film, soft-baked at 90 °C, exposed to 365 – 405 nm UV light through a photomask and developed using OCG 934. Grafted oCVD PEDOT was grown on top of the PR-patterned Si wafer, and then the PR pattern was lifted off via ultrasonication for 5 minutes in acetone.

#### **4.2.5 Capillary force lithography<sup>15</sup>**

PS ( $MW_n=40,000$  from PolySciences) was spin-coated to form 140 nm thick film on top of oCVD PEDOT films grafted to PET substrates. Pre-patterned polyurethane mold was applied on the PS film spun on PEDOT and pressed at the temperature of 100 ~ 110 °C for 30 ~ 60 minutes to force PS siphoned into the capillary of patterned mold, formed the pattern. Oxygen plasma etching was utilized to transfer the positive tone pattern to the directly grafted PEDOT layer.

#### **4.2.6 e-beam lithography**

PMMA ( $MW_n=950,000$  from MicroChem 3.5 wt% in chlorobenzene) was spin-coated to form 200 nm thick film on top of . Negative tone patterning PMMA was obtained at a dose of 800  $\mu\text{C}/\text{cm}^2$  and developed for 60 s with 1:3 solution of isopropanol – methylisobutylketone. Oxygen plasma etching was applied utilized to transfer the pattern to the directly grafted PEDOT layer.

#### 4.2.7 Analysis

Film thicknesses were measured on a Tencor P-10 profilometer. Conductivity measurements were done with a four point probe (Model MWP-6, Jandel Engineering, Ltd). Tape test was performed according to the standard test method (ASTM D3359-97)<sup>21</sup>. FTIR spectra were obtained via Nexus 870, Thermo Electron Corporation. Ultrasonication of PEDOT film was performed in pure water for 15 to 180 minutes by a 100 W ultrasonicator (Cole-Parmer, Model 8891R). The surface morphology and surface damage, such as delamination, buckling, and cracking of PEDOT film was examined by optical microscopy (Olympus, Model CX41) with the maximum magnification of X1000. Wrinkled surfaces of PEDOT/PS film were monitored with AFM (Digital Instruments, Dimension 3100). Images of the PEDOT patterns were obtained with Environmental Scanning Electron Microscopy, (FEI/Philips XL30 FEG ESEM).

#### 4.3 Results and Discussion

The proposed mechanism (Fig. 4-1a) for grafting PEDOT was inspired by Kovacic's report<sup>22</sup> that benzene could be polymerized to form doped polyphenylene using Friedel-Craft catalysts, such as  $\text{AlCl}_3$ ,  $\text{CuCl}_2$ ,  $\text{FeCl}_3$ , and  $\text{MoCl}_5$ <sup>22</sup>. The Friedel-Craft catalysts facilitate the formation of radical cations from benzene, toluene, chlorobenzene, phenol, biphenyl, and naphthalene<sup>22</sup>. The Kovacic mechanism has striking similarities with the proposed mechanisms for oxidative polymerization of other conjugated polymers (Fig. 4-1b) including polypyrrole<sup>23</sup>, polythiophene<sup>18, 24, 25</sup> and PEDOT<sup>18, 26</sup>. The main difference

is the choice of the aromatic monomer. The current work rests on the hypothesis that Kovacic's mechanism is also extensible to solid surfaces containing aromatic rings (Fig. 4-1c). If the conditions used to create radical cations from the monomers simultaneously produce radical cations on the substrate, the reaction of these two species by the mechanism shown in Fig. 4-1c would result in covalent grafting. This attachment scheme forms bonds directly between the substrates containing aromatic rings and the monomer units of the growing conductive polymers without employing any additional linker molecules. The same conditions that give rise to grafting will result in continued propagation of the covalent polymer chain through oxidative polymerization. Both grafting and growth occur in a single synthetic step. In support of this hypothesis, the same conductivity is measured for oCVD films grown on substrates containing aromatic groups (grafted) and on substrates on which no grafting occurs, indicating negligible impact of the grafted layer on electronic properties. Post-deposition rinsing with methanol yields oCVD PEDOT films having negligible Friedel-Craft catalyst incorporation<sup>17</sup>.

Fourier transformed infrared (FTIR) spectroscopic analysis (Fig. 4-2) supports the hypothesis of grafting between an oCVD PEDOT film and a PS substrate. The shaded band centered at  $\sim 3000\text{ cm}^{-1}$  of highlights peaks observed in pure PS (Fig. 4-2a) are absent in pure PEDOT (Fig. 4-2b). A PS film spun on PEDOT film (termed as PS-on-PEDOT) and oCVD PEDOT deposited on PS film (termed as PEDOT-on-PS) were respectively prepared. The chemical composition of the PS-on-PEDOT is the same as that of PEDOT-on-PS. However, it is hypothesized that only the PEDOT-on-PS sample has a strong chemical grafting between the layers while the PS-on-PEDOT has only a weak physical attachment.

The FTIR spectra from bilayer films of PEDOT-on-PS (Fig. 4-2c) and PS-on-PEDOT (Fig. 4-2d) peaks are essentially indistinguishable and contain representative peaks for both PS and PEDOT. However, after a 5s rinse with tetrahydrofuran (THF), a good solvent for PS, the characteristic peaks of PS in FTIR spectrum of the ungrafted PS-on-PEDOT are completely removed (Fig. 4-2e). On the other hand, the characteristic peaks of PS in the FTIR spectrum of the grafted PEDOT-on-PS (Fig. 4-2f) were detected even after a one-hour soaking in THF. Considering the high solubility of PS in THF<sup>27</sup>, the retention of PS the grafted PEDOT-on-PS after soaking in THF strongly supports the present of strong covalent bonding between PS and PEDOT.

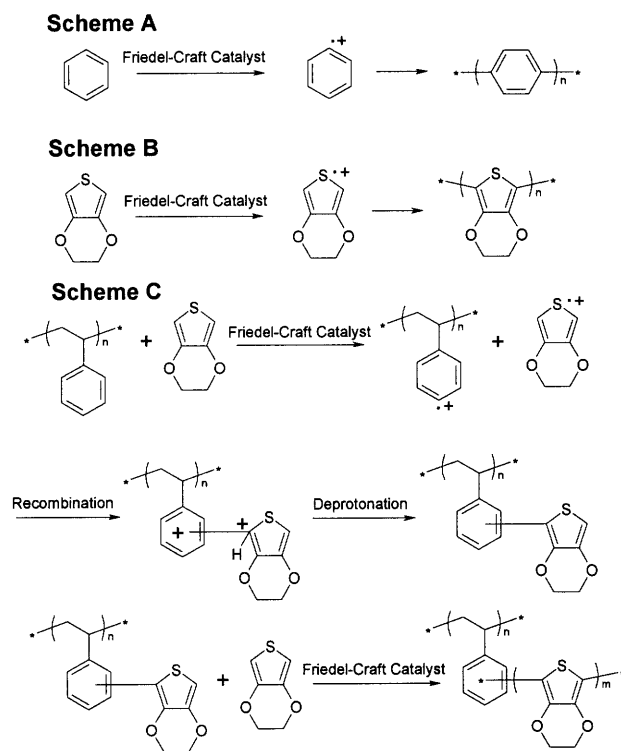


**Figure 4-1** A schematic representation of the reaction mechanism involved in grafting PEDOT films onto aromatic polymeric substrates.

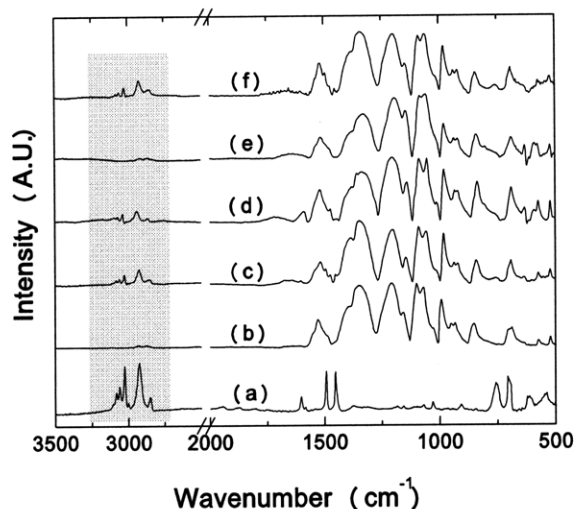


**Figure 4-2** FT-IR spectra of (a) standard PS (200 nm, MW = 250K); (b) oCVD PEDOT (60 nm); (c) ungrafted PS-on-PEDOT; (d) grafted PEDOT-on-PS; (e) ungrafted PS-on-PEDOT after 5 s of rinsing with THF; (f) grafted PEDOT-on-PS after one hour of soaking in THF.

The grafting scheme is anticipated to be universal whenever both the substrate surface and oCVD monomer can be activated with Friedel-Craft catalyst. Thus, numerous oxidatively polymerized conductive polymers have the potential to be robustly adhered to substrates containing aromatic groups or to which aromatic groups have been linked. Conversely, no improvement in the adhesion strength should be observed when the substrate is devoid of aromatic groups. Indeed, evaluation of adhesion after tape testing (ASTM D3359-97)<sup>21</sup> and ultrasonication confirms the chemical selectivity of the inherent grafting procedure towards different polymeric substrates. Figure 4-3a reveals that tape

testing resulted in no delamination of PEDOT films inherently grafted to PC. Identical results were obtained for PEDOT on PS, PET, polyethylenephthalate (PEN), polyurethane (PU), and poly(acrylonitrile-butadiene-styrene) (ABS), substrates which all contain aromatic functional groups. Additionally, strong adhesion promotion was also observed for oCVD polyaniline and polypyrrole films deposited on PET substrates. As expected for a nonaromatic substrate, severe adhesive failure (Fig. 4-3a) resulted when the same synthetic procedure and testing was carried out for PEDOT growth onto polypropylene (PP). Delamination was also observed for PEDOT on polyethylene (PE), polytetrafluoroethylene (PTFE), and polyethyleneoxide (PEO) substrates, materials containing no aromatic rings. In contrast, the full thickness of PEDOT film grafted on PET was also retained after ultrasonication in water for 3 hours. No delamination was observed and more than 90% of initial conductivity was retained after the ultrasonication. Most likely, the slight loss in conductivity results from dopant wash-out.

Enhanced adhesion was also obtained when the grafting technique was expanded to additional types of substrates by introducing linker materials containing active sites for the Friedel-Craft catalyst. For example, a linker material, phenyltrichlorosilane (PTCS)<sup>14</sup> was used to create phenyl groups covalently linked to glass surfaces. The presence of phenyl groups at the surface was confirmed by the change of static contact angle with water from less than 10° to  $65 \pm 2^\circ$  (data not shown). The resultant grafted oCVD PEDOT film survived one hour of ultrasonication (Fig. 4-3b). For substrates having bulk compositions devoid of aromatic groups, when the linker was not used, the integrity of the PEDOT film was lost during 5 min of ultrasonication (Fig. 4-3b). These observations consistently



support the hypothesis of grafting through the aromatic group of the linker. Silanes react with various inorganic substrates, including quartz, native oxide on Si wafers, aluminum, copper, stainless steel, as well as glass<sup>27</sup>. Indeed, all of above-mentioned substrates displayed a similar enhancement of adhesion strength to PEDOT when the linker was employed.

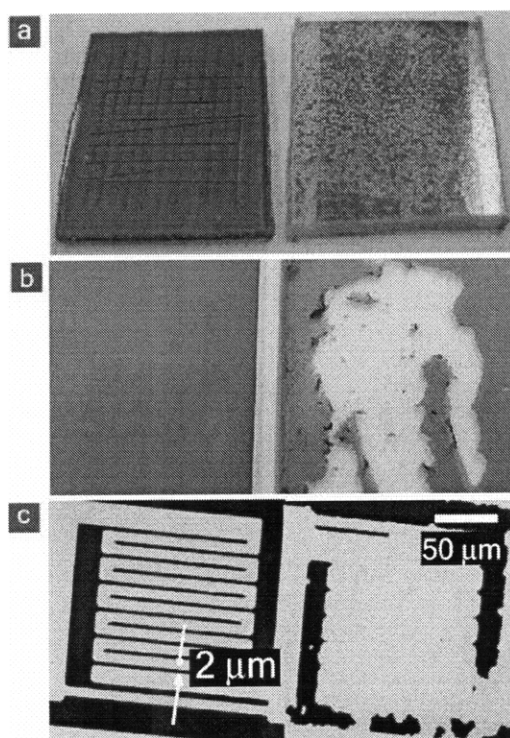


**Figure 4-3** (a) PEDOT grafted on PET (left) and PEDOT on PP, ungrafted (right) after tape testing; (b) PEDOT grafted (left) and ungrafted (right) on glass after the ultrasonication for 5 min.; (c) Conventional lift-off photolithography pattern on Si wafers with ungrafted PEDOT (left) and with grafted PEDOT (right). The scale bars represent a length of 50  $\mu\text{m}$ .

Grafting of the conducting polymer film to the substrate minimizes delamination problems during patterning as clearly demonstrated by comparing the negative tone patterns on Si for the grafted and ungrafted PEDOT. For the ungrafted case (Fig. 4-3c, right), acetone caused liftoff of smaller features. However, a well-resolved and complete pattern was successfully obtained from grafted PEDOT (Fig. 4-3c, left). In previous studies, patterning organic conducting layer were obtained through modification of the standard lithography process<sup>7</sup>. However, by grafting, well defined PEDOT patterns were easily obtained without any modification of the standard photolithographic lift-off patterning process used for common inorganic metals such as Pt, Cr, and Au<sup>19</sup>.

In order to verify the effectiveness of grafting toward enhanced adhesion of PEDOT onto the underlying polymeric layer, surface deformation induced by swelling stress was investigated. A grafted PEDOT/PS bilayer film and an ungrafted PEDOT/PEO bilayer supported on Si wafers were prepared. Upon exposure to the vapor of a selected solvent, the underlying polymeric layer became gradually swells, leading to a considerable volumetric expansion. However, the top surface of PEDOT layer can retain its intrinsic solid-like characteristics during the swelling of the underlying layer, leading to the formation of in-plane compressive stress within the bilayer films of PEDOT/polymer. Eventually, the accumulated compressive stress was released as a generation of surface wrinkles by buckling deformation<sup>28, 29</sup>.

In case of grafted PEDOT film on PS layer (Figs. 4-4a and 4-4b), gradual swelling of PS film by THF solvent could be interpreted from the uniformly generated surface wrinkles. In particular, initial emergence of periodic perturbational waves occurs when the compressive

stress exceeds the critical buckling stress. Note that the onset of buckling confirms the presence of strong binding (adhesion) between PEDOT and underlying PS layer, which causes the film to wrinkle uniformly with a specific periodicity over the entire film surface, as demonstrated through Fourier transform analysis, shown as the inserts to Figs. 4-4a and 4b. On the other hand, as shown in Figs.4-4c and 4d, swelling of non-grafted PEDOT film on PEO layer results in random deformation of surface. The absence of binding between PEDOT and PEO allows for interfacial slip and results in the non-uniform localization of swollen PEO under the PEDOT layer.

The enhanced adhesion by the grafting process can be utilized to obtain well-defined high-density patterns of conducting polymer over the entire surface of the substrate. Three different patterning processes of 1) optical patterning of conventional photolithography, 2) stamping patterning of capillary force lithography, and 3) writing patterning of e-beam lithography were utilized to pattern grafted oCVD conducting polymer films without any modification of standard patterning protocol. All of the independent patterning processes could form very well-defined patterns of PEDOT (Fig. 4-3c and 4-5). Figure 4-5 displays patterned PEDOT films grafted on a flexible transparent PET substrate. The low surface roughness of oCVD PEDOT (root mean square roughness is less than 3 nm) allows high-density patterns to be obtained from capillary force lithography<sup>15</sup>, over an area of 2 mm × 3mm with minimum feature size down to 120 nm on flexible PET substrates. A variety of patterns (Figs. 4-5b to 5d) are readily resolved on flexible polymer substrates without any notable regions of failure. Furthermore, finer feature size pattern can also be obtained via e-

beam writing lithography, and well defined 60 nm lines were successfully obtained (Fig. 4-5d) in PEDOT grafted onto flexible PET substrate.

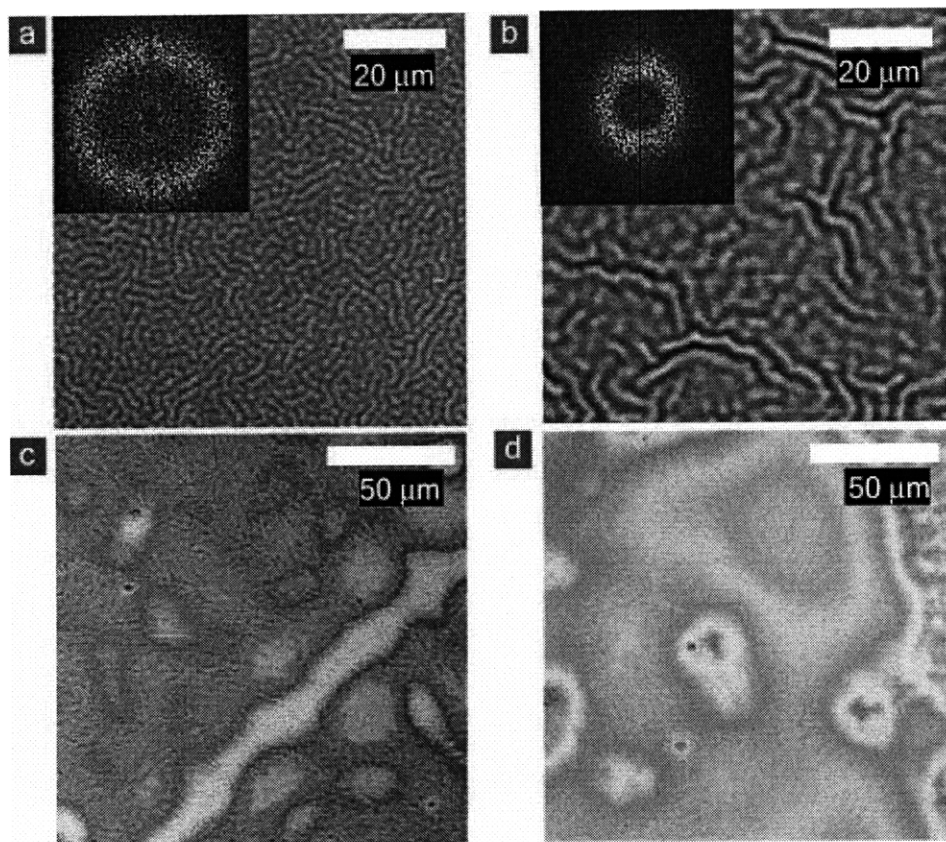


**Figure 4-4** Atomic force microscope (AFM) of PEDOT films on PS after treatment with THF vapors for (a) 5 s and (b) 15 s. Rings appearing in the corresponding fast Fourier transforms (insets) indicates that the patterns of surface wrinkles are isotropic and of single length-scale<sup>29</sup> of  $2.1 \pm 0.3 \text{ } \mu\text{m}$  and  $3.9 \pm 0.9 \text{ } \mu\text{m}$  for (a) and (b), respectively. This uniform wrinkling confirms the strong adhesion of grafted PEDOT on PS. Uniform surface wrinkling is absent in the optical microscope images of the PEDOT films on PEO after treatment with water vapor for (c) 15 min, and (d) 30 min., consistent with the lack of PEDOT grafting to the non-aromatic PEO layer.

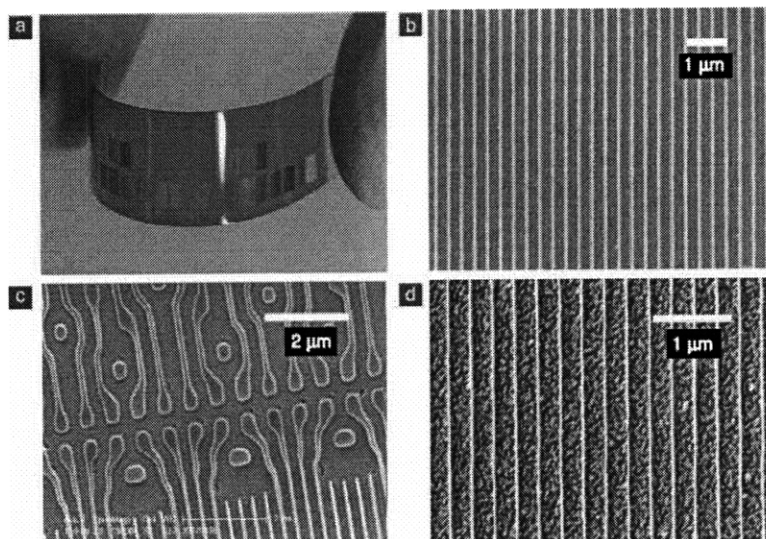


**Figure 4-5** PEDOT pattern on flexible PET substrate by capillary force lithography; (a) image of patterned PEDOT film on flexible PET substrate; (b) 120 nm line pattern; (c) complex pattern; (d) 60 nm line pattern of PEDOT film grafted on flexible PET substrate by e-beam lithography.

#### 4.4 Conclusion

In summary, grafting of conducting polymer films (PEDOT, polypyrrole, and polyaniline) on aromatic organic substrates was successfully obtained via a linker-free one-step oCVD process. This grafting scheme relies on the ability of the Friedel-Craft catalyst to form radical cations on the substrate under the conditions oCVD conducting polymer growth. The grafted film exhibited a dramatic increase in adhesion strength. By using silane coupling agents containing an aromatic ring, the grafting process can also be extended to common inorganic substrates such as aluminum and glass. With directly grafted PEDOT, 60 nm features sizes were obtained on flexible and transparent polymeric substrates. The

ability to graft conducting polymers on common substrates has the potential to revolutionize the fabrication of integrated circuitry for flexible electronics. This easy, one-step grafting process offers a wide process window and versatility in applications to various flexible substrates. In particular, this linker-free technique eliminates the tedious additional processes for grafting and opens up the possibility of mass-production of grafted flexible conducting layers at low cost.

### **Acknowledgements**

This research was supported by the U.S. Army through the Institute for Soldier Nanotechnologies, under Contract DAAD-19-02-D-0002 with the U.S. Army Research Office. The authors thank Dr. Sreeram Vaddiraju for valuable comments. The authors thank Kevin Kyungbum Ryu for photolithography. This work made use of MIT's shared scanning-electron-beam-lithography facility in the Research Laboratory of Electronics.)

### **References**

---

1. Forrest, S.R. The path to ubiquitous and low-cost organic electronic appliances on plastic. *Nature* **428**, 911-918 (2004).
2. Briseno, A.L. et al. Patterning organic single-crystal transistor arrays. *Nature* **444**, 913-917 (2006).
3. Ahn, J.H. et al. Heterogeneous three-dimensional electronics by use of printed semiconductor nanomaterials. *Science* **314**, 1754-1757 (2006).

4. Khang, D.Y., Jiang, H.Q., Huang, Y. & Rogers, J.A. A stretchable form of single-crystal silicon for high-performance electronics on rubber substrates. *Science* **311**, 208-212 (2006).
5. Groenendaal, L., Zotti, G., Aubert, P.H., Waybright, S.M. & Reynolds, J.R. Electrochemistry of poly(3,4-alkylenedioxythiophene) derivatives. *Advanced Materials* **15**, 855-879 (2003).
6. Sun, Y.R. et al. Management of singlet and triplet excitons for efficient white organic light-emitting devices. *Nature* **440**, 908-912 (2006).
7. DeFranco, J.A., Schmidt, B.S., Lipson, M. & Malliaras, G.G. Photolithographic patterning of organic electronic materials. *Organic Electronics* **7**, 22-28 (2006).
8. Muller, C.D. et al. Multi-colour organic light-emitting displays by solution processing. *Nature* **421**, 829-833 (2003).
9. Holdcroft, S. Patterning pi-conjugated polymers. *Advanced Materials* **13**, 1753-1765 (2001).
10. Letierrier, Y. et al. Mechanical integrity of transparent conductive oxide films for flexible polymer-based displays. *Thin Solid Films* **460**, 156-166 (2004).
11. Chen, Z., Cotterell, B. & Wang, W. The fracture of brittle thin films on compliant substrates in flexible displays. *Engineering Fracture Mechanics* **69**, 597-603 (2002).
12. Crawford, G.P. Flexible flat panel displays (John Wiley & Sons, Hoboken, N.J., 2005).
13. Li, Z.F. & Ruckenstein, E. Patterned conductive polyaniline on Si(100) surface via self-assembly and graft polymerization. *Macromolecules* **35**, 9506-9512 (2002).

14. Ruckenstein, E. & Li, Z.F. Surface modification and functionalization through the self-assembled monolayer and graft polymerization. *Advances in Colloid and Interface Science* **113**, 43-63 (2005).
15. Suh, K.Y. & Lee, H.H. Capillary force lithography: Large-area patterning, self-organization, and anisotropic dewetting. *Advanced Functional Materials* **12**, 405-413 (2002).
16. Im, S.G. & Gleason, K.K. Systematic Control of the Electrical Conductivity of Poly (3, 4-ethylenedioxythiophene) via Oxidative Chemical Vapor Deposition (oCVD) *Macromolecules* **40**, 6552-6556 (2007).
17. Im, S.G., Olivetti, E.A. & Gleason, K.K. Doping level and work function control in oxidative chemical vapor deposited poly (3,4-ethylenedioxythiophene). *Applied Physics Letters* **90**, 152112 (2007).
18. Lock, J.P., Im, S.G. & Gleason, K.K. Oxidative chemical vapor deposition of electrically conducting poly(3,4-ethylenedioxythiophene) films. *Macromolecules* **39**, 5326-5329 (2006).
19. Ryan, R.W. et al. Dielectric-assisted trilayer lift-off process for improved metal definition. *Journal of Vacuum Science & Technology B* **16**, 2759-2762 (1998).
20. Kymissis, I., Dimitrakopoulos, C.D. & Purushothaman, S. Patterning pentacene organic thin film transistors. *Journal of Vacuum Science & Technology B* **20**, 956-959 (2002).
21. Annual Book of ASTM Standards D3359 (1997).



22. Kovacic, P. & Jones, M.B. Dehydro Coupling of Aromatic Nuclei by Catalyst Oxidant Systems - Poly(Para-Phenylene). *Chemical Reviews* **87**, 357-379 (1987).
23. Sadki, S., Schottland, P., Brodie, N. & Sabouraud, G. The mechanisms of pyrrole electropolymerization. *Chemical Society Reviews* **29**, 283-293 (2000).
24. Kirchmeyer, S. & Reuter, K. Scientific importance, properties and growing applications of poly(3,4-ethylenedioxythiophene). *J Mater Chem* **15**, 2077-2088 (2005).
25. Ha, Y.H. et al. Towards a transparent, highly conductive poly(3,4-ethylenedioxythiophene). *Advanced Functional Materials* **14**, 615-622 (2004).
26. Kim, J., Kim, E., Won, Y., Lee, H. & Suh, K. The preparation and characteristics of conductive poly(3,4-ethylenedioxythiophene) thin film by vapor-phase polymerization. *Synthetic Metals* **139**, 485-489 (2003).
27. Barton, A.F.M. CRC handbook of polymer-liquid interaction parameters and solubility parameters (CRC Press, 1990).
28. Yoo, P.J., Suh, K.Y., Kang, H. & Lee, H.H. Polymer elasticity-driven wrinkling and coarsening in high temperature buckling of metal-capped polymer thin films. *Physical Review Letters* **93** (2004).
29. Yoo, P.J. & Lee, H.H. Morphological diagram for metal/polymer bilayer wrinkling: Influence of thermomechanical properties of polymer layer. *Macromolecules* **38**, 2820-2831 (2005).

## **Chapter Five**

### **CONFORMAL COVERAGE OF POLY (3,4-ETHYLENEDIOXYTHIOPHENE) FILMS WITH TUNABLE NANOPOROSITY VIA OXIDATIVE CHEMICAL VAPOR DEPOSITION (OCVD)**

**Sung Gap Im**, David Kusters, Wonjae Choi, Salmaan H. Baxamusa, Richard van de Sanden, and Karen K. Gleason, 'Conformal Coverage of Poly (3,4-ethylenedioxythiophene) films with tunable nanoporosity via Oxidative Chemical Vapor Deposition (oCVD)', *ACS Nano*, 2(2008), 1959-1967

## ABSTRACT

Novel nano-porous poly (3,4-ethylenedioxythiophene) (PEDOT) films with basalt-like surface morphology are successfully obtained via a one-step, vapor phase process of oxidative chemical vapor deposition (oCVD) by introducing a new oxidant,  $\text{CuCl}_2$ . The substrate temperature of the oCVD process is a crucial process parameter for controlling electrical conductivity and conjugation length. Moreover, the surface morphology is also systemically tunable through variations in substrate temperature, a unique advantage of oCVD process. By increasing the substrate temperature, the surface morphology becomes more porous, with the textured structure on the nanometer scale. The size of nanopores and fibrils appears uniformly over  $25 \text{ mm} \times 25 \text{ mm}$  areas on the Si wafer substrates. Conformal coverage of PEDOT films grown with the  $\text{CuCl}_2$  oxidant (C-PEDOT) is observed on both standard trench structures with high aspect ratio and fragile surfaces with complex topology, such as paper, results which are extremely difficult to be achieved with liquid phase based processes. The tunable nano-porosity and its conformal coverage on various complex geometries are highly desirable for many device applications requiring controlled, high interfacial area, such as supercapacitors, Li-ion battery electrodes, and sensors. For example, highly hydrophilic surface with the static water contact angle down to less than  $10^\circ$  is obtained solely by changing surface morphology. By applying fluorinated polymer film onto the nano-porous C-PEDOT via initiative chemical vapor deposition (iCVD), the C-PEDOT surface also shows the contact angle higher than  $150^\circ$ . The hierarchical porous structure of fluorinated polymer coated C-PEDOT on paper mat shows superhydrophobicity and oil repellency.

**KEYWORDS:** poly (3,4-ethylenedioxythiophene) (PEDOT), oxidative chemical vapor deposition (oCVD), oxidant, CuCl<sub>2</sub>, FeCl<sub>3</sub>, nanostructure, conformal coverage, superhydrophobicity, oleophobicity

## 5.1 Introduction

Nanostructured materials have drawn significant research interest as their properties are often unique with respect to bulk materials of identical chemical composition.<sup>1</sup> Controlling the properties of these materials requires structural control on the nanometer scale.<sup>2</sup> A number of chemical and physical methodologies have been applied to synthesize nanostructured metals, inorganics, polymers, and carbon nanotubes, having a variety of potential applications, including circuit integration, microfluidics, and biomedical devices.<sup>3,</sup>

4

Conducting polymers are regarded as one of the most promising materials for nanostructured devices.<sup>5, 6</sup> Poly(3,4-ethylenedioxythiophene) (PEDOT) is a particularly interesting conducting polymer due to its excellent environmental stability and high optical transparency in its electrically conductive state.<sup>7, 8</sup> Moreover, since it has a moderate bandgap with low redox potential and exceptionally high conductivity, PEDOT has been applied to various electronic devices such as electrochemical cells,<sup>7</sup> chemical sensors,<sup>9, 10</sup> and transparent, flexible electrodes for organic electronics.<sup>11</sup> Currently, nanostructured PEDOT has been reported using various synthesis schemes.<sup>5</sup> For example, Jang *et. al.*

fabricated PEDOT nanorods for a sensing application by using micelle intermediated interfacial oxidative polymerization.<sup>9</sup> Abidian *et. al.* synthesized PEDOT nanotubes for controlled drug release by utilizing electrospun fibers as a template in electrochemical polymerization.<sup>12</sup> However, these synthetic methodologies require multi-step procedures and strict control over reaction conditions.

Previously, we have demonstrated an *in situ* deposition of well-defined, optically transparent PEDOT films on a variety of substrates, including Si wafers, paper, aluminum foil, and plastic substrates by using oxidative chemical vapor deposition (oCVD).<sup>13-16</sup> The oCVD film growth was achieved through vapor phase introduction of both the oxidant, FeCl<sub>3</sub>, and the monomer, 3,4-ethylenedioxythiophene (EDOT). The electrical conductivity, doping level, and work function of the oCVD PEDOT could be controlled by varying substrate temperature ( $T_{\text{sub}}$ ),<sup>13, 14</sup> and the maximum electrical conductivity achieved was greater than 700 S/cm.<sup>13, 15</sup> The oCVD PEDOT could also be grafted on various organic plastic substrates such as polystyrene (PS), polycarbonate (PC), and polyethyleneterephthalate (PET).<sup>15</sup>

In this report, we describe a new synthetic scheme to fabricate nano-porous, basalt-like PEDOT films by introducing a new oxidant, CuCl<sub>2</sub>, to the oCVD process. Both CuCl<sub>2</sub> and FeCl<sub>3</sub> are oxidants which are categorized as Friedel-Craft catalysts.<sup>15</sup> The surface morphology and nanostructure of the resultant films could be systematically controlled by changing  $T_{\text{sub}}$ . The nanostructured PEDOT could also be conformally coated on various geometries, including trenches with high aspect ratio and complex, fragile surfaces without damaging the subtle surface structure, which is difficult to achieve via a non-CVD processes.<sup>17</sup> Water and ethanol droplet contact angles on these nano-porous PEDOT films

showed that the contact angle was highly dependent on surface morphology. Superhydrobicity and oleophobicity was also readily obtained via vapor phase, initiative chemical vapor deposition (iCVD) of fluorinated polymer film on nanostructured oCVD PEDOT. The size-tunable nano-porous PEDOT film has a high surface area, and thus may find direct application in various devices that require high interfacial areas such as sensors, lithium secondary batteries, and supercapacitors.<sup>8</sup>

## 5.2 Experimental

The detailed procedure of the oCVD process and the reactor configuration are described in detail elsewhere.<sup>13-16</sup> Si wafers, quartz plates, and paper were used as substrates for the oCVD of PEDOT. To monitor conformality, PEDOT was deposited on trenches with various aspect ratios patterned on Si wafer which were supplied from Analog Devices. Process pressure was maintained between 50 and 100 mTorr and the flow rate of evaporated EDOT monomer was metered through a mass flow controller at 5 sccm. The substrate temperature was varied between 20 – 100 °C by a PID controller. The oxidizing agent was evaporated from a resistively heated crucible. For C-PEDOT films, the oxidizing agent was  $\text{CuCl}_2$  and was evaporated at a temperature greater than 380 °C. For F-PEDOT films, the oxidizing agent was  $\text{FeCl}_3$  and was evaporated at 300 °C.

The total deposition time was 60 minutes. The thickness of PEDOT was controlled by the loading amount of  $\text{CuCl}_2$  and the deposition time. After deposition, the film was rinsed with methanol for about 30 minutes to remove any residual oxidizing agent and EDOT monomer.

The iCVD process was also described in detail elsewhere.<sup>18</sup> Perfluorodecyl acrylate monomer and tert-butyl peroxide initiator were vaporized at room temperature and introduced into the iCVD chamber at flow rates of approximately 0.3 sccm and 1.3 sccm, respectively. The polymerization reaction was initiated by heating a filament array to 280 °C. The process pressure was controlled at 100 mTorr by a throttling butterfly valve. Film thicknesses were monitored *in situ* by interferometry; approximately 25 nm of the PFA film was deposited in 10 min.

PEDOT film thickness was measured with a profilometer (Tencor, P-10) and the sheet resistance was measured with a four-point probe (MWP-6, Jandel Engineering Ltd.). The conductivity was calculated from the sheet resistance and measured thickness. FTIR spectra were collected on a Nexus 870, Thermo Electron Corporation. The surface morphology of PEDOT film was imaged by both SEM (FEI/Philips XL30 FEG ESEM) and AFM (Dimension 3100, Digital Instruments, Ltd.). The sampling size of roughness of PEDOT film was fixed at  $2 \times 2 \mu\text{m}^2$ . The static contact angle was measured within 30 s after placing 2 – 4  $\mu\text{L}$  of deionized water and ethanol droplets on the substrates (VCA2000, AST Inc.).

All chemicals were purchased from Aldrich and used without any further purification.

19

## **5.3 Results and Discussion**

### **5.3.1 FTIR Spectra**

The Fourier transform infrared (FTIR) spectra of oCVD PEDOT with  $\text{CuCl}_2$  as an oxidizing agent (C-PEDOT, afterward) at three different values of  $T_{\text{sub}}$  (Fig. 5-1a-c) match

the spectra for oCVD PEDOT with  $\text{FeCl}_3$  as an oxidizing agent (F-PEDOT, afterward) at  $T_{\text{sub}} = 55\text{ }^\circ\text{C}$  (Fig. 5-1d). The detailed peak assignments were recently reported elsewhere.<sup>13</sup> This result indicates that  $\text{CuCl}_2$  successfully oxidized the EDOT monomer to form PEDOT. Due to its insolubility, the molecular weight of PEDOT could not be measured with conventional method such as gel-permeation chromatography (GPC).<sup>13</sup> However, compared to oligomeric PEDOT,<sup>20</sup> the peaks in the FTIR spectra of C-PEDOT are broadened by the doping effect,<sup>21</sup> which demonstrates that doped C-PEDOT was successfully polymerized. The intensity of the  $\text{C}=\text{C}$ <sup>13, 20</sup> peak at  $1520\text{ cm}^{-1}$  is known to increase as the conjugation length of PEDOT grows.<sup>22</sup> Thus, the gradual decrease in the intensity of the  $1520\text{ cm}^{-1}$  peak as the substrate temperature decreases (Fig. 5-1b and 5-1a) represents a decrease in the conjugation length of C-PEDOT. It is well known that variation in conjugation length directly affects the electrical conductivity of PEDOT.<sup>23</sup> The increase in conjugation length and conductivity with increasing substrate temperature has also been observed in F-PEDOT<sup>13, 14</sup> produced by oCVD. However, the absolute value of conductivity was highly affected by the oxidant used. For C-PEDOT, the maximum conductivity obtained was  $32\text{ S/cm}$  at  $T_{\text{sub}} = 80\text{ }^\circ\text{C}$  which is almost one order lower than that of F-PEDOT.<sup>13, 15</sup> Two possible reasons for this difference are lower oxidation potential of  $\text{Cu}^{2+}$  ( $E_0 = +0.153\text{ eV}$ ) compared with  $\text{Fe}^{3+}$  ( $E_0 = +0.771\text{ eV}$ )<sup>24</sup> and the lower density of the oCVD films formed using  $\text{CuCl}_2$ , as will be discussed below.



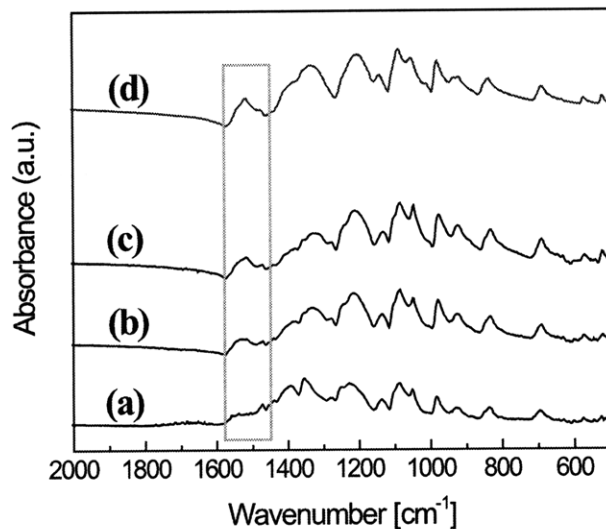


Figure 5-1. FTIR spectra of PEDOT films via oCVD process with (a-c)  $\text{CuCl}_2$  or (d)  $\text{FeCl}_3$  as an oxidant; (a)  $T_{\text{sub}} = 20\text{ }^\circ\text{C}$ , conductivity was 0.22 S/cm; (b)  $T_{\text{sub}} = 50\text{ }^\circ\text{C}$ , conductivity was 3.3 S/cm; (c)  $T_{\text{sub}} = 80\text{ }^\circ\text{C}$ , conductivity was 11.3 S/cm; (d)  $T_{\text{sub}} = 55\text{ }^\circ\text{C}$ , conductivity was 11.2 S/cm. The rectangle highlights an absorption region associated with conjugation in the oCVD PEDOT.

### 5.3.2 Surface Morphology

The surface morphology of the C-PEDOT (Fig. 5-2a-c) as imaged via scanning electron microscopy (SEM) differed from that of the smooth F-PEDOT (Fig. 5-2d). F-PEDOT had a root mean squared (RMS) roughness of less than 4 nm determined by atomic force microscopy (AFM). At the surface of F-PEDOT, shallow (<10 nm height) wrinkles of relative uniform spacing were also observed and are most likely formed by the reaction residue filtrated out from F-PEDOT during the rinsing process. On the other hand, the

surface morphology of C-PEDOT is highly dependent on the substrate temperature used for film growth.

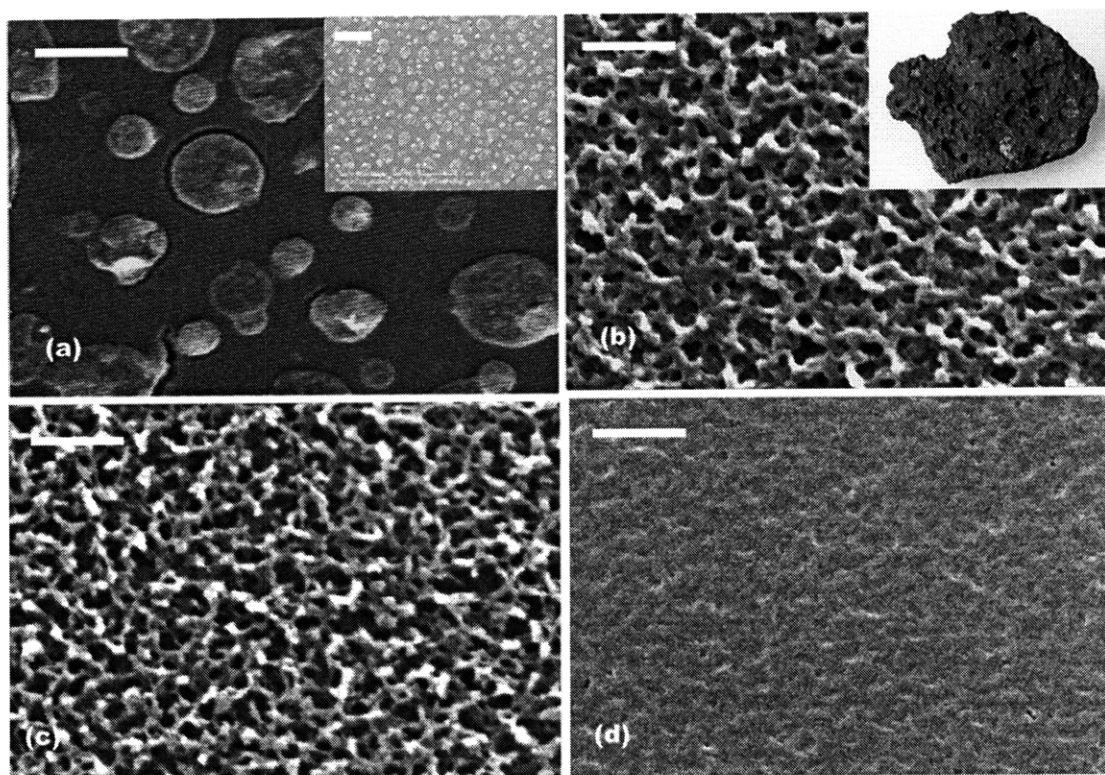


Figure 5-2. SEM images of (a-c) C-PEDOT and (d) F-PEDOT, respectively; (a)  $T_{\text{sub}} = 20$  °C; (b)  $T_{\text{sub}} = 50$  °C; (c)  $T_{\text{sub}} = 80$  °C; (d)  $T_{\text{sub}} = 55$  °C. Each scale bars represents 500 nm. Scale bar in the inset of (a) represents 5  $\mu\text{m}$ . Inset of (b) is the digital camera image of basalt. Copyright (2008) by Andrew Alden, geology.about.com, reproduced under educational fair use.

At  $T_{\text{sub}} = 20\text{ }^{\circ}\text{C}$ , two distinct regions can be observed in C-PEDOT: a relatively dense and smooth area surrounding large, porous domains with rounded edges whose size ranges from *ca* 200 to 300 nm diameters. Some of these porous domains merged to form larger regions having diameters of 500 ~ 1100 nm (Fig. 5-2a, inset). At the higher  $T_{\text{sub}}$  of 50  $^{\circ}\text{C}$ , the surface morphology of C-PEDOT is entirely that of a highly interconnected, porous structure. The pore size ranged from 50 to 150 nm and the diameter of the fibrils ranged between 40 and 100 nm. The relatively narrow size distribution of the nanopores and fibril structures was observed over the entire area of the 25 mm  $\times$  25 mm substrate. At  $T_{\text{sub}} = 80\text{ }^{\circ}\text{C}$ , the surface morphology was similar to that at  $T_{\text{sub}} = 50\text{ }^{\circ}\text{C}$ , but the film is more porous.

The formation of pores in C-PEDOT is hypothesized to be related to the unique behavior of the  $\text{CuCl}_2$  oxidant. The  $\text{CuCl}_2$  is typically heated to temperatures of 380 – 420  $^{\circ}\text{C}$  inside a crucible located within the oCVD reactor.  $\text{CuCl}_2$  is known to decompose to  $\text{CuCl}$  vapor and  $\text{Cl}_2$  gas at temperatures higher than 300  $^{\circ}\text{C}$ .<sup>25</sup> While  $\text{CuCl}$  is known as a Lewis acid, its oxidation power is weak.<sup>25</sup> On the other hand,  $\text{Cl}_2$  is a strong oxidant<sup>25</sup> and is capable of oxidizing the EDOT monomer to form a radical cation, the first step in the growth of conductive PEDOT chains. The vaporized  $\text{CuCl}$  is easily condensed at the substrate because it is essentially involatile at temperatures lower than 100  $^{\circ}\text{C}$ . On the other hand,  $\text{Cl}_2$  is highly volatile ( $T_{\text{bp}} = -34.04\text{ }^{\circ}\text{C}$ <sup>24</sup>) even at the lower temperature of the substrate. Since EDOT dimers and higher molecular weight EDOT oligomers are nearly involatile,<sup>13</sup> further step growth polymerization reactions are confined to the substrate. Therefore, a mixture of EDOT monomer, EDOT oligomers, and  $\text{CuCl}$  is formed on the relatively cold substrate. The  $\text{CuCl}$  at the substrate can be readily re-oxidized to form  $\text{CuCl}_2$  in the presence of  $\text{Cl}_2$ , such as  $\text{Cl}_2$  or residual  $\text{O}_2$  in the reactor. Thus, the oxidative polymerization of EDOT can

be performed by both  $\text{Cl}_2$  and  $\text{CuCl}_2$  at the surface of substrate. However, since  $\text{Cl}_2$  is so volatile, it is likely that most of oxidation reactions at the surface of substrate are performed solely by  $\text{CuCl}_2$ . As  $\text{CuCl}_2$  is mild oxidant and the oxidation reaction is relatively slower than that of  $\text{FeCl}_3$ , the oxidative polymerization with  $\text{CuCl}_2$  releases the gaseous reaction byproduct of  $\text{HCl}$ <sup>13, 16, 26</sup> more slowly than that with  $\text{FeCl}_3$ . Thus, the formation of bubbles in PEDOT film is most likely derived from the competing processes between the release of gaseous byproduct and the condensation of polymerized PEDOT film. If film has grown over the site of the release of the gaseous byproducts, the bubbles which eventually escape lead to the formation of pores. At low  $T_{\text{sub}}$  the reaction is slow, allowing the entrapment of  $\text{HCl}$  vapor before the release of vapor occurs. Indeed in Fig. 5-2a, corresponding to the lowest  $T_{\text{sub}}$  C-PEDOT, features resulting from gas-evolution are observed only over part of the surface in island-like domains. The roughened surface of inside these domains strongly implies the evolution of gas in this domain during the deposition process. The effused gas slowly forces the formation of expanded domains, and these bubbles collapse when the gas escapes. Each of the island domains contained at least one “vent-hole” through which the volatile gaseous component effused out. The observation from the magnified images supports the hypothesis that pores are formed by the outgassing of bubbles formed during the polymerization reaction.

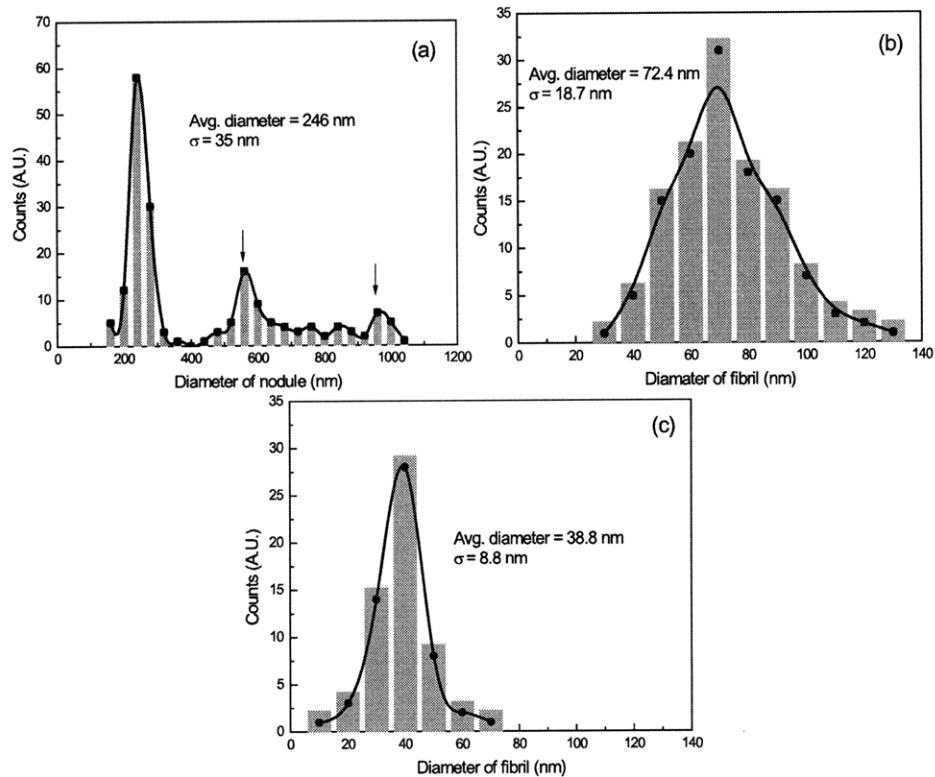


Figure 5-3. Size distribution of diameter of (a) nodules of C-PEDOT at  $T_{\text{sub}}=20\text{ }^{\circ}\text{C}$  and fibrils of C-PEDOT at (b) at  $T_{\text{sub}}=50\text{ }^{\circ}\text{C}$  and (c) at  $T_{\text{sub}}=80\text{ }^{\circ}\text{C}$ , respectively. Arrows denoted in (a) represent the peak position of merged nodules.

The enlarged image of inset of Fig. 5-2a demonstrates that the morphology of nodular structure is uniformly distributed. The size distribution of nodules in the image of inset of Fig. 5-2a is shown in Fig. 5-3a. The mean diameter of individual nodules was about 250 nm and showed a reasonably narrow distribution (the standard deviation was 35 nm), suggesting a relatively constant rate of gas evolution and effusion during the deposition. The distribution could not be fitted with one Gaussian curve and the distribution had some

separate, additional peaks with the size of greater than 500 nm, which clearly supports the hypothesis of formation of larger nodules by merging individual nodules of uniform size distribution.

At higher substrate temperatures, the rapidly growing film temporarily entrains the gaseous byproduct, which is finally released through the burst of vapor bubbles over the entire surface of the film (Fig. 5-2b and 5-2c). This vigorous effusion not only enlarged the pore size in the film, but also added mechanical stress to the fibril. Consequently, the fibril diameter decreased significantly (20 – 60 nm) and the length of the fibril increased. Some of the fibril texture was disconnected by the mechanical stress of the gaseous byproduct effusion, causing pores to merge and increasing the overall porosity of the film. The size distributions of fibrils in Fig 5-2b and c demonstrate narrow Gaussian curves (Fig. 5-3b and c). At  $T_{\text{sub}} = 50\text{ }^{\circ}\text{C}$ , mean diameter of fibrils was about 72 nm, which became thinner (mean diameter = 39 nm) with narrower distribution at  $T_{\text{sub}} = 80\text{ }^{\circ}\text{C}$ . The estimated RMS roughness of C-PEDOT at  $T_{\text{sub}} = 50\text{ }^{\circ}\text{C}$  was more than 20 nm and the depth of the pore was generally larger than 50 nm. Considering the total film thickness measured by profilometry was 75 nm, it follows that the interconnected texture structure was maintained throughout the thickness of C-PEDOT film. The SEM images (Fig. 5-2b and 5-2c) of the nano-porous structure in C-PEDOT deposited at higher substrate temperatures also strongly support the hypothesis that a gaseous vapor evolved out from the solid PEDOT surface as bubbles during the oCVD process. Moreover, the observed size distribution infers that the rate of vapor effusion rate was relatively constant with respect to  $T_{\text{sub}}$ , which strongly suggests that the nano-porous structure can be tuned systematically by controlling  $T_{\text{sub}}$  during the oCVD process. Analogous porous structures in other materials are formed by the mechanism of

gas evolution. For example, Styrofoam<sup>TM</sup>, a well-known packaging material, is produced by the thermal expansion of a gaseous blowing agent such as pentane or CO<sub>2</sub> in solid polystyrene. Another well-known example is basalt, which is formed by the rapid cooling of lava at the surface of earth (Fig. 5-2b, inset). The entrapped water or air vapor in solidified lava results in the characteristic porous structure of basalt, which has morphological similarity to the surface structure of C-PEDOT.

In the case of F-PEDOT, the strong oxidant FeCl<sub>3</sub> can oxidize EDOT so quickly that the rate of gaseous byproduct release is much faster than that of condensation of PEDOT film. Therefore, gaseous HCl can easily escape at the surface of formed PEDOT and smooth F-PEDOT is formed by oCVD process (Fig. 5-2d). In other words, the nano-porous structure can be formed in the course of competing process of oxidation reaction and condensation, and it follows that the slow oxidation reaction with CuCl<sub>2</sub> plays a critical role in forming this basalt-like structure.

### 5.3.3 Conformal Coverage on Complex Geometries

In addition to resulting in different surface morphologies on flat substrates, the change in oxidants impacts the degree of conformality over nonplanar microstructured substrates. Trenches (8 μm deep × 2 μm wide) in silicon were used to examine the conformal coverage of oCVD PEDOT grown with different oxidants at substrate temperatures less than 100°C. Fig. 5-4a and b demonstrate the cross-sectional SEM images of C-PEDOT (a) and F-PEDOT (b) on these standard trenches deposited at T<sub>sub</sub> = 50 °C. For F-PEDOT, the vaporized FeCl<sub>3</sub> has very high sticking probability, nearing unity, because it is almost non-

volatile at  $T_{\text{sub}}$  less than 100 °C.<sup>17</sup> Since the evaporated  $\text{FeCl}_3$  from the heating crucible is directional, most of  $\text{FeCl}_3$  is condensed at near the entrance region of the trench. The resultant cross-sectional image clearly shows that F-PEDOT was deposited mostly on the entrance of trench and no film was observed at the bottom and the sidewall of the trench. On the other hand, the oCVD of C-PEDOT involves highly volatile  $\text{Cl}_2$  vapor in the deposition process.  $\text{Cl}_2$  has much lower sticking probability compared with  $\text{FeCl}_3$  vapor due to extremely high volatility. The lower sticking probability allows non-directional flux of oxidant in the trench, which can be materialized as a conformal coverage of the trench.<sup>17</sup> Fig. 5-4a demonstrates the conformal growth of about 120 nm thick C-PEDOT in the trench. The nano-porous, basalt-like structure could be observed in both side walls and bottom of the nanometer scale conformally covered trench. Although the oCVD procedure is almost same between C-PEDOT and F-PEDOT, the dramatic difference in conformality supports the hypothesis of the involvement of volatile  $\text{Cl}_2$  in C-PEDOT deposition, which is one of unique advantages that  $\text{CuCl}_2$  oxidant can offer. This conformal coverage is unique properties of CVD process, which is very difficult to achieve in other liquid phase based methods.<sup>17</sup> For comparison, Fig. 5-4c shows the result of spin-casting and polymerizing a liquid phase mixture of EDOT and  $\text{FeCl}_3$  solution in methanol is an extremely nonconformal coverage. The solution was trapped at the bottom of the trench but depleted at the side wall and upper mouth area. The resultant feature was highly irregular compared to the original shape of trench.



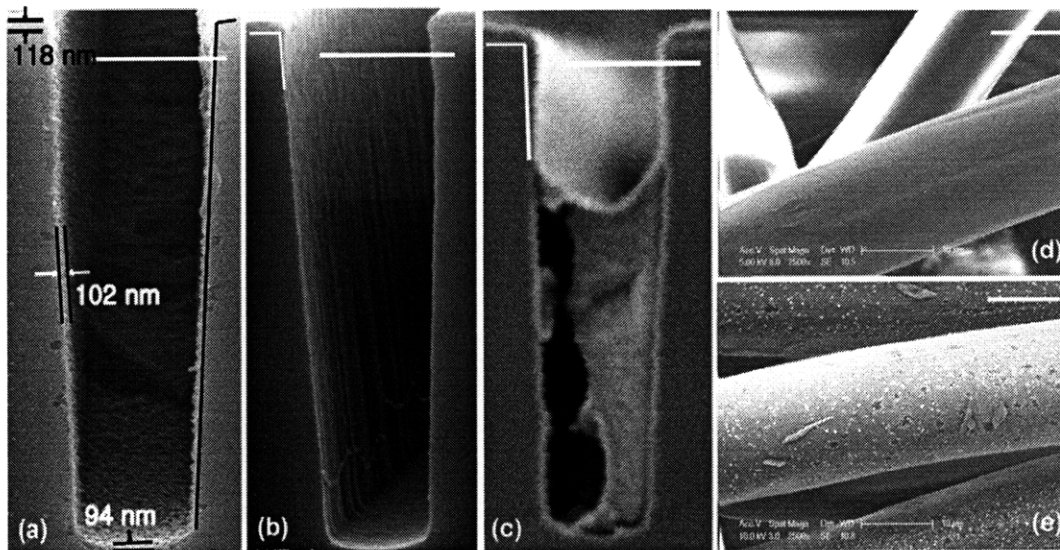


Figure 5-4. Cross-sectional SEM images of (a) C-PEDOT and (b) F-PEDOT deposited on trenches and (c) EDOT and  $\text{FeCl}_3$  mixture solution was spin-cast to form highly anisotropic PEDOT on trench. Each scale bars represents  $2 \mu\text{m}$ . Black line in the right side of (a) and white line in the left side of (b) and (c) show the borders between Si trench and C-PEDOT film. SEM images of conformally coated C-PEDOT film on paper mat (d) before and (e) after the deposition of C-PEDOT film. Each scale bars represents  $10 \mu\text{m}$ .

The conformal coverage can also be achieved on various convex and concave surfaces. Since oCVD is a vapor phase based process, oCVD PEDOT can be conformally deposited on various soft, vulnerable substrates without damaging the substrate structure. Fig. 5-4d and e demonstrate the C-PEDOT deposited at  $T_{\text{sub}} = 80 \text{ }^\circ\text{C}$  on a paper mat whose fiber diameter was  $15 \sim 25 \mu\text{m}$  long. The SEM images showed that C-PEDOT was conformally deposited around the fibers of the paper mat while maintaining the initial features of the

mat. The nano-structure of C-PEDOT was also observed at the surface of micro-structured paper mat. Combined with the microstructure offered from the paper mat, the nano structure from C-PEDOT on paper mat has a hierarchical, huge surface area, advantageous for various applications such as flexible electrodes with high surface areas and supercapacitors.

### 5.3.4 Superhydrophobicity and Oil Repellency

One of the properties that the nano-porous structure can affect is wettability.<sup>6, 18, 27-29</sup> On a smooth, flat, and chemically homogeneous surface, the contact angle,  $\theta$ .  $\theta$  is defined by Young's equation

$$\cos \theta = \frac{\gamma_{SV} - \gamma_{SL}}{\gamma_{LV}} \quad (1)$$

where  $\gamma_{SV}$ ,  $\gamma_{SL}$ ,  $\gamma_{LV}$  is solid-vapor, solid-liquid, and liquid-vapor interfacial tension, respectively. In Young's equation, the  $\theta$  is solely determined by the chemical composition of solid, liquid, and vapor, involved. When the surface is roughened, the apparent contact angle ( $\theta^{app}$ ) can be altered by a geometric factor, given by Wenzel's equation

$$\cos \theta^{app} = r \cos \theta \quad (2)$$

where  $r$  is a ratio of true surface area to the horizontal projection of surface area.<sup>18, 27</sup> Assuming the chemical composition of surface is identical, the  $\theta^{app}$  can be modulated solely by altering surface morphology. If  $\theta$  is less than  $90^\circ$ ,  $\theta^{app}$  is always less than  $\theta$  because  $r$  in eq. (2) is always larger than one. Therefore, if the flat surface is hydrophilic, the roughened surface becomes more hydrophilic and the surface is more wettable.

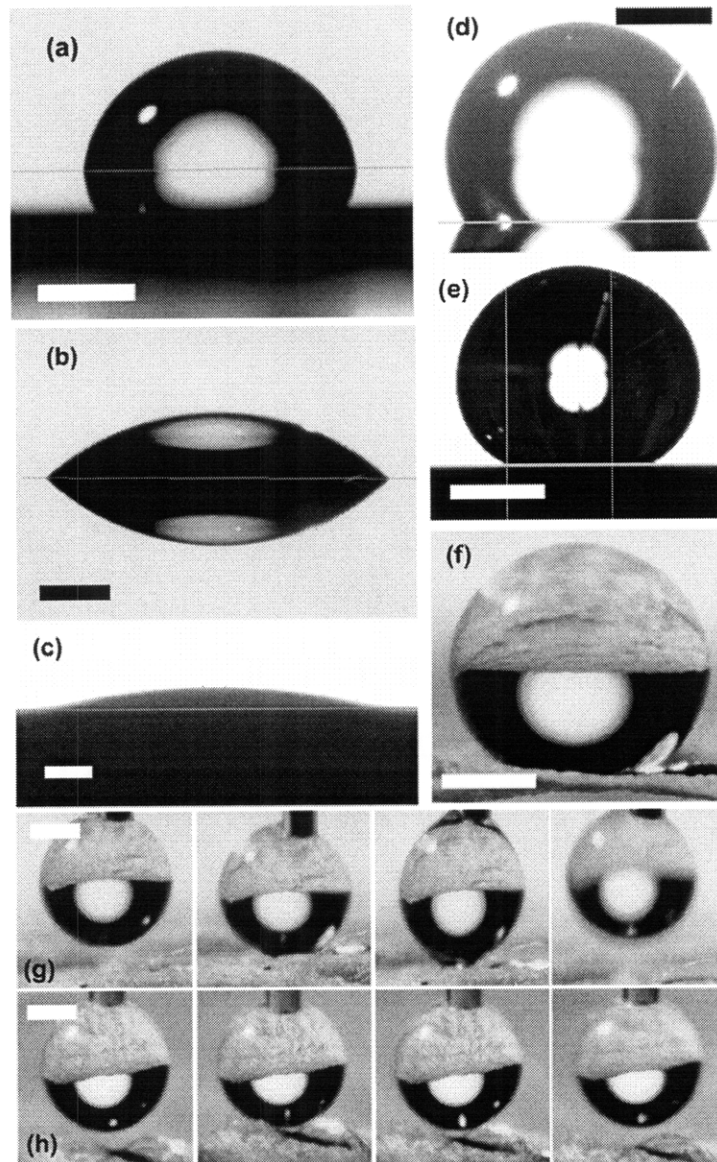


Figure 5-5. Water droplet contact angle variations of PEDOT film according to the surface roughness; (a) F-PEDOT, RMS roughness = 3.7 nm,  $\theta = 84^\circ$ ; (b) C-PEDOT, RMS roughness = 22.7 nm,  $\theta = 37^\circ$ ; (c) C-PEDOT, RMS roughness = 43.0 nm,  $\theta = 10^\circ$  respectively. Contact angle variations of PFA-modified PEDOT film; (d) F-PEDOT,  $\theta =$

120°; (b) C-PEDOT,  $\theta = 150^\circ$ . (f) digital camera image of PFA-modified C-PEDOT coated paper mat. A series of picture captured from CCD camera for advancing and receding water droplet on (g) PFA-modified paper mat and (h) PFA-modified C-PEDOT coated paper mat, respectively. Each scale bar represents 1 mm.

The effect of high surface roughness on C-PEDOT on wettability was evaluated by measuring  $\theta$  for water (Fig. 5-5a-c) on the surface. Compared to the contact angle of F-PEDOT whose surface roughness is relatively low (Fig. 5-5a), the contact angle of C-PEDOT displays a large decrease of contact angle (Fig. 5-5b and c). As the RMS roughness increases, the contact angle decreases significantly. Considering that the chemical compositions of F-PEDOT and C-PEDOT are almost identical, the contact angle difference mainly derives from morphological effect. With a surface roughness of higher than 40 nm, the contact angle of C-PEDOT surface is  $10^\circ$ , which is very close to being superhydrophilic.

Analogously, if the  $\gamma_{SV}$  is smaller than  $\gamma_{SL}$  in eq. 1, then CA is greater than  $90^\circ$  and the  $\theta^{app}$  with the roughness of  $r$  is greater than  $\theta$  of flat surface, according to equation 2. As the morphology of C-PEDOT surface is significantly rough, the surface can be rendered strongly hydrophobic by coating with a low surface energy material. For this purpose, a 25-nm thick, fluorinated acrylate (poly(perfluorodecyl acrylate), PFA) polymer film with low surface energy ( $\gamma_{SV} = 9.3$  mN/m) was deposited via initiative chemical vapor deposition (iCVD).<sup>18, 28</sup> The CA of water on PFA-modified F-PEDOT was  $120^\circ$ , which was similar to the contact angle of water on a pure PFA film,  $118^\circ$  (Fig. 5-5d).<sup>28</sup> On the other hand, 120-nm thick nano-porous C-PEDOT film coated with 25 nm of PFA showed a large increase in

contact angle, to  $150\pm 3^\circ$ , which is close to superhydrophobic surface (Fig. 5-5e).<sup>18</sup> Neither the surface morphology of the basalt-like structure nor the conductivity of the C-PEDOT film was significantly altered by subsequent iCVD deposition. Since the iCVD PFA film was conformally covered both C-PEDOT and F-PEDOT film, the chemical composition of surface is practically identical,<sup>28</sup> and the increase of contact angle in C-PEDOT is solely due to the nano-porous, textured morphology.

If a surface shows superhydrophobicity ( $\theta > 150^\circ$ ), the water is believed to form a composite interface with the surface texture, termed the Cassie regime.<sup>18, 27</sup> In the Cassie regime,  $\theta^{app}$  is calculated as the average of  $\theta$  of the solid and the air, given by

$$\cos \theta^{app} = -1 + \phi_s (1 + \cos \theta) \quad (3)$$

where  $\phi_s$  is the fraction of solid-liquid contact area.<sup>27</sup> When the surface texture is so rough that the water cannot penetrate into the valleys of the structure, small pockets of air become entrapped and the water sits partially on air. If the area ratio of the air region over surface is close to 1, the composite interface between water/solid/air becomes practically air-like, which is extremely hydrophobic and exhibits very low hysteresis. By combining our nanoscale roughness with the microscale textures of the paper mat, the C-PEDOT surface could be made even more hydrophobic. This is actually the technique used by the famous lotus leaf.<sup>29</sup> As shown in Figure 5-4d, the one-step oCVD process can easily form a hierarchical structure of nanometer scale roughness of C-PEDOT on the micrometer scale roughness of the paper mat.

Although the exact value of  $\theta^{app}$  was difficult to determine because the extremely rough surface of paper mat made it difficult to obtain a flat baseline for the contact angle

measurement (Fig. 5-5f), the measured contact angle was higher than  $163^\circ$ . Moreover, the water droplet was not pinned on the C-PEDOT coated paper mat and showed negligible hysteresis. A series of pictures was captured to elucidate the hysteresis of advancing and receding water droplet on PFA-modified paper mat as a control (termed as control mat afterward, Fig. 5-5g) and C-PEDOT-paper mat (termed as sample mat afterward, Fig. 5-5h). The highly micro-porous control mat resulted in the Cassie state when water droplet was applied. No increase in the advancing contact angle was observed when the water droplet was pressed on the mat. However, a decrease in the receding contact angle was clearly observed when the water droplet was siphoned from the control mat. Although the water sits on the air in the microscale pores between fibers, a considerable amount of control mat area was in contact with the water droplet. Hence, in spite of the low surface energy of PFA film, the wet area can be pinned adhesively with water droplet, which possibly caused the receding angle hysteresis in control mat.<sup>27</sup> On the other hand, sample mat has enormously tortured surface area in nanometer scale, compared with control mat. With this nano-scale surface curvature, penetration of water into the micro-scale is even further reduced, which greatly decreases the contact surface area,  $\phi_s$  in equation 3. Consequently, adhesive pinning<sup>27</sup> is greatly depressed and the sequential CCD camera images clearly show that no hysteresis between advancing and receding angle.

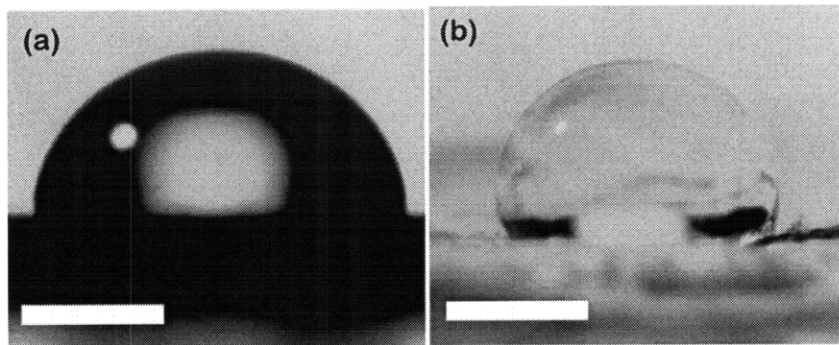


Figure 5-6. Ethanol droplet contact angles on (a) PFA-modified C-PEDOT film on Si wafer ( $\theta = 88^\circ$ ) and (b) PFA-modified C-PEDOT coated paper mat ( $\theta = 113^\circ$ ), respectively. Each scale bar represents 1 mm.

Furthermore, the oil repellency – termed as oleophobicity – could also be observed from PFA-modified C-PEDOT film on Si wafer (Fig. 5-6a) and sample mat (Fig. 5-6b). Since the surface tension of most of oil is generally much lower than that of water ( $\gamma_{LV} = 71.99$  mN/m at  $25^\circ\text{C}$ )<sup>24</sup>, it is extremely difficult to achieve oleophobicity.<sup>18, 29</sup> The contact angle of ethanol droplet ( $\gamma_{LV} = 21.97$  mN/m at  $25^\circ\text{C}$ )<sup>24</sup> on PFA-modified C-PEDOT film on Si wafer was  $88^\circ$  (Fig. 5-6a), which is almost two-fold greater than the CA of flat PFA-coated Si wafer ( $43^\circ$ ), which shows that the surface roughness of C-PEDOT plays a critical role in the oil repellency. According to the equation 2,  $\theta^{pp}$  of ethanol droplet in Fig. 5-6a should decrease since  $\theta$  of ethanol droplet is less than  $90^\circ$ . However, the observed result is reversed, which might be from metastable Cassie state or local pinning effect in Wenzel state.<sup>29</sup> The receding angle from this droplet was practically  $0^\circ$ , which can occur also from both highly hysteric Cassie state or strongly textured Wenzel state. To investigate this

aspect further, we have deposited ethanol on the sample mat. Ethanol did not penetrate into the fabrics, which conclusively supports the formation of Cassie state on sample mat and  $\theta^{APP}$  was  $113^\circ$ . The observed water and oil repellency of highly conductive PEDOT film can greatly enhance the self-cleaning ability, which potentially has a wide impact on anti-corrosion, anti-fouling from polluted water and fatty liquid.<sup>29</sup>

## 5.4 Conclusion and outlook

In conclusion, a new nanostructured PEDOT film was obtained via oCVD process by introducing new oxidant of  $\text{CuCl}_2$ . The obtained C-PEDOT film showed high electrical conductivity up to 32 S/cm. Substrate temperature was a critical process parameter in oCVD that controls the conductivity of C-PEDOT film, as was same in F-PEDOT. A basalt-like nano-porous structure was uniformly obtained from C-PEDOT deposited at  $T_{\text{sub}}$  higher than  $50^\circ\text{C}$ . The pore size and porosity could be systematically tuned by modulating substrate temperature. The C-PEDOT film showed ultimately improved conformality on the substrate. Conformal coverage on standard trench in Si and on paper fiber mats was clearly visible in the SEM images with retention of the complex surface structure. As an example of the effect of morphology, the contact angle decreases according to increase of the surface roughness and an extremely hydrophilic surface was successfully obtained. Moreover, on microstructured substrates, highly conductive and superhydro/oleophobic surface, such as non-wettable conducting paper could also be obtained easily by subsequent oCVD and iCVD process. The regularly nanostructured, hierarchical nanostructure has great potential for a variety of applications. For instance, highly hydrophilic conductive



PEDOT film can be used for advanced electrochemical applications, such as bio-sensors. Achieving high surface area layer on planar substrates and conformal coating of high surface area substrates are enabling features for devices such as supercapacitor and batteries, where high interfacial area is desired.

### **ACKNOWLEDGMENT**

This research was supported by the U.S. Army through the Institute for Soldier Nanotechnologies, under Contract DAAD-19-02-D-0002 with the U.S. Army Research Office. The authors thank Edward F. Gleason in Analog Devices for the supply of trench wafers.

### **REFERENCES**

1. Murray, C.B., Kagan, C.R. & Bawendi, M.G. Synthesis and characterization of monodisperse nanocrystals and close-packed nanocrystal assemblies. *Annual Review of Materials Science* **30**, 545-610 (2000).
2. Park, J. et al. Ultra-large-scale syntheses of monodisperse nanocrystals. *Nature Materials* **3**, 891-895 (2004).
3. Langer, R. & Peppas, N.A. Advances in biomaterials, drug delivery, and bionanotechnology. *Aiche Journal* **49**, 2990-3006 (2003).
4. Sarikaya, M., Tamerler, C., Jen, A.K.Y., Schulten, K. & Baneyx, F. Molecular biomimetics: nanotechnology through biology. *Nature Materials* **2**, 577-585 (2003).

5. Jang, J. in *Emissive Materials: Nanomaterials* 189-259 (2006).
6. Chiou, N.R., Lui, C.M., Guan, J.J., Lee, L.J. & Epstein, A.J. Growth and alignment of polyaniline nanofibres with superhydrophobic, superhydrophilic and other properties. *Nature Nanotechnology* **2**, 354-357 (2007).
7. Groenendaal, L., Zotti, G., Aubert, P.H., Waybright, S.M. & Reynolds, J.R. Electrochemistry of poly(3,4-alkylenedioxythiophene) derivatives. *Advanced Materials* **15**, 855-879 (2003).
8. Groenendaal, B.L., Jonas, F., Freitag, D., Pielartzik, H. & Reynolds, J.R. Poly(3,4-ethylenedioxythiophene) and its derivatives: Past, present, and future. *Advanced Materials* **12**, 481-494 (2000).
9. Jang, J., Chang, M. & Yoon, H. Chemical sensors based on highly conductive poly(3,4-ethylene-dioxythiophene) nanorods. *Advanced Materials* **17**, 1616-+ (2005).
10. Sotzing, G.A., Briglin, S.M., Grubbs, R.H. & Lewis, N.S. Preparation and properties of vapor detector arrays formed from poly(3,4 ethylenedioxy)thiophene-poly(styrene sulfonate)/insulating polymer composites. *Analytical Chemistry* **72**, 3181-3190 (2000).
11. Sirringhaus, H. et al. High-resolution inkjet printing of all-polymer transistor circuits. *Science* **290**, 2123-2126 (2000).
12. Abidian, M.R., Kim, D.H. & Martin, D.C. Conducting-polymer nanotubes for controlled drug release. *Advanced Materials* **18**, 405-+ (2006).

13. Im, S.G. & Gleason, K.K. Systematic Control of the Electrical Conductivity of Poly (3, 4-ethylenedioxythiophene) via Oxidative Chemical Vapor Deposition (oCVD) *Macromolecules* **40**, 6552-6556 (2007).
14. Im, S.G., Olivetti, E.A. & Gleason, K.K. Doping level and work function control in oxidative chemical vapor deposited poly (3,4-ethylenedioxythiophene). *Applied Physics Letters* **90**, 152112 (2007).
15. Im, S.G., Yoo, P.J., Hammond, P.T. & Gleason, K.K. Grafted Conducting Polymer Films for Nano-patterning onto Various Organic and Inorganic Substrates by Oxidative Chemical Vapor Deposition *Advanced Materials* **19**, 2863-2867 (2007).
16. Lock, J.P., Im, S.G. & Gleason, K.K. Oxidative chemical vapor deposition of electrically conducting poly(3,4-ethylenedioxythiophene) films. *Macromolecules* **39**, 5326-5329 (2006).
17. Gates, S.M. Surface Chemistry in the Chemical Vapor Deposition of Electronic Materials. *Chemical Reviews* **96**, 1519-1532 (1996).
18. Ma, M.L., Mao, Y., Gupta, M., Gleason, K.K. & Rutledge, G.C. Superhydrophobic fabrics produced by electrospinning and chemical vapor deposition. *Macromolecules* **38**, 9742-9748 (2005).
19. Aasmundtveit, K.E. et al. Structure of thin films of poly(3,4-ethylenedioxythiophene). *Synthetic Metals* **101**, 561-564 (1999).
20. Tran-Van, F., Garreau, S., Louarn, G., Froyer, G. & Chevrot, C. Fully undoped and soluble oligo(3,4-ethylenedioxythiophene)s: spectroscopic study and

- electrochemical characterization. *Journal of Materials Chemistry* **11**, 1378-1382 (2001).
21. Skotheim, T.A., Elsenbaumer, R.L. & Reynolds, J.R. Handbook of conducting polymers (M. Dekker, New York, 1998).
  22. Im, S.G., Olivetti, E.A. & Gleason, K.K. Systematic control of the electrical conductivity of poly (3,4-ethylenedioxythiophene) via oxidative chemical vapor deposition (oCVD). *Surface & Coatings Technology* **201**, 9406-9412 (2007).
  23. Baughman, R.H. & Shacklette, L.W. Conjugation Length Dependent Transport in Conducting Polymers from a Resistor Network Model. *Journal of Chemical Physics* **90**, 7492-7504 (1989).
  24. Lide, D.R. CRC Handbook of Chemistry and Physics (Taylor and Francis Group, LLC, Boca Raton, FL, 2008).
  25. Cotton, F.A. & Wilkinson, G. Advanced Inorganic Chemistry: a comprehensive text (John Wiley and Sons, New York, 1998).
  26. Sadki, S., Schottland, P., Brodie, N. & Sabouraud, G. The mechanisms of pyrrole electropolymerization. *Chemical Society Reviews* **29**, 283-293 (2000).
  27. Lafuma, A. & Quere, D. Superhydrophobic states. *Nature Materials* **2**, 457-460 (2003).
  28. Ma, M.L. et al. Decorated electrospun fibers exhibiting superhydrophobicity. *Advanced Materials* **19**, 255-+ (2007).
  29. Tuteja, A. et al. Designing superoleophobic surfaces. *Science* **318**, 1618-1622 (2007).

# **Chapter Six**

## **OXIDATIVE CHEMICAL VAPOR DEPOSITED POLY (3,4- ETHYLENEDIOXYTHIOPHENE) FILMS FOR ORGANIC PHOTOVOLTAIC CELL APPLICATIONS**

## Abstract

Oxidative chemical vapor deposited (oCVD) poly (3,4-ethylenedioxythiophene) (PEDOT) was successfully applied as a buffer layer in efficient organic photovoltaic (oPV) cells. First of all, to stabilize the interfacial contact of oCVD PEDOT on anode metal oxide, oCVD PEDOT was grafted to the indium tin oxide (ITO) surface using redox-active carboxylic acid containing 2-thiophene acetic acid (2-TAA) as a coupling agent. Contact angle measurement before and after 2-TAA treatment confirmed the tight chemisorption of this coupling agent on the ITO surface. On top of this surface, oCVD PEDOT was deposited and the PEDOT film showed enhanced adhesion to the ITO surface over silane-treated surfaces. With this interface stabilized, oPV cells were fabricated and the device performance was measured and compared with a conventional control cell using a PEDOT:PSS buffer layer. Although the oCVD cell showed low shunt resistance and non-ideal J-V behavior compared with the control cell, decreased series resistance in the oCVD cell ultimately lead to a comparable device with power conversion efficiency (PCE) of 5.2% under green light illumination. The hydrophobicity and stabilized interface formed with oCVD PEDOT play an important role in the observed high efficiency. For maximized oPV cell PCE using oCVD PEDOT as a buffer layer, further oCVD PEDOT optimization is required with respect to controlling surface roughness and surface concentration of Cl<sup>-</sup> ions.

**KEYWORDS:** poly (3,4-ethylenedioxythiophene) (PEDOT), oxidative chemical vapor deposition (oCVD), organic photovoltaic (oPV) cell, short circuit current ( $J_{sc}$ ), open circuit voltage ( $V_{oc}$ ), fill factor (FF)

## 6.1 Introduction

Polymer-based organic photovoltaic (oPV) cells have drawn significant research interest for their potential applicability to renewable solar energy conversion.<sup>1</sup> Since the pioneering work of Tang,<sup>2</sup> the performance of oPV cells has rapidly improved and power conversion efficiencies (PCE) ~5% under an air mass 1.5 global (AM 1.5G) illumination have been demonstrated by several research groups.<sup>1,3-5</sup> Simulation results have shown that PCE is expected to increase to ~10% via further optimization of donor-acceptor energy levels.<sup>6</sup> The best performing oPV cells to date contain a bulk-heterojunction (BHJ), which is defined by a phase-segregated, bicontinuous mixture to maximize the interfacial area between the donors and acceptor materials.<sup>7</sup> The final oPV devices are created by sandwiching the BHJ donor-acceptor composite between a transparent metal oxide anode, such as indium tin oxide (ITO), and a metal cathode. When light illuminates the oPV cell, the donor material, which is typically a conjugated polymer, absorbs the light to form excitons, the excited states of an electron-hole pair. The formed excitons are diffused via charge transfer or exciton diffusion and dissociate into electron and hole charges at the donor-acceptor interface, forced by the applied external charge. The dissociated charges are collected at the electrode through a bicontinuous pathway to the electrodes to generate the

photocurrent. The efficiency of oPV cells consists of the product of stepwise efficiencies of each process of light absorption, exciton or energy diffusion, exciton dissociation, and charge transfer. Therefore, to maximize the efficiency of oPV cell, it is necessary to optimize each process.

The current research to optimize the performance of oPV cells has focused on 1) the optimization of the mechanistic processes to generate photocurrent,<sup>6, 8</sup> 2) tuning the morphology of bicontinuous donor-acceptor composites,<sup>5</sup> 3) the application of new organic electronic materials,<sup>9</sup> and 4) controlling the interface between the electrode and the active composite layer.<sup>3</sup> In particular, the ohmic contact between the electrode and the active layer is highly desirable, as it facilitates the charge injection into the device.<sup>3</sup> In many cases, higher work function materials have been used as a buffer layer for this purpose. Poly(3,4-ethylenedioxythiophene) doped with poly(styrenesulfonic acid) (PEDOT:PSS) is a well-known buffer layer for use with ITO anodes,<sup>10</sup> since it has a higher work function (~5.2 eV)<sup>11</sup> compared to ITO (4.7 ~ 4.9 eV) and facilitates charge injection into the oPV cells. In addition, spin-coated PEDOT:PSS films greatly reduce the surface roughness of the anode which greatly decreases the leakage current in the device.<sup>3, 10</sup> However, the low conductivity of the PEDOT:PSS system can cause increased series resistance. Moreover, in PEDOT:PSS, phase segregation occurs between PSS and PEDOT, and acidic PSS-rich (78 atomic %) phase is dominant at the surface of PEDOT:PSS, which can cause device degradation.<sup>12</sup>

Previously, we have demonstrated an *in situ* deposition of well-defined, optically transparent PEDOT films on a variety of substrates, including Si wafers, paper, aluminum



foil, and plastic substrates by using oxidative chemical vapor deposition (oCVD).<sup>11, 13-15</sup> The oCVD film growth was achieved through vapor phase introduction of both the oxidant, FeCl<sub>3</sub>, and the monomer, 3,4-ethylenedioxythiophene (EDOT). The oCVD PEDOT has also been grafted on various organic plastic substrates such as polystyrene (PS), polycarbonate (PC), and polyethyleneterephthalate (PET).<sup>14</sup> By introducing a different oxidant, CuCl<sub>2</sub>, to the oCVD process, nano-porous, basalt-like PEDOT films with high surface area were obtained. The nanostructured PEDOT were also conformally coated on various geometries, including trenches with high aspect ratio and complex, fragile surfaces without damaging the subtle surface structure. Such features are difficult to achieve via a non-CVD processes.<sup>16</sup> It was shown that the electrical conductivity and doping level of the oCVD PEDOT could be controlled by varying substrate temperature ( $T_{\text{sub}}$ ),<sup>11, 13</sup> and the maximum electrical conductivity achieved was greater than 700 S/cm.<sup>13, 14</sup> The work function of oCVD PEDOT was systemically tuned from 5.1~5.4 eV by varying the conditions of the oCVD process.<sup>11</sup>

These oCVD PEDOT films, combining high conductivity and high work function, are an ideal fit for application as a buffer layer in oPV cells. In this work, oCVD PEDOT was used as a buffer layer in oPV cells which showed high PCE and large short circuit current ( $J_{\text{sc}}$ ). The performance is similar with that of fully optimized oPV devices utilizing PEDOT:PSS.

## **6.2 Experimental**

### **6.2.1 ITO/glass substrate cleaning**

The ITO/glass substrates were obtained from Thin Film Devices (sheet resistance = 10-100  $\Omega$ /square). The substrates were initially scrubbed with a soft cloth and ultrasonicated in deionized (DI) water with detergent for 30 minutes. The substrates were then ultrasonicated in DI water, 2-propanol, acetone, and methanol for 20 minutes each. Finally, the substrates were treated with oxygen plasma for 5 minutes. The process pressure was 100 mTorr, and oxygen was introduced at a flow rate of 20 sccm. 100 W of 13.56 MHz power source was applied with continuous RF discharge.

### **6.2.2 ITO surface modification<sup>17</sup>**

For surface modification of ITO, 10 mg of 2-thiophene acetic acid (2-TAA) (Aldrich, 97%) was dissolved in 10 ml of ethanol. ITO substrates were submerged in the solution which was stirred with magnetic bar for 2 hrs at 70 °C. After the treatment, the substrates were rinsed with copious ethanol and DI water.

### **6.2.3 oCVD of PEDOT film**

The oCVD process procedure and the reactor configuration are described in detail elsewhere.<sup>11, 13-15</sup> Pre-patterned, ITO-coated glass was used as substrates for the oCVD of PEDOT. Process pressure was maintained between 50 and 100 mTorr and the flow rate of evaporated EDOT monomer was metered through a mass flow controller at 5 sccm. The substrate temperature was varied between 20 – 100 °C by a PID controller. The oxidant, FeCl<sub>3</sub>, was evaporated from a resistively heated crucible at a temperature greater than 300 °C. The total deposition time was 30 minutes. The thickness of oCVD PEDOT films was

maintained at about 25 nm, controlled by the loading amount of FeCl<sub>3</sub> and the deposition time. After the deposition, the film was rinsed with methanol for about 30 minutes to remove any residual oxidant and EDOT monomer.

#### **6.2.4 PEDOT:PSS spin-coating**

For comparison, conventional PEDOT:PSS (AI4083, H.C. Starck) in water solution was filtered through 0.45  $\mu\text{m}$ , spin-coated at 4000 rpm for 60 s, and annealed at 210 °C for 5 minutes to form 50-100 nm thick PEDOT:PSS films on the ITO/glass substrates.

#### **6.2.5 oPV cell fabrication**

oCVD PEDOT coated ITO/glass substrates were transferred to nitrogen-filled glove-box. 30 mg/ml of poly(3-hexylthiophene) (P3HT) (American Dye Source, Inc., MW=20,000-70,000) and [6,6]-phenyl C<sub>61</sub> butyric acid methyl ester (PCBM) (American Dye Source, Inc.) chlorobenzene (Sigma Aldrich) were prepared respectively and mixed with 1:1 volumetric ratio. The mixture solution was applied on PEDOT substrates and spin-coated at 1000 rpm for 60 s, and pre-annealed at 80 °C for 20 minutes to form an 80-90 nm thick P3HT:PCBM layer. After the substrates were cooled down, the substrates were transferred to evaporation chamber and 50 nm of Mg:Ag (9:1) in evaporation ratio film was deposited and capped with 50 nm thick Ag film. The base pressure of evaporation chamber was lower than  $2 \times 10^{-7}$  mTorr. The overlap area between anode and cathode defines the device area, which is 0.0121 cm<sup>2</sup>.

## 6.2.6 Characterization

PEDOT film thickness was measured with a profilometer (Tencor, P-10) and the sheet resistance was measured with a four-point probe (MWP-6, Jandel Engineering Ltd.). The conductivity was calculated from the sheet resistance and measured thickness. The surface morphology of PEDOT film was imaged by AFM (Dimension 3100, Digital Instruments, Ltd.). The sampling size for determining the roughness of PEDOT film was fixed at  $2 \times 2 \mu\text{m}^2$ . The static contact angle was measured within 30 s after placing 2 – 4  $\mu\text{L}$  of deionized water and ethanol droplets on the substrates (VCA2000, AST Inc.). The J-V characteristics of oPV cells were monitored in glove-box using a Keithley 647 source meter and a Lamina LED light engine with emission center 532 nm. The light intensity was calibrated with a standard Si photodiode and was determined to be  $78 \text{ W/cm}^2$ , unless mentioned otherwise. The series and shunt resistance were calculated from the inverse slope of J-V curve at 1.2 V and -0.2 V, respectively.

## 6.3 Results and Discussion

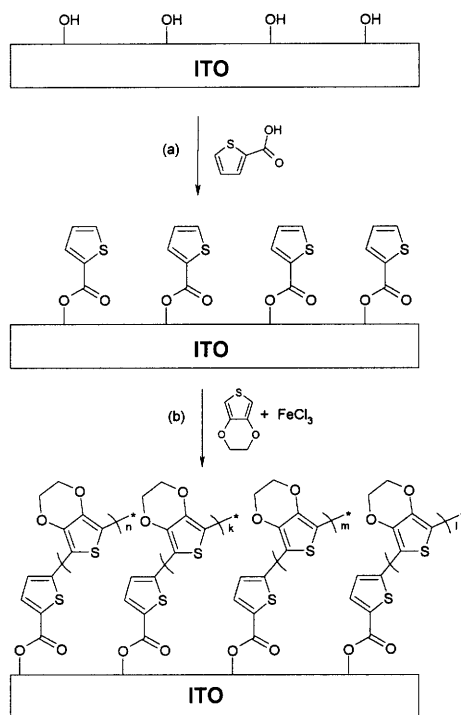
### 6.3.1 ITO surface modification

To optimize oPV cell performance, it is essential to form an ohmic contact between the ITO anode and the organic active layer;<sup>1,3</sup> however, the polar, hydrophilic ITO surface is frequently incompatible with non-polar, hydrophobic organic films. This can lead to an unstable interface, causing high series resistance during device operation, and delamination of the organic layers during device fabrication and operation.<sup>17</sup> In particular, the subsequent device fabrication processes consist of a series of wet chemical steps, in which it is

important to maintain chemical and mechanical stability between the ITO anode and the PEDOT buffer layer.<sup>14</sup> Attempting to stabilize the oCVD PEDOT films on the ITO/glass surface, the ITO/glass was pre-treated with silane coupling agents, well-known for their use on metal oxide surfaces. This is a procedure which we have previously demonstrated greatly enhances adhesion of PEDOT on Si, glass, and alumina surfaces by grafting using phenyl containing trichlorosilane coupling agents.<sup>14</sup> However, this same pre-treatment procedure when applied to ITO surfaces, resulted in oCVD PEDOT films that were easily delaminated from the ITO surface. This clearly indicates that volatile indium hydroxide phase is dominant at the surface of ITO and the ITO surface is different from ordinary stable metal oxide surfaces.

ITO consists of mostly indium oxide but a substantially high amount of tin is intentionally incorporated (up to 10% in indium oxide) for desired electrical and optical properties.<sup>17, 18</sup> This induces a high concentration of oxygen defects and can cause surface instabilities. The indium oxide is easily hydrolyzed with ambient moisture – the hydrolysis constant is  $10^{10}$  times higher than that of tin oxide – and the oxygen defects accelerate the hydrolysis reaction with ambient water vapor, and thereby the ITO surface is dominated by indium hydroxide ( $\text{In}(\text{OH})_3$ ) rather than indium oxide ( $\text{InO}_3$ ).<sup>17</sup> Therefore, the silane coupling agent can be easily removed from the ITO surface, although the silane compounds should form quite strong bonds with indium hydroxide.<sup>19</sup> Contact angle measurements clearly demonstrate this effect. Immediately following oxygen plasma treatment, the ITO surface showed a static water contact angle less than  $10^\circ$ . After 10-minutes of phenyltrichlorosilane (PTCS) treatment, the contact angle increased to  $55^\circ$  which indicates

silane compound coupling on the ITO surface.<sup>14</sup> However, after 10-minutes of ultrasonication cleaning in methanol the contact angle returns to 14°, which implies that most of the silane-coupled surface was removed from the ITO. Subsequent deposition of oCVD PEDOT on this silane treated ITO resulted in easy delamination from the ITO by ultrasonication. This is consistent with the contact angle measurement results showing that silane compounds are not stable coupling agents for ITO surface stabilization.



Scheme 6-1. Schematic procedure of grafting oCVD PEDOT on ITO surface using redox-active coupling agent: (a) surface treatment of oxygen-plasma cleaned ITO surface with 2-TAA for 2 hours at 70 °C in ethanol; (b) subsequent oCVD PEDOT deposition in which the FeCl<sub>3</sub> oxidant can activate both EDOT monomer and the thiophene ring at the surface of ITO to covalently attach PEDOT.

Alternatively, several redox-active molecules containing carboxylic acid, sulfonic acid, and phosphoric acid functionalities are known to chemisorb onto ITO surfaces.<sup>20</sup> For this reason, a thiophene containing carboxylic acid coupling agent, 2-TAA was applied to the ITO surface instead of PTCS. After treatment with 2-TAA, the contact angle increased to 57° which was maintained after ultrasonication. oCVD PEDOT was deposited on top of the 2-TAA treated ITO, and substantially enhanced adhesion was observed (Scheme 6-1).<sup>14</sup> A 10-minute ultrasonication test demonstrated that the oCVD PEDOT film was grafted to the ITO/glass surface. Combined with this mechanical stability, the surface-grafted oCVD PEDOT was not soluble in common organic solvents such as tetrahydrofuran (THF), *N,N'*-dimethylformamide (DMF), ethanol, and acetone. The chemical and mechanical stability offered by the redox-active coupling agent was beneficial for further device fabrication steps and prevented delamination of the following organic layers.

### 6.3.2 oPV Cell Performance

The equivalent circuit for oPV cells is demonstrated in Fig. 6-1a.<sup>21</sup> In general, the oPV cell shows diode-like behavior and the equivalent circuit represents the diode component which is composed of dark current unit ( $J_D$ ) and photo-generated unit ( $J_{ph}$ ) by the light illumination.<sup>21</sup> Assuming that the dark current characteristic is reasonably ideal diode-like,  $J_{ph}$  can be modulated by changing the intensity of light illumination. In general,  $J_{ph}$  is regarded as linear with respect to the light intensity. The degree of non-ideality of

oPV cell can be estimated by the value of the shunt resistance,  $R_{sh}$ , and series resistance,  $R_s$ .<sup>3, 21</sup> For ideal photovoltaic device behavior, both high  $R_{sh}$  and low  $R_s$  are required. In general,  $R_{sh}$  represents the leakage of charge current lost through the device, which is frequently related to imperfections of the film such as pinholes, roughness, and non-uniform surface.<sup>1</sup>  $R_s$  stems from the bulk resistance and/or charge barrier of the active layer and electrodes, contact resistance, and the resistance by the wire connections.<sup>1</sup> To minimize  $R_s$ , Ohmic contact between the electrodes and active layer is highly desirable to facilitate charge injection into the device.<sup>3</sup>

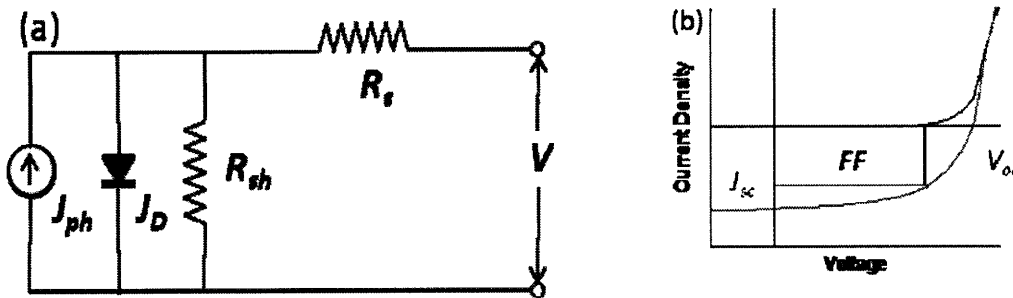


Fig. 6-1. (a) Equivalent circuit for oPV cells.  $J_{ph}$  is photo-generated current density,  $J_D$  is reverse saturation current,  $R_{sh}$  is shunt resistance, and  $R_s$  is series resistance. (b) Schematic of current-voltage characteristics of oPV cells under dark (black) and light (red) illumination.  $J_{sc}$  is short-circuit current,  $V_{oc}$  is open-circuit voltage, and  $FF$  is the fill factor that maximizes the power output from the cell.

In Fig. 6-1b, a characteristic J-V curve for oPV cells is illustrated. The current gain,  $J_{sc}$ , is the short-circuit current at  $V=0$  and the voltage gain,  $V_{oc}$ , is the open-circuit voltage



at  $J=0$  under the light illumination. The maximum possible power obtainable from oPV cells can be described by the fill factor,  $FF^1$ , which is defined as

$$FF = \frac{Power_{max}}{J_{sc} \times V_{oc}} \quad , \quad (1)$$

and the power conversion efficiency (PCE) of oPV cell can be defined as<sup>1</sup>

$$PCE = \frac{FF \cdot (J_{sc} \times V_{oc})}{Power_{light}} \quad . \quad (2)$$

All the necessary components that describe the performance of oPV cells such as  $J_{sc}$ ,  $V_{oc}$ ,  $FF$ ,  $R_s$ , and  $R_{sh}$  can be obtained through analysis of the J-V characteristics of the oPV cells.<sup>22</sup>

P3HT:PCBM BHJ was used as an active layer in the oPV cells used for our studies. The highest efficiency ( $\sim 5\%$  of PCE)<sup>3-5</sup> in polymer-based oPV cells has been realized using the P3HT:PCBM BHJ system as an active layer. P3HT and PCBM are miscible with each other, enabling systematic tuning and optimization of bicontinuous film morphology, leading to the highest PCE in oPV cells to date.<sup>1</sup> The high miscibility enables a 1:1 mixture ratio in P3HT:PCBM BHJ system, which is the optimal for achieving bicontinuous morphology.<sup>4</sup> Moreover, the post-treatment of P3HT:PCBM layer forms nano-scale, bicontinuous phase segregation, maximizing the interfacial area between P3HT and PCBM which greatly facilitates charge and exciton transfer between these donor-acceptor pairs.<sup>5</sup>

Recently, fullerene derivatives such as PCBM are regarded as one of the best performing acceptor materials, to date, for oPV cells. Fullerene derivatives retain exceptionally high electron affinity due to their high lowest unoccupied molecular orbital (LUMO) of about 4 eV.<sup>23</sup> The high LUMO energy level and high electron affinity greatly

stabilize the reduced state of fullerene derivatives, which is extremely difficult to achieve with other organic molecules. Moreover, fullerene derivatives have very high electron mobility of up to  $1 \text{ cm}^2/\text{V}\cdot\text{s}$  in field-effect transistors (FETs).<sup>24</sup> Further functionalization of fullerene derivatives for processibility purposes does not alter the electronic properties substantially, which clarifies the requirements of polymeric donor materials regardless of the functionalized derivatives tethered on fullerene.<sup>8</sup> PCBM is one of the most popular fullerene derivatives and is soluble in many organic solvents such as toluene, chloroform, and chlorobenzene.<sup>3, 4, 8</sup>

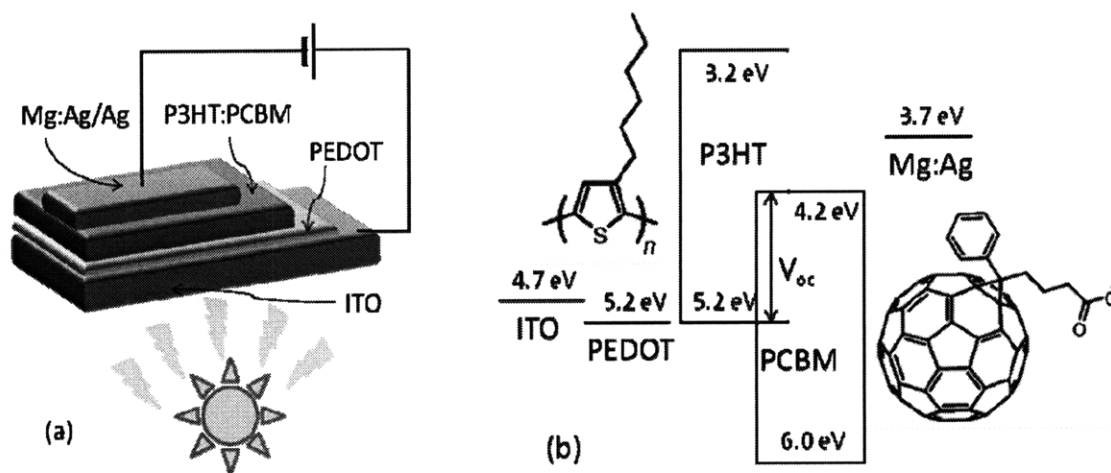


Fig. 6-2. (a) Schematic structure of P3HT:PCBM BHJ oPV cell. (b) Band structure diagram that shows the HOMO and LUMO energy levels of P3HT, PCBM, ITO, PEDOT, and Mg:Ag/Ag. The energy difference between the HOMO of donor and LUMO of acceptor is the theoretical maximum  $V_{oc}$ .

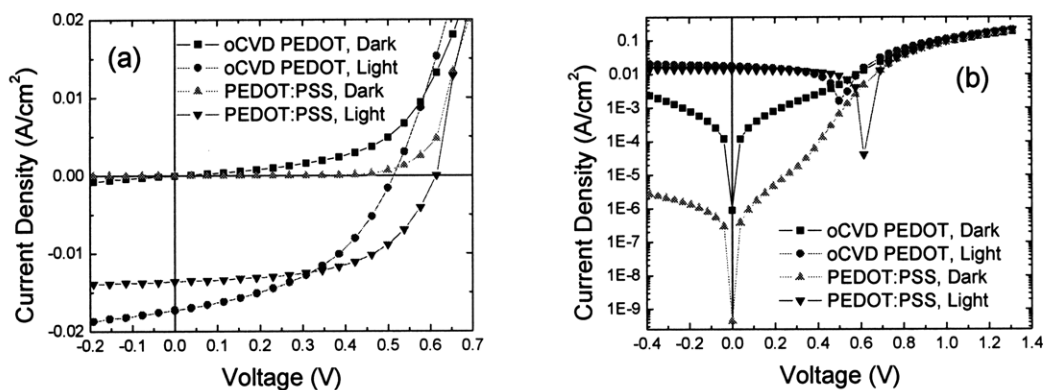


Figure 6-3. J-V curves of ITO/PEDOT/P3HT:PCBM/Mg:Ag/Ag bulk heterojunction (BHJ) device (a) linear scale, (b) logarithmic scale. PEDOT was either PEDOT:PSS or oCVD PEDOT.

Buffer layer	$V_{oc}$ (V)	$J_{sc}$ (mA/cm <sup>2</sup> )	FF	PCE (%)	$R_{sh}$ ( $\Omega \cdot \text{cm}^2$ )	$R_s$ ( $\Omega \cdot \text{cm}^2$ )
oCVD PEDOT	0.54	17	44	5.2	122	1.9
PEDOT:PSS	0.65	14	52	5.8	515	3.0

Table 6-1. Summary of device performance of P3HT:PCBM BHJ oPV cells with different anode buffer layers.  $R_s$  and  $R_{sh}$  were estimated as an inverse slope in the J-V curve at  $V=1.2\text{V}$  and  $0\text{V}$ , respectively.

J-V characteristics and the summary of device performance of oPV cells under the green light illumination ( $78\text{W}/\text{cm}^2$ , wavelength = 532 nm) are shown in Fig. 6-3 and Table 6-1. Since the green light illumination was different from the commonly used AM 1.5G simulated solar illumination light source,<sup>22</sup> it was impossible to compare the device performance of the oPV cells fabricated in this work directly with the literature performance of P3HT:PCBM BHJ oPV cells. However, a relative comparison of device performance of the oPV cell with oCVD PEDOT film (oCVD cell, afterward) and the oPV cell with PEDOT:PSS film (control cell, afterward) was possible.

Compared with the control cell, the oCVD cell showed about four times lower shunt resistance and 30 % lower series resistance. The J-V behavior of the oCVD cell slightly deviated from ideal diode behavior. The estimated rectification ratio for the oCVD cell (calculated at  $V = 0.5\text{ V}$  to  $V = -0.5\text{V}$ ) was order  $10^2$  which is low compared with  $\sim 10^3$  for the control cell,. Accordingly, the  $V_{oc}$  of the oCVD cell was  $\sim 0.1\text{ V}$  lower than that of the control cell and the fill factor was slightly lower as well. However, the decrease in series resistance in the oCVD cell facilitates charge injection and leads to an increase in  $J_{sc}$ . Overall, the PCE difference between the oCVD cell and the control cell was less than 1%, which is quite promising considering the process parameters of the oCVD PEDOT deposition were not yet optimized for subsequent device performance. The decrease in series resistance can be explained by many advantageous properties of the oCVD PEDOT buffer layer. oCVD PEDOT is about 100 times more conductive than PEDOT:PSS film, which directly reduces the series resistance of the buffer layer. Moreover, the surface of PEDOT:PSS film favors the PSS-rich state, which can act as an insulating layer and

increase the series resistance. Secondly, oCVD PEDOT is hydrophobic, which is favorable for interaction with the hydrophobic P3HT:PCBM layer. Additionally, the hydrophobic PEDOT film interacts favorably with the chlorobenzene solvent used for applying P3HT:PCBM, ensuring good contact of P3HT:PCBM layer with the oCVD PEDOT.<sup>1</sup> Contrastingly, PEDOT:PSS is very hydrophilic and does not favor organic solvents, such as chlorobenzene,<sup>5</sup> which can lead to interfacial defects in the resulting oPV cell. Finally, mobile Cl<sup>-</sup> dopants in oCVD PEDOT layer might facilitate charge mobility in the oPV cell. Compared with the practically immobile PSS dopants, Cl<sup>-</sup> dopants could easily diffuse into the P3HT:PCBM active layer under the applied bias, which could partially dope the interface between oCVD PEDOT and P3HT:PCBM layer and enhance the charge mobility.<sup>25</sup>

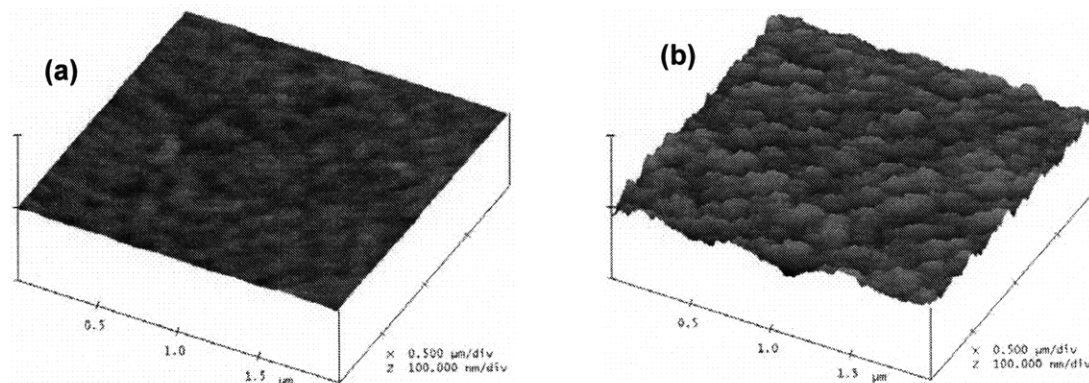


Figure 6-4. AFM image of (a) PEDOT:PSS film and (b) oCVD PEDOT film coated on Si wafer. The scanned area was  $2 \times 2 \mu\text{m}^2$  and height scale is 100 nm. The calculated root-mean squared roughness of PEDOT:PSS and oCVD PEDOT was 0.34 nm and 5.4 nm, respectively.

Greatly decreased shunt resistance and non-ideal J-V characteristics are responsible for reduced PCE and lowered  $V_{oc}$ . One of the main reasons for this shunt resistance reduction is the roughness of the oCVD PEDOT film compared with the PEDOT:PSS film. Atomic force microscopy (AFM) images of PEDOT:PSS and oCVD PEDOT films are shown in Fig. 6-4. Compared with the spin-coated PEDOT:PSS film, which are known to be pin-hole free,<sup>10</sup> the oCVD PEDOT film shows more than 10 times higher roughness. Although this film roughness is very small relative to the thickness of P3HT:PCBM active layer (~90 nm), the rough surface characteristics can cause a non-uniform electric field to the P3HT:PCBM active layer that can lead to charge leakage paths.<sup>10</sup> Although the rough surface can induce interfacial defects in the oCVD oPV cell, the much larger surface area of oCVD PEDOT films can also enhance the charge injection efficiency and there should be a trade-off in the buffer layer roughness. Similarly, the  $Cl^-$  ions at the interface of the oCVD PEDOT and P3HT:PCBM layers can facilitate charge injection; however, the ions can also act as charge traps in the active layer leading to non-ideal J-V characteristics in the oPV cell.<sup>25</sup> Further device optimization and controlling of oCVD parameters is required for maximized PCE from oCVD cells.

## 6.4 Conclusion

oCVD PEDOT was successfully applied as a buffer layer in efficient oPV cells. oCVD PEDOT was grafted to the ITO anode surface using redox-active carboxylic acid containing 2-TAA as a coupling agent. The ITO surface was highly susceptible to

hydrolysis reaction and the surface was not stable with common silane-based coupling agents. Contact angle measurement before and after 2-TAA treatment confirmed the tight chemisorption of this coupling agent on the ITO surface. On top of this surface, oCVD PEDOT was deposited and the PEDOT film showed enhanced adhesion to the ITO surface compared with similar silane-treated surfaces. With this interface stabilized, oPV cells were fabricated and the device performance was measured and compared with a conventional control cell using a PEDOT:PSS buffer layer. Although the oCVD cell showed low shunt resistance and non-ideal J-V behavior compared with the control cell, decreased series resistance in the oCVD cell ultimately lead to a comparable device with PCE of 5.2% under green light illumination. The hydrophobicity and stabilized interface formed with oCVD PEDOT play an important role in the observed high efficiency. For maximized oPV cell PCE using oCVD PEDOT as a buffer layer, further oCVD PEDOT optimization is required with respect to controlling surface roughness and surface concentration of Cl<sup>-</sup> ions.

## **Acknowledgement**

This research was supported by the U.S. Army through the Institute for Soldier Nanotechnologies, under Contract DAAD-19-02-D-0002 with the U.S. Army Research Office.

## **References**

1. Thompson, B.C.; Frechet, J.M.J. Organic photovoltaics - Polymer-fullerene composite solar cells. *Angewandte Chemie-International Edition* **2008** *47*, 58-77.
2. Tang, C.W. 2-LAYER ORGANIC PHOTOVOLTAIC CELL. *Applied Physics Letters* **1986** *48*, 183-185.
3. Ko, C.J.; Lin, Y.K.; Chen, F.C.; Chu, C.W. Modified buffer layers for polymer photovoltaic devices. *Applied Physics Letters* **2007** *90*, 3.
4. Li, G.; Shrotriya, V.; Huang, J.S.; Yao, Y.; Moriarty, T.; Emery, K.; Yang, Y. High-efficiency solution processable polymer photovoltaic cells by self-organization of polymer blends. *Nature Materials* **2005** *4*, 864-868.
5. Ma, W.L.; Yang, C.Y.; Gong, X.; Lee, K.; Heeger, A.J. Thermally stable, efficient polymer solar cells with nanoscale control of the interpenetrating network morphology. *Advanced Functional Materials* **2005** *15*, 1617-1622.
6. Scharber, M.C.; Wuhlbacher, D.; Koppe, M.; Denk, P.; Waldauf, C.; Heeger, A.J.; Brabec, C.L. Design rules for donors in bulk-heterojunction solar cells - Towards 10 % energy-conversion efficiency. *Advanced Materials* **2006** *18*, 789-+.
7. Halls, J.J.M.; Walsh, C.A.; Greenham, N.C.; Marseglia, E.A.; Friend, R.H.; Moratti, S.C.; Holmes, A.B. EFFICIENT PHOTODIODES FROM INTERPENETRATING POLYMER NETWORKS. *Nature* **1995** *376*, 498-500.
8. Brabec, C.J.; Sariciftci, N.S.; Hummelen, J.C. Plastic solar cells. *Advanced Functional Materials* **2001** *11*, 15-26.
9. Gunes, S.; Neugebauer, H.; Sariciftci, N.S. Conjugated polymer-based organic solar cells. *Chemical Reviews* **2007** *107*, 1324-1338.



10. Kirchmeyer, S.; Reuter, K. Scientific importance, properties and growing applications of poly(3,4-ethylenedioxythiophene). *J Mater Chem* **2005** *15*, 2077-2088.
11. Im, S.G.; Olivetti, E.A.; Gleason, K.K. Doping level and work function control in oxidative chemical vapor deposited poly (3,4-ethylenedioxythiophene). *Applied Physics Letters* **2007** *90*, 152112.
12. Greczynski, G.; Kugler, T.; Keil, M.; Osikowicz, W.; Fahlman, M.; Salaneck, W.R. Photoelectron spectroscopy of thin films of PEDOT-PSS conjugated polymer blend: A mini-review and some new results. *Journal of Electron Spectroscopy and Related Phenomena* **2001** *121*, 1-17.
13. Im, S.G.; Gleason, K.K. Systematic Control of the Electrical Conductivity of Poly (3, 4-ethylenedioxythiophene) via Oxidative Chemical Vapor Deposition (oCVD) *Macromolecules* **2007** *40*, 6552-6556.
14. Im, S.G.; Yoo, P.J.; Hammond, P.T.; Gleason, K.K. Grafted Conducting Polymer Films for Nano-patterning onto Various Organic and Inorganic Substrates by Oxidative Chemical Vapor Deposition *Advanced Materials* **2007** *19*, 2863-2867.
15. Lock, J.P.; Im, S.G.; Gleason, K.K. Oxidative chemical vapor deposition of electrically conducting poly(3,4-ethylenedioxythiophene) films. *Macromolecules* **2006** *39*, 5326-5329.
16. Gates, S.M. Surface Chemistry in the Chemical Vapor Deposition of Electronic Materials. *Chemical Reviews* **1996** *96*, 1519-1532.

17. Armstrong, N.R.; Carter, C.; Donley, C.; Simmonds, A.; Lee, P.; Brumbach, M.; Kippelen, B.; Domercq, B.; Yoo, S.Y. Interface modification of ITO thin films: organic photovoltaic cells. *Thin Solid Films* **2003** *445*, 342-352.
18. Fan, J.C.C.; Goodenough, J.B. X-RAY PHOTOEMISSION SPECTROSCOPY STUDIES OF SN-DOPED INDIUM-OXIDE FILMS. *Journal of Applied Physics* **1977** *48*, 3524-3531.
19. Cui, J.; Wang, A.; Edleman, N.L.; Ni, J.; Lee, P.; Armstrong, N.R.; Marks, T.J. Indium tin oxide alternatives - High work function transparent conducting oxides as anodes for organic light-emitting diodes. *Advanced Materials* **2001** *13*, 1476-+.
20. Paniagua, S.A.; Hotchkiss, P.J.; Jones, S.C.; Marder, S.R.; Mudalige, A.; Marrikar, F.S.; Pemberton, J.E.; Armstrong, N.R. Phosphonic acid modification of indium-tin oxide electrodes: Combined XPS/UPS/contact angle studies. *Journal of Physical Chemistry C* **2008** *112*, 7809-7817.
21. Yoo, S.; Domercq, B.; Kippelen, B. Intensity-dependent equivalent circuit parameters of organic solar cells based on pentacene and C-60. *Journal of Applied Physics* **2005** *97*, 9.
22. Yip, H.L.; Hau, S.K.; Baek, N.S.; Ma, H.; Jen, A.K.Y. Polymer solar cells that use self-assembled-monolayer-modified ZnO/Metals as cathodes. *Advanced Materials* **2008** *20*, 2376-+.
23. Allemand, P.M.; Koch, A.; Wudl, F.; Rubin, Y.; Diederich, F.; Alvarez, M.M.; Anz, S.J.; Whetten, R.L. 2 DIFFERENT FULLERENES HAVE THE SAME CYCLIC

- VOLTAMMETRY. *Journal of the American Chemical Society* **1991** *113*, 1050-1051.
24. Singh, T.B.; Marjanovic, N.; Matt, G.J.; Gunes, S.; Sariciftci, N.S.; Ramil, A.M.; Andreev, A.; Sitter, H.; Schwodiauer, R.; Bauer, S. High-mobility n-channel organic field-effect transistors based on epitaxially grown C-60 films. *Organic Electronics* **2005** *6*, 105-110.
25. Romero, D.B.; Schaer, M.; Zuppiroli, L.; Cesar, B.; Francois, B. EFFECTS OF DOPING IN POLYMER LIGHT-EMITTING-DIODES. *Applied Physics Letters* **1995** *67*, 1659-1661.

## Chapter Seven

### A DIRECTLY PATTERNABLE, CLICK- ACTIVE POLYMER FILM VIA INITIATED CHEMICAL VAPOR DEPOSITION (ICVD)

**Sung Gap Im**, Byeong-Su Kim, Long Hua Lee, Wyatt E. Tenhaeff, Paula T. Hammond, and Karen K. Gleason, 'A Directly Patternable, "Click-Active Polymer Film via Initiative Chemical Vapor Deposition (iCVD)', *Macromolecular Rapid Communications*, 29(2008), 1648-1654.

## **Abstract**

A new one-step synthetic pathway is demonstrated for depositing the “click chemistry” active polymer coating of poly (propargyl methacrylate) (PPMA) via initiated chemical vapor deposition (iCVD) process utilizing a commercially available monomer. The complete retention of the pendent acetylene groups in PPMA was clearly observed in Fourier Transform Infrared spectroscopy (FTIR) and X-ray photoelectron spectroscopy (XPS) spectra. Using the proper surface treatment, iCVD PPMA can be chemically grafted onto the substrate, which provides sufficient stability to enable PPMA film to be click functionalized with various azide conjugate. The click functionalization was successfully demonstrated using azido-fluorescent dye onto patterned PPMA film in micron scale and the fluorescent dye was precisely aligned with the patterned PPMA film. Moreover, The iCVD PPMA itself exhibits e-beam sensitivity and hence can be directly patterned via electron beam (e-beam) lithography without requiring a conventional resist layer. Direct e-beam exposure of this multifunctional iCVD layer, a 200 nm pattern, and QD particles were selectively conjugated on the substrates via click chemistry. Combined with the advantages which iCVD can provide, the functional PPMA films can be utilized in various surface modification applications.

**Key words:** initiated chemical vapor deposition (iCVD), poly (propargyl methacrylate(PPMA), click chemistry, patterning, e-beam, fluorescence microscopy.

## 7-1 Introduction

Nanopatterned functional surfaces are excellent vehicles for exploring the interfacial interactions of biological components and can be utilized for applications including controlled drug release, biosensors, and artificial skin.<sup>1-3</sup> The desire for immobilization onto specific surface sites with high adhesion and high selectivity has motivated widespread interest in “click” chemistry, which quickly and selectively creates covalent linkages. One of the most efficient and versatile click reactions is the Huisgen 1,3-dipolar cycloaddition<sup>4</sup> in which the reaction of azides and terminal alkyne groups are catalyzed by Cu(I). These Sharpless-type click reactions display fast reaction rates, are highly regioselective, and can be performed in various solvents, including water at biologically relevant temperatures (25 – 70 °C).<sup>5</sup>

The high reactivity of the desired azide or alkyne groups presents challenges for both the synthesis and patterning of click active surfaces. Multistep synthesis has been successful. For example, a self-assembled monolayer initially formed with bromo-termination was subsequently converted to the azido-terminated functionality.<sup>6</sup> Alternatively, non-commercially available monomers have been synthesized for subsequent polymerization. For example, alkyne-functionalized paracyclophane monomers were synthesized and subsequently polymerized by chemical vapor deposition (CVD) process to obtain clickable surface.<sup>7</sup> Similarly, an azido-functionalized methacrylate was synthesized for use in an atom transfer radical polymerization (ATRP).<sup>8</sup>

The direct patterning of clickable surfaces is also challenging due to the high reactivity of clickable functionalities. For example, azides can be easily photolyzed with

ultraviolet light (UV).<sup>9</sup> The undesirable attack of alkyne functionality by the radicals generated in the course of polymerization also leads to highly branched and crosslinked polymers.<sup>8</sup> For these reasons, the clickable surface had been difficult to pattern by traditional lithographic approaches. Hence most of patterned click functionalization were focused to areally confined click reaction rather than the patterning of clickable surface itself. For instance, microcontact printing of alkynes was applied on azide surface to form 5  $\mu\text{m}$  stripe pattern.<sup>6, 7</sup> Alternatively, electrochemical activation of Cu(I) catalyst was selectively applied on Au electrode with azide self-assembled monolayers (SAMs) with the separation of 10  $\mu\text{m}$  between the two electrodes.<sup>10</sup>

Synthesis of click active surface which could be directly patterned by irradiation would enable traditional lithography to be employed for the creation of high resolution patterns. In this report, poly (propargyl methacrylate) (PPMA) films were successfully synthesized by initiated CVD (iCVD) in one step from the commercially available monomer. The mild temperatures of the iCVD process permit retention of delicate functional groups.<sup>11</sup> Feature sizes of 200 nm were achieved by direct electron beam (e-beam) lithography. As the PPMA itself is sensitive to e-beam exposure, the need a conventional resist layer is avoided. Grafting of the iCVD PPMA layer to the substrate was achieved in order to obtain mechanical and chemical stability of polymer films for this nanometer scale resolution. Click chemistry employing the pendant alkyne of the PPMA was demonstrated before and after patterning. Thus, iCVD PPMA exhibits the dual functions of “clickability” and direct e-beam patternability at the nanometer scale.

## 7.2 Experimental

### 7.2.1 iCVD

The procedure of iCVD process was described in detail elsewhere.<sup>12</sup> PMA (Alfa Aesar, 98 %) and tert-butyl peroxide (Aldrich, 98 %) were purchased and used without further purification. PMA and initiator were vaporized at room temperature and introduced into the iCVD chamber at a flow rate of approximately 4 sccm and 1.5 sccm, respectively. The flow rates were controlled with mass flow controllers, MKS 1490A and MKS 1152C. The polymerization reaction was initiated with the filament at 280 °C. The process pressure was 800 mTorr - controlled by PID controllable butterfly valve (MKS 248 flow control valve). Film thicknesses were monitored *in situ* by interferometry; approximately 200 nm of the PPMA film was deposited in 20 min.

### 7.2.2 Plasma polymerization

Plasma polymerized PPMA film was obtained in parallel plate chamber with 150 mm diameter electrodes. The process pressure was 100 mTorr, and PMA was introduced at a flow rate of 5 sccm. 5 W of 13.56 MHz power source was applied with continuous RF discharge. After 10 minutes, plasma polymerized PPMA film was obtained with a thickness of 100 nm.

### 7.2.3 Surface grafting

0.5 ml of TCVS (from Aldrich, 97 %) was placed in the dessicator. Oxygen plasma treated Si wafer was exposed to TCVS vapor at 25 °C for less than 5 minutes. The process



pressure in the dessicator was 100 mTorr. Exactly the same iCVD conditions were applied to the silane treated Si wafer for grafted PPMA on Si wafer.

#### **7.2.4 Click chemistry**

4 mM of N<sub>3</sub>-coumarin (AnaSpec Inc., 97%), 1 mM of copper(II) sulfate, and 2 mM of sodium ascorbate were solubilized in 10 ml of DMF. A piece of grafted PPMA films (100 nm thick) on Si wafer was placed into the solution and stirred by magnetic bar at 25 °C for 16 hours. After the reaction, the sample was rinsed with DMF several times and dried with nitrogen purge. Ten minutes of ultrasonication was applied to the N<sub>3</sub>-coumarin functionalized PPMA film to remove physically adsorbed, unreacted reaction residue. Maintaining the same reaction conditions of N<sub>3</sub>-coumarin except for replacing the N<sub>3</sub>-coumarin with azido-biotin (Aldrich Inc.), resulted in biotin-functionalized pPA surface. The QD conjugation was achieved by soaking biotin-functionalized substrates in 1.0 mM of streptavidin-derivatized QD particle (Qdot<sup>®</sup> 605 streptavidin conjugate, Invitrogen) in water solution for 30 minutes. Afterward, the physically attached QDs were rinsed with excessive water and ultrasonicated for 10 minutes.

#### **7.2.5 Photolithography**

OCG 825 was used as the photoresist. After spin coated to form 1 μm thick film, it was soft-baked at 90 °C. The film was exposed to UV light with the photomask and developed with OCG 934, as the developer. On top of the patterned photoresist layer,

PPMA was deposited via iCVD technique and the PPMA film on photoresist pattern was lifted off via ultrasonication for 5 minutes in acetone.

### **7.2.6 e-beam lithography**

e-beam was directly irradiated on top of iCVD PPMA films, and Negative tone patterning was obtained at a dose of 50 mC/cm<sup>2</sup>. Developing for 90 s with DMF completes 200 nm feature size of PPMA pattern.

### **7.2.7 Measurement**

FTIR spectra were obtained via Nexus 870, Thermo Electron Corporation. XPS was done on a Kratos Axis Ultra spectrometer equipped with a monochromatized Al K $\alpha$  source. The measured XPS spectra were non-linear square fitted for quantitative analyses. The e-beam pattern was examined by optical microscopy (Olympus, Model CX41) with the maximum magnification of  $\times 1000$ . Fluorescence images were also gathered using AxioSkop 2 MAT, Zeiss with the excitation wavelength of 365 nm for N<sub>3</sub>-coumarin and 605 nm for red QD. AFM image was obtained using DI3100, Digital Instruments.

## **7.3 Results and Discussion**

Fig. 7-1a and 1b represent the Fourier transform infrared (FTIR) spectrum of PMA monomer and iCVD PPMA, respectively. Both spectra display the characteristic bands for alkynes – C-H stretch peak around 3200 cm<sup>-1</sup> and C $\equiv$ C stretch peak around 2100 cm<sup>-1</sup>.<sup>13</sup> The nearly identical intensity of the two FTIR peaks distinctly indicates the retention of the

pendant “click-active” alkyne functionalities during the iCVD polymerization process. In contrast, the film resulting from plasma polymerization of PMA contains virtually no characteristic alkyne peaks in FTIR spectra, which demonstrates that the alkynes are completely destroyed by the applied plasma (Fig. 7-1c). Instead, the increase of  $sp^3$  C-H peak intensity around  $3000\text{ cm}^{-1}$  in Fig. 7-1c infers that the decomposed alkynes are converted to click-inert alkyl groups. The contrast between Figs. 7-1b and 1c clearly displays the non-destructive characteristics of iCVD process relative to the plasma polymerization.

The C=C stretch peak around  $1600\text{ cm}^{-1}$  observed for the PMA monomer (Fig. 7-1a) disappears in iCVD PPMA (Fig. 7-1b), which clearly represents that the PMA monomer fed into the chamber is converted to PPMA polymer film on Si wafer by the iCVD vinyl polymerization process.<sup>14</sup> The increase of the  $sp^3$  C-H peak intensity around  $3000\text{ cm}^{-1}$  in Fig. 7-1b also supports the radical polymerization via iCVD process.

Chemical and mechanical stability in solvents is essential for subsequent click functionalization and patterning processes because they consist of a series of wet chemical steps. For this purpose, PPMA film was covalently grafted onto the Si wafer surface by using pre-treatment of a vinyl containing silane coupling agent, trichlorovinyl silane (TCVS) and subsequent iCVD process to achieve solvent resistance of the polymer layer.<sup>15</sup> Ultrasonication and tape tests demonstrated the greatly enhanced adhesion of iCVD PPMA grafted on to the Si surfaces (data not shown).<sup>15</sup> The surface grafted PPMA was not soluble in common organic solvents such as tetrahydrofuran (THF), *N,N'*-dimethylformamide

(DMF), and acetone. No distinctive change was observed in FTIR spectra between before and after the solvent exposure.

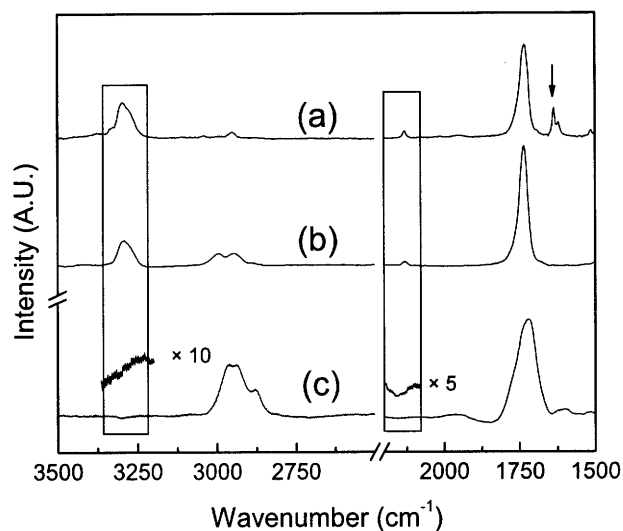


**Figure 7-1.** FTIR spectra of (a) PMA monomer, (b) iCVD PPMA, and (c) plasma polymerized PPMA. Rectangular regions represent C-H stretch peak in alkyne group (around  $3200\text{ cm}^{-1}$ ) and  $\text{C}\equiv\text{C}$  stretch peak in alkyne group (around  $2100\text{ cm}^{-1}$ ). The arrow represents  $\text{C}=\text{C}$  stretch peak in the monomer (a) (around  $1600\text{ cm}^{-1}$ ) which, due to vinyl polymerization, is absent in the iCVD film (b). The iCVD film (b) clearly returns clickable alkyne group while this functionality is destroyed by plasma polymerization (c).

The X-ray photoelectron spectroscopy (XPS) spectra of iCVD PPMA are shown in Fig.7-2 and 7-3a. As expected, the XPS survey scan (Fig.7-3a, bottom) reveals only oxygen and carbon in a ratio of 23:77, which corresponds within 1% error of the theoretical O:C ratio of 2:7. The C 1s high resolution scan spectrum (Fig. 7-2a) was non-linear least

squares fit using four Gaussian peaks, providing quantitative analysis that also matched with the known chemical structure of PPMA.<sup>16</sup> The calculated ratio of each carbon (C1:C2:C3:C4) was 57.5:14.1:14.3:14.2, which is very close to the theoretical ratio of 4:1:1:1. Of particular interest for a “clickable” surface, is the intense peak at 284.8 eV corresponds to the carbons in alkyne group and  $\alpha$ -methyl, methylene backbone. Thus XPS confirms that the alkyne groups identified in the bulk iCVD PPMA film by FTIR, are also present at the surface where their reactivity is desired. The O 1s high resolution scan spectrum can also be non-linear least squares fit to two independent peaks corresponding to the two distinct oxygen sites in acrylate group. The calculated ratio was 52:48 which approximately matches with theoretical ratio of 1:1. Therefore, the XPS analysis distinctly displays that the surface composition of iCVD PPMA film is fully consistent with the expected molecular structure of PPMA. Moreover, these XPS results corroborate the FTIR results and support the hypothesis that most of the reactive alkyne functionality survived the iCVD polymerization reaction.

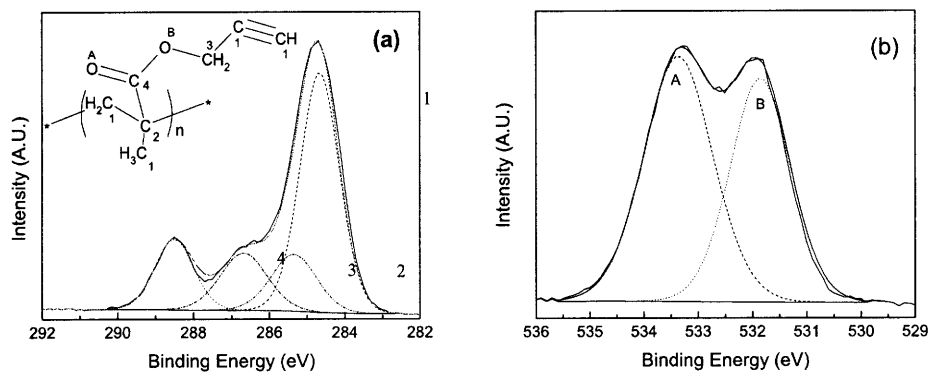
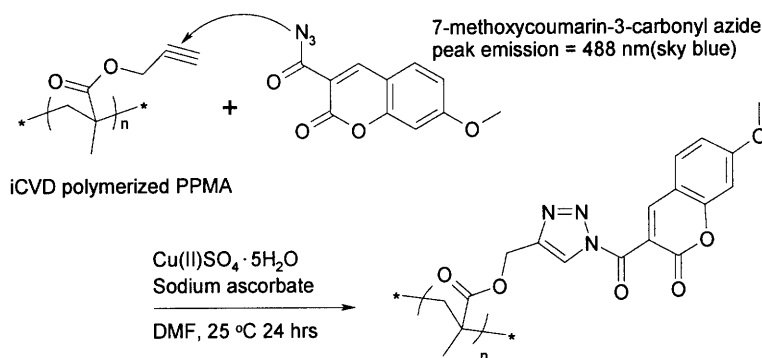


**Figure 7-2.** XPS high resolution spectra of PPMA; (a) C 1s and (b) O 1s, respectively. The chemical structure is labeled with numbers, providing the assignment for (a), and capital letters, which correspond to the assignment for (b).



**Scheme 7-1.** Click reaction between iCVD PPMA and azido functionalized fluorescent dye, N<sub>3</sub>-coumarin.

Onto this alkyne surface, click functionalization was applied by introducing azide conjugates. The click reactivity of the PPMA surface was assessed using a surface sensitive spectroscopy, X-ray photoelectron spectroscopy (XPS) and a fluorescence microscopy measurement of a fluorescent dye functionalized PPMA surface by click reaction. For this purpose, an azido-derivatized blue fluorescent dye, 7-methoxycoumarin-3-carbonyl azide (N<sub>3</sub>-coumarin, peak emission = 488 nm) was chosen as a conjugate. The Huisgen 1,3-dipolar cycloaddition between N<sub>3</sub>-coumarin and iCVD PPMA was performed with copper(II) sulfate and excess of sodium ascorbate in DMF solvent. Sodium ascorbate reduces copper(II) sulfate to yield Cu(I) ions that catalyze the cycloaddition reaction to form triazole linkage between iCVD PPMA and N<sub>3</sub>-coumarin (scheme 7-1). After the

reaction, repeated rinsing and ultrasonication were applied to eliminate all physisorbed species during the functionalization step. The grafting of iCVD PPMA to the substrate turned out to be a critical step for preventing the iCVD layer from delaminating during click functionalization, which enables the use of various organic solvents and purification with ultrasonication. XPS was applied on iCVD PPMA film before and after the N<sub>3</sub>-coumarin functionalization. A new indicative nitrogen peak around 400 eV was detected in N<sub>3</sub>-coumarin functionalized iCVD PPMA surface in the XPS survey scan spectrum, which was absent in the XPS scan of freshly prepared iCVD PPMA (Fig. 7-3a). Since N<sub>3</sub>-coumarin does not contain nitrogen except at the azido group, the nitrogen at the polymer surface originated from the “click”-linkage of triazole group. Therefore, the appearance of new nitrogen peak indicates that the cycloaddition of N<sub>3</sub>-coumarin was successfully achieved. The N 1s high resolution scan XPS spectrum also confirms the attachment of N<sub>3</sub>-coumarin on iCVD PPMA surface via click chemistry (Fig. 7-3b). The nitrogen peak were non-linear least squares fit to two peaks, which were assigned as the amide bond in triazole (1 in Fig. 7-3a) at 400.8 eV and two N=N bond in triazole (2 in Fig. 7-3a) at 399.2 eV.<sup>16</sup> The ratio of peak areas was calculated into approximately 1:2, which is consistent with the chemical structure N<sub>3</sub>-coumarin functionalized PPMA.<sup>17</sup>

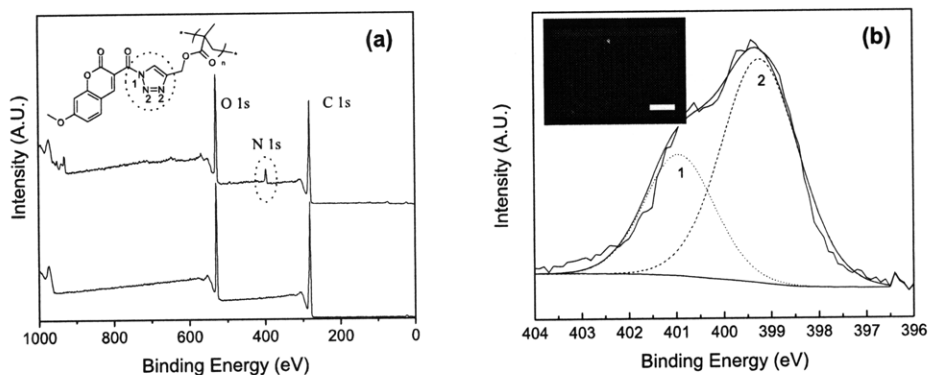


**Figure 7-3.** XPS (a) Survey scan of PPMA (bottom) and N<sub>3</sub>-coumarin functionalized PPMA films (top) and (b) high resolution N 1s scan data of N<sub>3</sub>-coumarin functionalized PPMA films via click reaction, respectively. Dotted circles in (a) highlight the newly formed N 1s peak by click addition reaction. Inset in (b) represents a fluorescence microscope image of patterned PPMA film click-functionalized with N<sub>3</sub>-coumarin. Scale bar in the inset represents 20 μm. Each superscripted numbers in chemical formula of click functionalized PPMA in (a) corresponds to peaks assigned in XPS N 1s spectrum in (b).

The chemical selectivity of the click reaction with iCVD PPMA was assessed by applying clickable fluorescent dye onto pre-patterned PPMA. To pattern PPMA, a conventional patterning process of photolithography was applied on PPMA.<sup>15</sup> To minimize the potential damage on alkyne functionality in PPMA film during the photolithography process, only photoresist (PR) layer was pre-patterned first. Subsequently, iCVD PPMA was grafted on PR-patterned Si wafer. The lift-off of patterned PR with acetone completes the patterning of PPMA film. The covalently grafted PPMA film was mechanically and



chemically strong enough to enable acetone-based lift-off process without damaging the click active alkyne functionality. A well-defined 2  $\mu\text{m}$  size line pattern was easily obtained according to the patterned PR film. The same click chemistry was applied onto this patterned PPMA surface, and fluorescence microscope image (inset in Fig. 7-3b) shows a sharp contrast of fluorescence from the blue  $\text{N}_3$ -coumarin dye. The fluorescence image was precisely aligned with the PPMA pattern. No fluorescence image degradation was observed after 10 minutes of ultrasonication, confirming that the binding of fluorescent dye on PPMA film is covalently bound rather than just physically adsorbed.

Furthermore, iCVD PPMA film could also be patterned with e-beam lithography. PPMA showed an especially advantageous property that the film itself was e-beam sensitive, and indeed a well-defined pattern in nanometer scale was easily obtained with the e-beam irradiation directly onto iCVD PPMA film. The atomic force microscopy (AFM) image of the e-beam patterned iCVD PPMA film (Fig. 7-4b) shows that the e-beam irradiated area was developed out with DMF for 90 ~ 120 s, and 200 nm stripe patterns were obtained with the dosage of 50  $\text{mC}/\text{cm}^2$  at 50 keV acceleration voltage. The e-beam sensitivity of PPMA allows an easy fabrication of nano-pattern without the use of additional e-beam resist, which substantially simplifies the whole patterning process (Fig. 7-4a-B) compared with a standard e-beam lithography procedure (Fig. 7-4a-A). Moreover, the direct patterning process can also remove the potential occasion of damaging clickable alkyne group from e-beam resist involved process, such as thermal annealing, organic solvents of e-beam resist in spin coating and resist removal. In addition, the developer of direct e-beam patterning, DMF is also widely used as an organic solvent for the click

chemistry and the developer does not destroy the patterned PPMA surface any further. Therefore, if DMF is chosen as a solvent for click reaction of e-beam patterned PPMA, the development process can also be directly included in click reaction step so that the development and click reaction occurs simultaneously and the patterning-functionalization process can be further simplified.

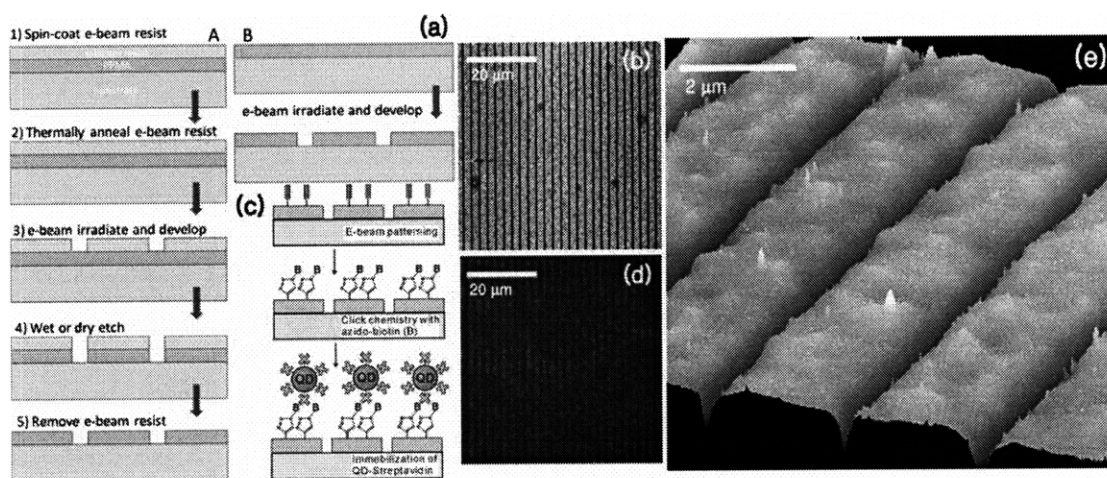


Figure 7-4. (a) Schematic patterning procedure of standard e-beam lithography (A) and direct e-beam patterning with e-beam sensitive PPMA film (B) and (b) AFM image of e-beam patterned iCVD PPMA. (c) Schematic procedure of QD-streptavidin immobilization onto the patterned polymer film by biotin-streptavidin binding via click reaction. (d) fluorescence microscope image and (e) Enlarged 3-D AFM image of e-beam patterned PPMA film conjugated with QD particles via click chemistry, respectively.

The e-beam sensitivity of PPMA film is attributable to the methacrylate backbone of PPMA. It is well known that a variety of methacrylate polymers such as poly (methyl

methacrylate) (PMMA), poly (2-hydroxyethyl methacrylate), and poly (methyl methacrylic acid) are known to retain e-beam patternability.<sup>18-20</sup> Previously, negative-tone e-beam patterning of iCVD poly (glycidyl methacrylate) films was also reported.<sup>19</sup> As one of the methacrylate polymers, iCVD PPMA also displayed e-beam sensitivity. However, compared with one of the standard e-beam resist, PMMA, PPMA requires about 10 ~ 50 times higher e-beam dose for the same level pattern resolution. We suspect that during e-beam exposure some of the alkyne groups in PPMA cross-link simultaneously with the depolymerization of methacrylate group. Hence, a higher dose of e-beam is required as compared with acrylate resist with inert methyl side group.

On top of 200 nm line patterned iCVD PPMA surface using e-beam lithography, larger QD particles ( $\lambda_{em} = 605$  nm, ca 15 nm) were used to assess the pattern fidelity in click functionalization. First of all, azido-derivatized biotin was conjugated on pre-patterned iCVD PPMA substrates by click reaction. Afterward, streptavidin-functionalized QD particles are spread onto the biotin-functionalized PPMA film and strong biotin-streptavidin binding was successfully formed in 30 minutes (Fig. 7-4c). After the QD conjugation, a 10-minute ultrasonication was applied to remove physically adsorbed QDs and other unreacted residue. The click functionalization of e-beam patterned PPMA film could be clearly observed by using fluorescence microscopy and AFM (Fig. 7-4d and e). The fluorescence from click functionalized QDs is overlapped exactly with the pre-patterned e-beam pattern of PPMA film (Fig. 7-4d). Similarly, the surface of unexposed area from e-beam irradiation shows a high surface density of QDs, which appear shown as white dots in the AFM image (Fig. 7-4e). On the other hand, negligible amount of QD

particles were observed on the etched out area. This obvious contrast in QD particle density on the surface is totally consistent with the fluorescence microscope image. Same as preceding, the mechanical and chemical stability gifted by grafting agent again ensures the reliable e-beam patterning and click reaction of the iCVD PPMA. The dual functionality of clickability and e-beam sensitivity in the iCVD PPMA can offer a powerful tool for various selective surface modification applications.

#### **7.4 Conclusion**

In conclusion, a new rapid synthetic pathway for depositing the click-active polymer coating of PPMA was obtained via a simple one-step iCVD process from a commercially available monomer, PMA. The pendent alkyne groups in PPMA were clearly observed in FTIR and XPS spectra. By introducing surface grafting agent to the iCVD process, the chemical and mechanical stability of the iCVD clickable layer was greatly enhanced. The well-defined alkyne surface functionality enables click chemistry through selective reactivity with azides. Furthermore, PPMA film also demonstrated sensitivity to e-beam irradiation, which enabled clickable substrates having nanometer scale patterns. Direct e-beam exposure of this multifunctional iCVD layer, a 200 nm pattern, and QD particles were selectively conjugated on the substrates via click chemistry. Because the iCVD layer itself is e-beam sensitive, no additional resist layer was required. Combined with the advantages of CVD process, such as conformal coverage, non-sensitiveness to the substrates, and ability to be grafted on various substrates,<sup>11</sup> the clickable iCVD polymer e-beam sensitive layer can be a design platform for immobilized

bio-devices including biosensors, bio-assays, drug discovery, and bio micro-electro-mechanical systems (bio-MEMS), microfluidic devices, and tissue engineering.<sup>1</sup>

### **Acknowledgements**

This research was supported by the U.S. Army through the Institute for Soldier Nanotechnologies, under Contract DAAD-19-02-D-0002 with the U.S. Army Research Office. This work made use of MIT's shared scanning-electron-beam-lithography facility in the Research Laboratory of Electronics.

### **References**

1. Kane, R.S.; Takayama, S.; Ostuni, E.; Ingber, D.E.; Whitesides, G.M. Patterning proteins and cells using soft lithography. *Biomaterials* **1999** *20*, 2363-2376.
2. Falconnet, D.; Csucs, G.; Grandin, H.M.; Textor, M. Surface engineering approaches to micropattern surfaces for cell-based assays. *Biomaterials* **2006** *27*, 3044-3063.
3. Senaratne, W.; Andruzzi, L.; Ober, C.K. Self-assembled monolayers and polymer brushes in biotechnology: Current applications and future perspectives. *Biomacromolecules* **2005** *6*, 2427-2448.
4. Kolb, H.C.; Finn, M.G.; Sharpless, K.B. Click chemistry: Diverse chemical function from a few good reactions. *Angewandte Chemie-International Edition* **2001** *40*, 2004-+.

5. Lutz, J.F. 1,3-dipolar cycloadditions of azides and alkynes: A universal ligation tool in polymer and materials science. *Angewandte Chemie-International Edition* **2007** *46*, 1018-1025.
6. Rozkiewicz, D.I.; Janczewski, D.; Verboom, W.; Ravoo, B.J.; Reinhoudt, D.N. "Click" chemistry by microcontact printing. *Angewandte Chemie-International Edition* **2006** *45*, 5292-5296.
7. Nandivada, H.; Chen, H.Y.; Bondarenko, L.; Lahann, J. Reactive polymer coatings that "click". *Angewandte Chemie-International Edition* **2006** *45*, 3360-3363.
8. Sumerlin, B.S.; Tsarevsky, N.V.; Louche, G.; Lee, R.Y.; Matyjaszewski, K. Highly efficient "click" functionalization of poly(3-azidopropyl methacrylate) prepared by ATRP. *Macromolecules* **2005** *38*, 7540-7545.
9. Pandurangi, R.S.; Lusiak, P.; Kuntz, R.R.; Volkert, W.A.; Rogowski, J.; Platz, M.S. Chemistry of bifunctional photoprobes. 3. Correlation between the efficiency of CH insertion by photolabile chelating agents and lifetimes of singlet nitrenes by flash photolysis: First example of photochemical attachment of Tc-99m-complex with human serum albumin. *Journal of Organic Chemistry* **1998** *63*, 9019-9030.
10. Devaraj, N.K.; Dinolfo, P.H.; Chidsey, C.E.D.; Collman, J.P. Selective functionalization of independently addressed microelectrodes by electrochemical activation and deactivation of a coupling catalyst. *Journal of the American Chemical Society* **2006** *128*, 1794-1795.

11. Tenhaeff, W.T.; Gleason, K.K. Initiated and Oxidative Chemical Vapor Deposition of Polymeric Thin Films: iCVD and oCVD *Advanced Functional Materials* **2008** *18*, 969-1140.
12. Chan, K.; Gleason, K.K. Initiated chemical vapor deposition of linear and cross-linked poly(2-hydroxyethyl methacrylate) for use as thin-film hydrogels. *Langmuir* **2005** *21*, 8930-8939.
13. Lin-Vien, D. The Handbook of Infrared and Raman Characteristic Frequencies of Organic Molecules; Academic Press: Boston, 1991;xvi, 503 p.
14. O'Shaughnessy, W.S.; Gao, M.L.; Gleason, K.K. Initiated chemical vapor deposition of trivinyltrimethylcyclotrisiloxane for biomaterial coatings. *Langmuir* **2006** *22*, 7021-7026.
15. Im, S.G.; Yoo, P.J.; Hammond, P.T.; Gleason, K.K. Grafted Conducting Polymer Films for Nano-patterning onto Various Organic and Inorganic Substrates by Oxidative Chemical Vapor Deposition *Advanced Materials* **2007** *19*, 2863-2867.
16. Moulder, J.F.; Stickle, W.F.; Sobol, P.E.; Bomben, K.D. Handbook of X-ray Photoelectron Spectroscopy; Chastain, J. & Jr., R.C.K.: Eden Prairie, MN, 1995.
17. Rohde, R.D.; Agnew, H.D.; Yeo, W.S.; Bailey, R.C.; Heath, J.R. A non-oxidative approach toward chemically and electrochemically functionalizing Si(111). *Journal of the American Chemical Society* **2006** *128*, 9518-9525.
18. Helbert, J.N. Handbook of VLSI microlithography : principles, technology, and applications Noyes Publications Park Ridge, N.J., 2001.

19. Mao, Y.; Felix, N.M.; Nguyen, P.T.; Ober, C.K.; Gleason, K.K. Towards all-dry lithography: Electron-beam patternable poly(glycidyl methacrylate) thin films from hot filament chemical vapor deposition. *Journal of Vacuum Science & Technology B* **2004** *22*, 2473-2478.
20. Mao, Y.; Gleason, K.K. Vapor-deposited fluorinated glycidyl copolymer thin films with low surface energy and improved mechanical properties. *Macromolecules* **2006** *39*, 3895-3900.



# Chapter Eight

## PATTERNING NANODOMAINS WITH ORTHOGONAL FUNCTIONALITIES: SOLVENTLESS SYNTHESIS OF SELF- SORTING SURFACES

**Sung Gap Im**, Ki Wan Bong, Byeong-Su Kim, Salmaan H. Baxamusa, Paula T. Hammond, Patrick S. Doyle, and Karen K. Gleason, 'Patterning Nanodomains with Orthogonal Functionalities: Solventless Synthesis of Self-Sorting Surfaces', *Journal of the American Chemical Society*, 130(2008), 14424-14425.

## **Abstract**

A simple method to fabricate a multi-functional patterned platform on the nanometer scale is demonstrated. The platform contains two reactive functional groups on the surface – one is an acetylene group which can be functionalized via click chemistry and the other is an amine group which can also be functionalized by classic carbodiimide chemistry with N-hydroxysuccinimide (NHS). The click-active and amine surface could be obtained from polymer coating of poly (propargyl methacrylate) (PPMA) via initiated chemical vapor deposition (iCVD) and poly allylamine (PAAm) via plasma polymerization process, respectively, utilizing commercially available monomers. Capillary force lithography (CFL) process was applied on a stacked film of PPMA layer on PAAm, and CFL could selectively pattern PPMA maintaining bottom PAAm layer intact, which completes the multi-functional nano-patterns. The minimum feature size of this nano-pattern was 110 nm. The entire fabrication process is solventless and low temperature, which can minimize the loss of functionalities. The click and NHS-reactions are highly orthogonal to each other so that non-specific immobilization can be minimized. These advantageous characteristics enable the covalent functionalization of two independent components in a one-pot functionalization process in a self-recognized way. The one-pot orthogonal functionalization was performed in an aqueous solution at room temperature, which is bio-compatible. Considering the versatility and generality of the reactions used here, we believe this platform can be easily extended to various bio-device applications.

**Key words:** initiated chemical vapor deposition (iCVD), poly (propargyl methacrylate(PPMA), poly allylamine (PAAm), click chemistry, patterning, orthogonality, fluorescence microscopy.

## 8-1 Introduction

Designed bio-active patterned functional surfaces can offer advantageous properties such as controlled adsorption and site-specific affinity.<sup>1, 2</sup> In particular, area-selective functionalization of multiple components onto a pre-designed surface<sup>2-6</sup> is highly desirable. Such a system can be utilized to detect and identify more than one analyte in biosensor applications, which enables fabrication of more effective bio-devices.<sup>3</sup> Moreover, the multi-functional surface can be used as a template to monitor the interaction among the adsorbed components from a complex mixture, such as an extracellular environment. To achieve this goal, a highly efficient, orthogonal functionalization scheme with high fidelity is desirable.

Although various multicomponent patterning strategies are well-established for semiconductor industries, the direct application of these schemes for bio-active platforms is still challenging because many biological components such as proteins and nucleic acids are susceptible to degradation during patterning.<sup>7</sup> For example, conventional photolithography (PL) utilizes harsh organic solvents and UV irradiation that can potentially lead to the destruction of bio-activity.<sup>3, 7</sup> Soft lithography techniques often result in the dehydration of biofunctionalities during the inking of stamps.<sup>6</sup> For these

reasons, patterned surfaces had been primarily functionalized only with one component on a selected area.<sup>8,9</sup> To achieve bio-active multifunctional surfaces, J. Katz *et al.* synthesized a new photosensitive terpolymer that can be processed under mild bio-compatible conditions;<sup>3</sup> however, the process involves a complicated synthesis. J. M. Slocik *et al.* used shadow mask patterning and plasma enhanced chemical vapor deposition (PECVD) for patterning of multiple components, but the resolution does not reach the nanometer scale domain and the use of thiol agents limits the type of substrates that can be used.<sup>5</sup> For nanometer scale multifunctional surfaces, a solventless patterning process that can be performed at mild condition using commercial reactants is highly desirable.

In this report, we propose a facile solventless method for synthesizing nanopatterned multi-functional surfaces. One nanodomain contains an acetylene group which can be functionalized via click chemistry. The other nanodomain contains surface amine groups which can be functionalized by carbodiimide chemistry with *N*-hydroxysuccinimide (NHS).<sup>4,8</sup> Both the click reaction and amine functionalization (NHS reaction, afterward) are well-understood, and have attractive characteristics such as high selectivity, high yield, fast reaction in aqueous phase at room temperature, and bio-compatibility.<sup>4,8</sup> Moreover, the click and NHS-reactions are highly orthogonal to each other so that non-specific immobilization can be minimized.<sup>4</sup> With these functionalities, we demonstrated the covalent functionalization of two independent components in a one-pot, self-sorted area-selective process, performed in an aqueous solution at room temperature, having conditions which are bio-compatible. Considering the versatility and generality of

the thin film deposition methods used here, we believe this platform can be easily extended to various bio-device applications.

## **8.2 Experimental**

### **8.2.1 Plasma polymerization of poly allylamine (PAAm)**

Plasma polymerized PAAm film was obtained in parallel plate chamber with 150 mm diameter electrodes. Allylamine (Aldrich, 99 %) was purchased and used without further purification. First, all the substrates were 100 W of oxygen plasma treated for 60 s at 50 mTorr of oxygen. Immediately after the oxygen plasma treatment, the plasma polymerization was initiated by applying 5 W of 13.56 MHz power source with continuous RF discharge. The process pressure was 100 mTorr, and allylamine was introduced at a flow rate of 20 sccm. After 10 minutes, plasma polymerized PAAm film was obtained with a thickness of 100 nm.

### **8.2.2 Initiated Chemical Vapor Deposition (iCVD) of poly (propargyl methacrylate) (PPMA)**

The procedure of iCVD process was described in detail elsewhere. Propargyl methacrylate (PMA) (Alfa Aesar, 98 %) and tert-butyl peroxide (Aldrich, 98%) were purchased and used without further purification. PMA and initiator were vaporized at room temperature and introduced into the iCVD chamber at a flow rate of approximately 3.75 sccm and 1.75 sccm, respectively. The flow rates were controlled with MKS 1490A mass flow controllers. The polymerization reaction was initiated with the filament at 280 °C. The

process pressure of 800 mTorr was maintained by a butterfly valve with PID control (MKS 248 flow control valve). Film thicknesses were monitored *in situ* by interferometry; approximately 200 nm of the PPMA film was deposited in 15 min.

### **8.2.3 Silane treatment for surface grafting of inorganic substrates**

0.5 ml of trichlorovinyl silane (TCVS) (from Aldrich, 97%) was placed in the dessicator. An oxygen plasma treated substrate was exposed to TCVS vapor at 25 °C for less than 5 minutes. The process pressure in the dessicator was 100 mTorr. Exactly the same plasma polymerization conditions were applied to the silane treated substrates for grafted PAAm on the substrates.

### **8.2.4 Capillary force lithography**

Sylgard 184 (Dow Chemical) was cast over a silicon wafer mold prepared by standard lithographic methods, degassed under vacuum and cured overnight at 70 °C. The cured poly (dimethyl siloxane) (PDMS) was peeled off the master. Similarly, poly (urethaneacrylate) (PUA) having carboxyl group. (MINS, Minuta Tech., Korea) was cast over pre-patterned Si wafer master and exposed to ultraviolet (UV) light (wavelength = 365 nm) for one minutes. The pre-cured PUA mold was carefully detached from Si wafer master and fully cured by UV treatment for four hours. The patterned PDMS or PUA mold was applied on iCVD PPMA and cured with 100 ~ 110 °C for 30 minutes to transfer the positive tone pattern of PPMA onto the grafted PAAm layer.

### **8.2.5 Surface Functionalization**

2.0 mg of 5-(and 6-)carboxyfluorescein, succinimidyl ester (NHS-fluorescein, Pierce Biotechnology Inc, Rockford, IL) 1.0 mg of tetramethylrhodamine-5-carbonyl azide (Azido-rhodamine, Invitrogen, Chicago, IL), 3.2 mg of copper(II) sulfate (Sigma Aldrich, 99%) and 8.0 mg of sodium ascorbate (Sigma Aldrich) were solubilized in 10 ml of a mixture of dimethyl sulfoxide (DMSO) and water (1:9 v/v). A piece of surface patterned film (200 nm thick) on Si wafer was placed into the solution and stirred by magnetic bar at 25 °C for 16 hours under the protection from light. After the reaction, the sample was extensively rinsed with a mixture of DMSO and water (1:9 v/v) and dried with gentle nitrogen purge.

### **8.2.6 Microscopy**

Fourier Transform infrared (FTIR) spectra were obtained via Nexus 870, Thermo Electron Corporation. Scanning electron microscopy (SEM) images were obtained with Environmental Scanning Electron Microscopy, (FEI/Philips XL30 FEG ESEM). Atomic force microscopy (AFM) image was obtained using DI3100, Digital Instruments. Fluorescence images were gathered using AxioSkop 2 MAT, Zeiss with the excitation wavelength of 488 nm for NHS-fluorescein and 605 nm for azido-rhodamine.

### 8.3 Results and Discussion

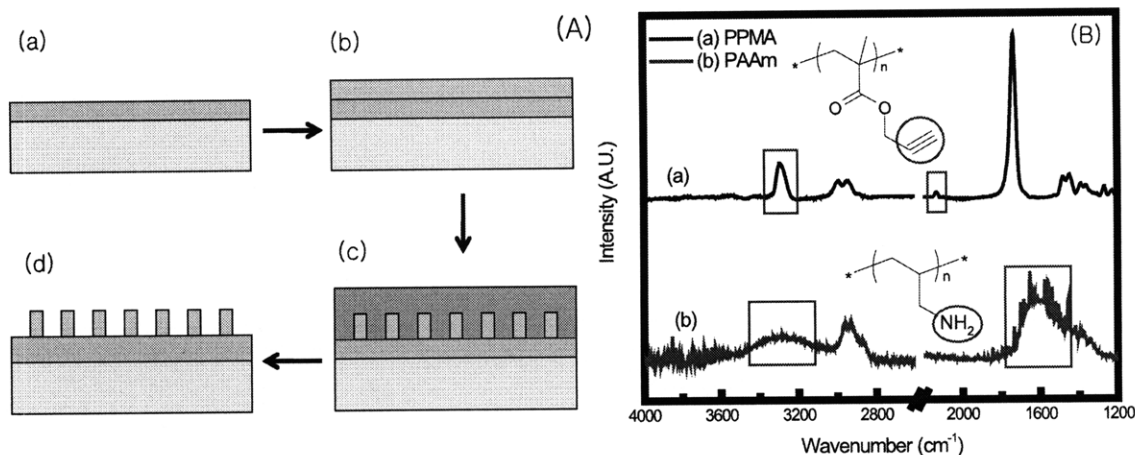


**Figure 8-1** (A) Schematic procedure of nano-pattern fabrication: (a) PECVD of PAAm; (b) iCVD of PPMA; (c) apply CFL mold to induce capillary rise; (d) remove CFL mold to complete the nano-pattern. (B) FTIR spectra of (a) iCVD PPMA and (b) PECVD PAAm.

In Fig. 8-1A, capillary force lithography (CFL)<sup>10</sup> nanopatterns the upper layer of a bilayer structure, exposing regions of the bottom material, thus creating a dual functional surface. Crosslinking allows the bottom layer to remain immobile during the CFL step. Vapor deposition allows the insoluble bottom layer to be directly synthesized. For the top layer, the use of solventless vapor deposition is also critical, as solvents used in conventional solution processing have the potential to dissolve the underlying layer of a multilayer.<sup>11</sup> Additionally, residual solvent can lead to biocompatibility issues.<sup>12</sup> In contrast to conventional photolithography, CFL does not require resists, developers, solvents, or chemically destructive irradiation that can deactivate the reactive functional groups.<sup>10</sup>



Moreover, since the patterning process of CFL utilizes solely thermal movement of polymer film regardless of the chemical properties of polymer films, we believe this procedure can be applicable to many different sets of functional polymer films.

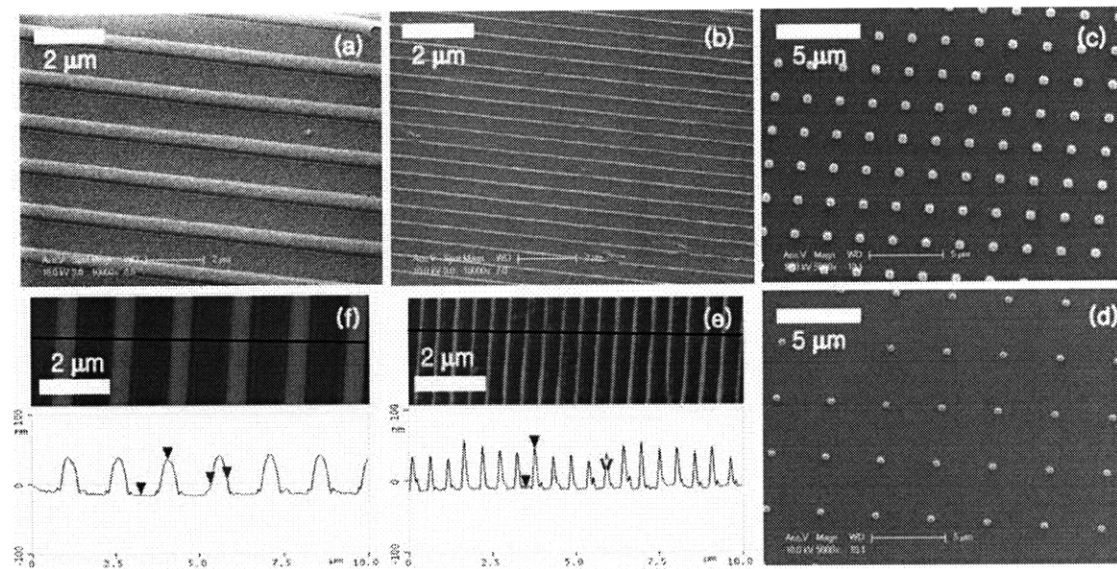


**Figure 8-2** Scanning electron microscope (SEM) and atomic images of nano-patterned platform of iCVD PPMA on PECVD PAAM background film via CFL; (a) 500 nm, (b) 110 nm stripe pattern, and (c) 800 nm, (d) 500 nm dot patterns, and atomic force microscope (AFM) image of (e) 110 nm and (f) 500 nm line pattern AFM image clear demonstrates the pattern fidelity and exposure of PAAM of the structure.

To create a bilayer with amine and acetylenic functional groups, first a 100 nm thick poly(allyl amine) (PAAM) film using PECVD to achieve crosslinking. Next, a 50 nm thick non-crosslinked poly(propargyl methacrylate) (PPMA) film was synthesized via

initiated chemical vapor deposition (iCVD). Conveniently, the monomers required for both layers are commercially available.

The Fourier Transform Infrared (FTIR) spectrum (Fig. 8-1B) clearly shows the N-H stretching peak ( $\sim 3200\text{ cm}^{-1}$ ) and the N-C stretching peak ( $\sim 1650\text{ cm}^{-1}$ ), demonstrating retention of the amine functionality in the PECVD PAAm layer.<sup>13</sup> Similarly, the characteristic peaks of the acetylene group (C-H stretch peak at  $\sim 3300\text{ cm}^{-1}$  and C $\equiv$ C stretch peak at  $\sim 2100\text{ cm}^{-1}$ )<sup>13</sup> were clearly observed in the FTIR spectrum of iCVD PPMA. The PECVD film was insoluble in common solvents for PAAm including water, methanol, and acetone, suggesting the presence of crosslinking commonly found in plasma deposited materials.<sup>14</sup> The iCVD PPMA films were soluble in acetone and dimethylformamide (DMF), suggesting limited or no crosslinking resulted from this less energetic vapor deposition method.<sup>14</sup>

For the CFL,<sup>10</sup> a poly(dimethylsiloxane) (PDMS) or a poly(urethaneacrylate) (PUA) mold<sup>15</sup> was placed on the PPMA/PAAm/Si substrate and a pressure of about 0.1 bar was applied to selectively induce the capillary rise of the PPMA layer. In general, a polymer film starts to deform when the temperature is raised beyond its glass transition temperature ( $T_g$ ). The PECVD PAAm film showed no detectable deformation when heated up to 110 °C. Considering that the reported  $T_g$  of standard PAAm is -6 °C,<sup>16</sup> the above results confirm that the PECVD PAAm film is highly crosslinked. On the other hand, a distinctive deformation was observed when the PPMA film was heated above 60 °C. After 30 minutes of pressing the CFL mold at the optimal temperature of 105 °C, well-resolved patterns were obtained over a 2 mm  $\times$  3 mm area (Fig. 8-2). The minimum feature size obtained was 110

nm. Highly anisotropic patterns were produced with high fidelity to the mold. Line-and-space patterns, dot arrays, and complex patterns were also obtained.

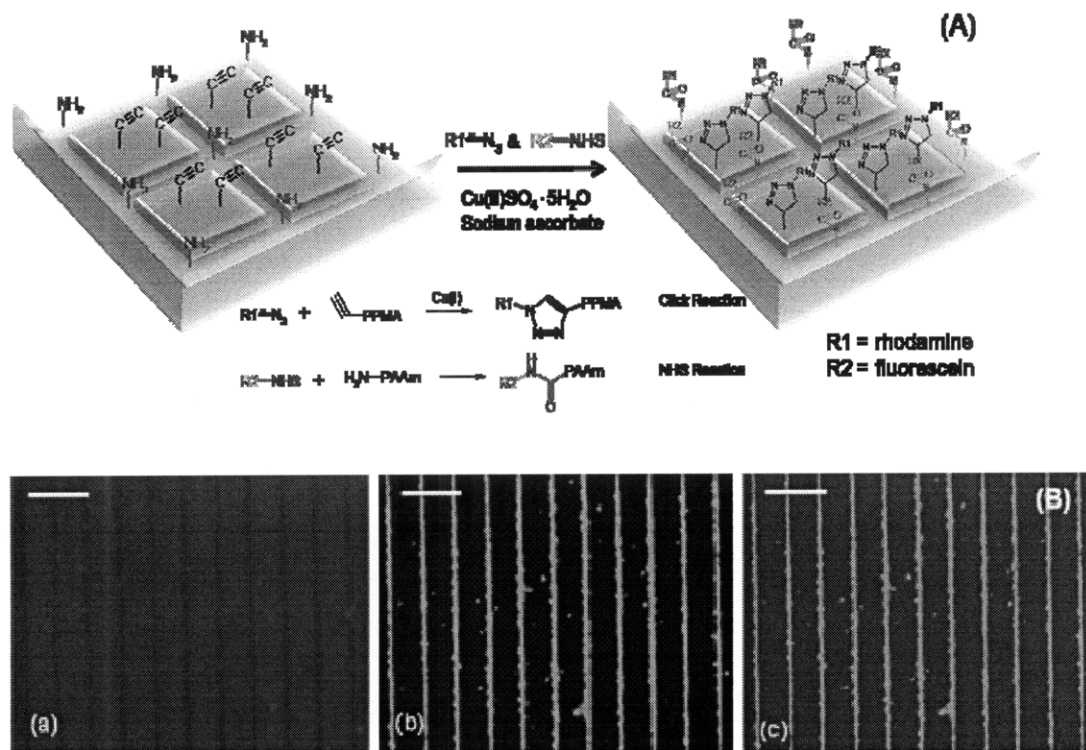


**Figure 8-3** (A) Schematic procedure of one-pot functionalization; (B) Fluorescence microscope image of (a) click functionalized red dye excited at 545 nm, (b) NHS functionalized green dye excited at 491 nm, and (c) overlapped image of (a) and (b). Each scale bars represents 30  $\mu m$ .

The orthogonal amine and acetylene functionalities on the surface enable the self-sorting two fluorescent dyes onto the nanopatterned domains during a one-pot functionalization step. For the click functionalization, the red dye, tetramethylrhodamine-5-

carbonyl azide (azido-rhodamine afterward,  $\lambda_{\text{abs}} = 545 \text{ nm}$ ,  $\lambda_{\text{em}} = 578 \text{ nm}$ ) in the presence of Cu(I) cation catalyst forms a triazole covalent linkage to the acetylene group of the PPMA patterned domain.<sup>8</sup> For the NHS functionalization, the green dye, 5-(and 6-) carboxyfluorescein, succinimidyl ester (NHS-fluorescein afterward,  $\lambda_{\text{abs}} = 491 \text{ nm}$ ,  $\lambda_{\text{em}} = 518 \text{ nm}$ ) forms a covalent peptide bond with the amine group in PAAm areas. The one-pot functionalization step from a mixture of the two dyes was performed in aqueous solution at room temperature for 20 h. A small amount of DMSO was added in the solution to improve the limited solubility of azido-rhodamine in the water (v/v ratio of water to DMSO was 9:1). The functionalized nano-pattern was thoroughly rinsed with water and nitrogen-dried.

The selective self-sorted pattern of fluorescent dyes was clearly observed by fluorescence microscopy (Fig. 8-3). During the one-pot functionalization, both surface groups recognized their conjugate functionalities in the dye and thus the surface was selectively tagged by the dye according to the pre-designed pattern. The overlapped fluorescent image clearly demonstrates that the top PPMA was completely dewetted from the bottom PAAm surface during the CFL.

#### **8.4 Conclusion**

In summary, we have demonstrated a dual functional nano-patterned platform with a minimum feature size of 110 nm. The fabrication process utilized sequential solventless CVD processes and patterned by a CFL process. By applying one-pot, biocompatible functionalization, the conjugate fluorescent dyes were assembled onto the pattern in a self-sorted fashion. Considering the ease of fabrication and the versatility and orthogonality of

the utilized functional groups, we believe this platform can be a powerful tool for bio-device applications in high throughput, multi-component systems.

### **Acknowledgements**

This research was supported by the U.S. Army through the Institute for Soldier Nanotechnologies, under Contract DAAD-19-02-D-0002 with the U.S. Army Research Office.

### **References**

1. Nie, Z.; Kumacheva, E. Patterning Surfaces with Functional Polymers. *Nature Materials* **2008** *7*, 277-290.
2. Xu, H.; Hong, R.; Lu, T.X.; Uzun, O.; Rotello, V.M. Recognition-directed orthogonal self-assembly of polymers and nanoparticles on patterned surfaces. *Journal of the American Chemical Society* **2006** *128*, 3162-3163.
3. Katz, J.S.; Doh, J.; Irvine, D.J. Composition-tunable properties of amphiphilic comb copolymers containing protected methacrylic acid groups for multicomponent protein patterning. *Langmuir* **2006** *22*, 353-359.
4. Malkoch, M.; Thibault, R.J.; Drockenmuller, E.; Messerschmidt, M.; Voit, B.; Russell, T.P.; Hawker, C.J. Orthogonal approaches to the simultaneous and cascade functionalization of macromolecules using click chemistry. *Journal of the American Chemical Society* **2005** *127*, 14942-14949.

5. Slocik, J.M.; Beckel, E.R.; Jiang, H.; Enlow, J.O.; Zabinski, J.S.; Bunning, T.J.; Naik, R.R. Site-specific patterning of biomolecules and quantum dots on functionalized surfaces generated by plasma-enhanced chemical vapor deposition. *Advanced Materials* **2006** *18*, 2095-+.
6. Zhou, F.; Zheng, Z.J.; Yu, B.; Liu, W.M.; Huck, W.T.S. Multicomponent polymer brushes. *Journal of the American Chemical Society* **2006** *128*, 16253-16258.
7. Sorribas, H.; Padeste, C.; Tiefenauer, L. Photolithographic generation of protein micropatterns for neuron culture applications. *Biomaterials* **2002** *23*, 893-900.
8. Lutz, J.F. 1,3-dipolar cycloadditions of azides and alkynes: A universal ligation tool in polymer and materials science. *Angewandte Chemie-International Edition* **2007** *46*, 1018-1025.
9. Suh, K.Y.; Langer, R.; Lahann, J. A novel photoderivable reactive polymer coating and its use for microfabrication of hydrogel elements. *Advanced Materials* **2004** *16*, 1401-+.
10. Suh, K.Y.; Lee, H.H. Capillary force lithography: Large-area patterning, self-organization, and anisotropic dewetting. *Advanced Functional Materials* **2002** *12*, 405-413.
11. Chan, K.; Gleason, K.K. Air-gap fabrication using a sacrificial polymeric thin film synthesized via initiated chemical vapor deposition. *Journal of the Electrochemical Society* **2006** *153*, C223-C228.

12. O'Shaughnessy, W.S.; Murthy, S.K.; Edell, D.J.; Gleason, K.K. Stable biopassive insulation synthesized by initiated chemical vapor deposition of poly(1,3,5-trivinyltrimethylcyclotrisiloxane). *Biomacromolecules* **2007** *8*, 2564-2570.
13. Lin-Vien, D. *The Handbook of Infrared and Raman Characteristic Frequencies of Organic Molecules*; Academic Press: Boston, 1991;xvi, 503 p.
14. Tenhaeff, W.E.; Gleason, K.K. Initiated and oxidative chemical vapor deposition of polymeric thin films: iCVD and oCVD. *Advanced Functional Materials* **2008** *18*, 979-992.
15. Kim, Y.S.; Baek, S.J.; Hammond, P.T. Physical and chemical nanostructure transfer in polymer spin-transfer printing. *Advanced Materials* **2004** *16*, 581-+.
16. Stone, F.W.; Stratta, J.J. *Encyclopedia of Polymer Science and Technology*; Union Carbide Corp., 2002;pp. 103~145.

# Chapter Nine

## A CONFORMAL NANO-ADHESIVE VIA INITIATED CHEMICAL VAPOR DEPOSITION FOR MICROFLUIDIC DEVICES

**Sung Gap Im**, Ki Wan Bong, Chia-Hua Lee, Patrick S. Doyle, and Karen K. Gleason, 'A Conformal Nano-adhesive via Initiated Chemical Vapor Deposition for Microfluidic Devices', *Lab on a Chip*, 8(2008), DOI: 10.1039/b812121d.



## **Abstract**

A novel high-strength nano-adhesive is demonstrated for fabricating nano- and microfluidic devices. While the traditional plasma sealing methods are specific for sealing glass to poly (dimethylsiloxane) (PDMS), the new method is compatible with a wide variety of polymeric and inorganic materials, including flexible substrates. Additionally, the traditional method requires that sealing occur within minutes after the plasma treatment. In contrast, the individual parts treated with the nano-adhesive could be aged for at least three months prior to joining with no measurable deterioration of post-cure adhesive strength. The nano-adhesive is comprised of a complementary pair of polymeric nanolayers. An epoxy-containing polymer, poly (glycidyl methacrylate) (PGMA) was grown by via initiated chemical vapor deposition (iCVD) on the substrate containing the channels. A plasma polymerized poly allylamine (PAAm) layer was grown on the opposing flat surface. Both CVD monomers are commercially available. The PGMA nano-adhesive layer displayed conformal coverage over the channels and was firmly tethered to the substrate. Contacting the complementary PGMA and PAAm surfaces, followed by curing at 70 °C, resulted in nano- and micro- channels structures. The formation of the covalent tethers between the complementary surfaces produces no gaseous by-products which would need to outgas. The nano-adhesive layers did not flow significantly as a result of curing, allowing the cross-sectional profile of the channel to be maintained. This enabled fabrication of channels with widths as small as 200 nm. Seals able to withstand >50 psia were fabricated employing many types of substrates, including silicon wafer, glass, quartz,

PDMS, polystyrene petri dishes, poly (ethylene terephthalate) (PET), polycarbonate (PC), and poly (tetrafluoro ethylene) (PTFE).

**Key words:** initiated chemical vapor deposition (iCVD), plasma polymerization, poly (glycidyl methacrylate) (PGMA), poly allylamine (PAAm), Epoxy curing, nano-adhesive, microfluidic device, adhesion strength.

## 9-1 Introduction

Microfluidic devices have drawn extensive interest from researchers in last decade due to their potential application in integrated analytical systems, biomedical devices, high throughput screening, and studies of chemical and biochemical reactions.<sup>1-3</sup> The advantages of miniaturized systems include the reduced consumption of reagents and analytes, low cost of manufacture, low consumption of power, high throughput, decreased production of by-product and increased portability.<sup>1</sup>

Microfluidic system fabrication incorporates many inorganic and polymeric materials. One of the most widely employed materials is poly (dimethylsiloxane) (PDMS).<sup>1</sup>  
<sup>4</sup> Complex layouts of microfluidic channels are created by simply casting PDMS prepolymer onto a silicon master containing the negative image.<sup>4</sup> The elastomeric nature of PDMS can conformally seal minor perturbations in the substrates. However, PDMS also has some drawbacks, including undesirable swelling in many organic solvents, hydrophobicity, and insufficient modulus for fabrication of nanometer scale channels.<sup>5,6</sup>

Polystyrene (PS),<sup>7</sup> poly (ethylene glycol) (PEG),<sup>8</sup> cyclo-olefin copolymers (COC),<sup>9</sup> and poly (methyl methacrylate) (PMMA)<sup>10</sup> have been utilized in microfluidic devices to a lesser degree, because of fabrication difficulties associated with these polymers.<sup>1, 4</sup> However, microfluidic devices fabricated with these materials potentially have many desirable attributes, including the reduction of undesirable swelling in organic solvents and decreased sagging when using higher modulus materials. Devices which can be mechanically flexed and which are comprised of smaller channels are also envisioned. Lower fabrication cost is another potential benefit.

One of the chief difficulties of employing alternate polymeric materials is that methods for sealing the microfluidic channels suffer from multiple limitations.<sup>11</sup> Strong seals can be achieved by fusion bonding<sup>12, 13</sup> and anodic bonding,<sup>14</sup> but these require high temperatures and high electric fields, respectively, which have the potential to damage low thermal stability substrates.<sup>11</sup> Surface modification with oxygen plasma<sup>1, 4, 15, 16</sup> or strong acid treatment<sup>15, 17</sup> allows formation of Si-O-Si covalent bonds at the interface with on Si-containing substrates such as glass, quartz, or PDMS.<sup>1</sup> However, the sealing must be performed in a short period of time following the surface treatment as the modified surface is unstable and rapidly recovers hydrophobicity.<sup>15</sup> In addition, this method is not suitable for carbon-based polymeric substrates.<sup>1</sup> Prepolymer<sup>5, 11</sup> or partially cured polymer materials<sup>8</sup> have also been utilized to seal chips, but the efficacy of these techniques is highly system-dependent. Adhesive bonding is one of the most common fabrication methods for microfluidic devices.<sup>18</sup> In spite of its ease of use and the resulting high bonding strength, the adhesive bonding process has some critical drawbacks. In this liquid-based

process, the adhesive deforms at the curing temperature, often causes clogging of the channel and/or deviation of the shape of channel from its initial design.<sup>19</sup> Additionally, delamination of adhesive layer from the substrates often causes the device failure.<sup>19</sup> To avoid these problems, several requirements on the adhesive layers can be suggested. First, the adhesive should be robustly anchored to the substrate before the sealing process. Second, the flow or deformation of the adhesive should be minimal during the sealing step. Next, the adhesive should conformally cover the substrates. Finally, the adhesive should be sufficiently thin to avoid blockage of the channel. For these reasons, it is essential to obtain conformally coated adhesive layer with nanometer scale thickness, which is firmly tethered on a substrate. However, these goals are extremely challenging to achieve with liquid-phase process, which often results in highly non-isotropic coverage of adhesive films on complex geometries.<sup>20, 21</sup>

Conformal coverage of many varieties of organic films at nanometer scale thicknesses has been achieved by initiated chemical vapor deposition (iCVD).<sup>20, 22, 23</sup> onto geometrical complex substrates including carbon nanotubes,<sup>24</sup> microparticles,<sup>22</sup> electrospun nanofibers,<sup>23</sup> and trenches with high aspect ratio.<sup>20</sup> The iCVD process is performed using room temperature substrates with commercially available cheap monomers.<sup>20, 25</sup> Thus, the iCVD surface modification layer can be applied to almost any type of substrate (metals, plastics, ceramics, etc.). Gas phase temperatures are generally less than 300 °C, which is sufficient for activating the initiator but mild enough to limit thermal decomposition of the monomer.<sup>22, 26</sup> Consequently, reactive functional groups present in the monomer are

retained to a high degree in the iCVD polymer film.<sup>25</sup> The retention of functional group is critical as these represent the potential adhesive sites.

Herein, we report a novel nano-adhesive layer deposited by the iCVD process. An epoxy-containing polymer, poly (glycidyl methacrylate) (PGMA) was used as a nano-adhesive layer. The PGMA coated substrate was brought into contact with the substrates covered with plasma polymerized poly (allylamine) (PAAm),<sup>27, 28</sup> and the ring-opening curing reaction of PGMA layer with conjugate PAAm layer was performed at the temperature of 70 °C to form a strong covalent bond between the two substrates. Both PGMA and PAAm layer could be easily obtained from commercially available cheap monomers. No leakage was observed up to the test pressure of 50 psia from the resulting microfluidic devices.<sup>15</sup>

## **9.2 Experimental**

### **9.2.1 Plasma polymerization of PAAm**

Plasma polymerized PAAm film was obtained in parallel plate chamber with 150 mm diameter electrodes. Allylamine (Aldrich, 99 %) was purchased and used without further purification. First, all the substrates were 100 W of oxygen plasma treated for 60 s at 50 mTorr of oxygen. Immediately after the oxygen plasma treatment, the plasma polymerization was initiated by applying 5 W of 13.56 MHz power source with continuous RF discharge. The process pressure was 100 mTorr, and allylamine was introduced at a flow rate of 20 sccm. After 10 minutes, plasma polymerized PAAm film

was obtained with a thickness of 100 nm.

### **9.2.2 iCVD of PGMA**

The procedure of iCVD process was described in detail elsewhere.<sup>26</sup> Before iCVD process, all the substrates were oxygen plasma treated, as in plasma polymerization. The plasma treated substrates was immediately transferred to iCVD vacuum chamber. GMA (Aldrich, 98 %) and tert-butyl peroxide (Aldrich, 98%) were purchased and used without further purification. GMA and initiator were vaporized at room temperature and introduced into the iCVD chamber at a flow rate of approximately 2.95 sccm and 1.75 sccm, respectively. The flow rates were controlled with MKS 1490A mass flow controllers. The polymerization reaction was initiated with the resistively heated tungsten (W) filament at 220 °C. The process pressure of 200 mTorr was maintained by a butterfly valve with PID control (MKS 248 flow control valve). Film thicknesses were monitored *in situ* by interferometry; approximately 200 nm of the PGMA film was deposited in 5 min.

### **9.2.3 Silane treatment for surface grafting of inorganic substrates**

0.5 ml of TCVS (from Aldrich, 97%) was placed in the dessicator. Oxygen plasma treated substrate – Si wafer, glass, quartz, and PDMS – was exposed to TCVS vapor at 25 °C for less than 5 minutes. The process pressure in the dessicator was 100

mTorr. Exactly the same iCVD and plasma polymerization conditions were applied to the silane treated substrates for grafted PGMA on the substrates.

#### **9.2.4 Curing nano-adhesive layers**

PGMA-coated substrates were bound to PAAm-coated substrates to seal the substrates. A PGMA grafted substrate was gently placed on PAAm grafted substrate and lightly pressed ( $\sim 0.1$  bar) to ensure the contact of two substrates. The bonding was completed by placing the coupled substrate into an oven at  $70\text{ }^{\circ}\text{C}$  for 12 hrs for curing the nano-adhesive layer.

#### **9.2.5 Fabrication of test microfluidic devices and leakage test**

Linear microfluidic channels were prepared in PDMS by standard soft lithographic techniques. Sylgard 184 (Dow Chemical) was cast over a silicon wafer mold prepared by standard lithographic methods, degassed under vacuum and cured overnight at  $70\text{ }^{\circ}\text{C}$ . The cured PDMS was peeled off the master, individual devices separated and fluidic connections were punched. Channels were straight and rectangular:  $200\text{ }\mu\text{m}$  wide,  $75\text{ }\mu\text{m}$  high. A nano-adhesive PGMA layer was applied onto this PDMS microfluidic channel, as described above. Separately, PAAm deposited Si wafer, PTFE, TCPS petri dish, PET, and PC film was prepared and the curing procedure completes the test microfluidic devices. The bond strength of nano-adhesive was tested

by performing burst pressure testing. The channel was filled with water and end of the channel closed. The inlet was attached to a water chamber pressurized with argon using a pressure regulator. The pressure was slowly increased until the channel was visibly observed to burst, leaking water out the side of the device, and the pressure at which this occurred is the reported burst pressure.

### **9.2.6 Microscopy**

For the cross sectional SEM, the nano-channel samples were cryomicrotomed and the images were obtained with Environmental Scanning Electron Microscopy, (FEI/Philips XL30 FEG ESEM).

## **7.3 Results and Discussion**

### **9.3.1 Adhesive Bonding**

Fig. 9-1 demonstrates schematically the procedure for bonding two different substrates. Channels were pre-patterned on one substrate, and the other substrate was kept flat. In general, the carbon-based polymeric substrates do not require the pretreatment. However, in case of polymeric substrates with low surface energy such as PTFE require the oxygen plasma treatment to activate the polymeric surface for better adhesion.<sup>29</sup> PGMA and PAAm films were deposited on this substrate via iCVD and plasma polymerization from commercially available monomers, respectively (Fig. 9-1a and b). No noticeable delamination was observed in PGMA and PAAm films even after 30 minutes of



ultrasonication in water. Strong bonding of adhesive layer on the substrate is essential for this nano-adhesive layer to form well sealed microfluidic devices, since the flaws in the interface between adhesives and substrates has been observed to be one of the major causes of leakage in microfluidic devices.<sup>19</sup>

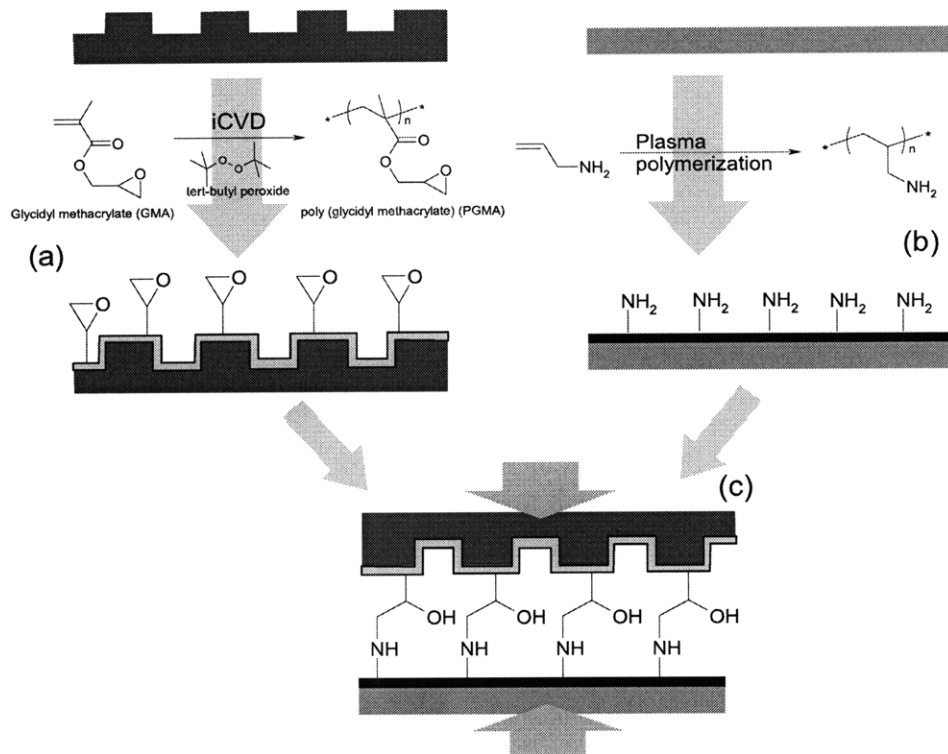


**Figure 9-1** Schematic of process for nano-adhesive bonding. Deposition of the (a) iCVD of PGMA onto a pre-patterned substrate and of the (b) plasma polymerized PAAm onto flat substrate, followed by curing at 70 °C to complete the bonding of two substrates (c). Note that the final adhesive bonding step produces no gaseous by-products and so avoids any potential issues arising due to outgassing.

Finally, the PGMA-grafted substrate was placed on the other PAAm-covered flat substrate. The stacked substrates are lightly pressed (~ 0.1 bar) and put into an oven at 70

°C for 12 hrs to induce a curing reaction between the epoxy and amine groups in the nano-additive film to complete the bonding of two substrates (Fig. 9-1c).<sup>30</sup> The ring-opening curing reaction is advantageous for this bonding process because of its relatively fast reaction rate at low temperature (25 ~ 100 °C). In addition, since curing occurs by an addition reaction, no gaseous reaction by-products evolve which might lead to leakage in the bonded substrates.<sup>29, 30</sup> Recently, H. Chen *et al* had also demonstrated a solventless adhesive bonding process using CVD polymer coatings to induce a strong covalent bonding between two substrates.<sup>31</sup> However, their process is condensation reaction having gaseous water by-product which can induce defects at the bonded interface, or bonding failure. In addition, the curing temperature of 140 °C is higher than glass-transition temperature ( $T_g$ ) for many of broadly used polymeric substrates including PS, PMMA, PET, poly vinylalcohol (PVA), polyacrylonitrile.<sup>32</sup> Using curing temperatures higher than  $T_g$ , can deform the polymeric substrates and the initial design of channel cannot be retained. In addition, the CVD reactants require special synthesis, which is barrier to further commercialization.

Many types of polymer substrates can be bonded with the procedure outlined above. For example, a pre-patterned polyurethane (PU) substrate was bonded with thin PC film (Fig. 9-2a). A test microfluidic device was fabricated by sealing pre-patterned PDMS substrate with PET film via nano-adhesive bonding (Fig. 9-2b and c). This microfluidic device did not fail even after the repeated flexing and the bondage was stable for a long storage (longer than 100 days). Even when mechanical stress was applied to the point where the polymer substrate failed, the seal remained intact,

evidence of excellent bond strength. In addition to the examples shown in Fig. 9-2, many other substrate pairs were successfully bonded including tissue-culture grade PS (TCPS) - PDMS, PTFE - PDMS, and PC - PET film.

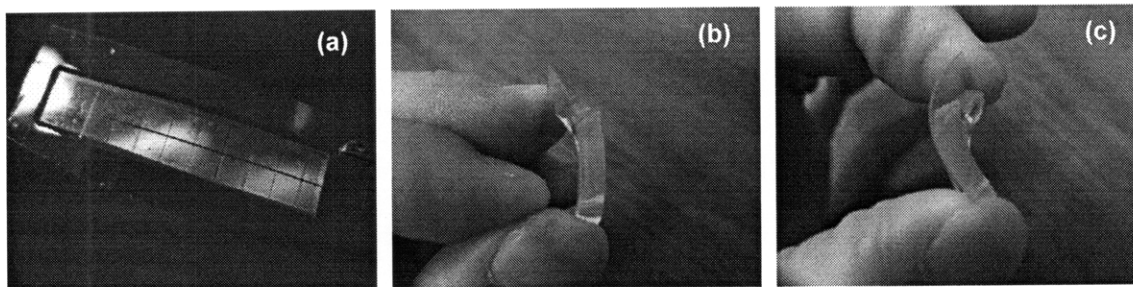


**Figure 9-2** Pre-patterned PU substrate bonded with PC film (a) and compressive (b) and tensile (c) stresses were applied to a test microfluidic device composed of pre-patterned PDMS substrate bonded with PET film.

Nano-adhesive films could also be grafted onto inorganic substrates including Si wafer, glass and quartz substrates by through a pre-treatment with a vinyl containing silane coupling agent, trichlorovinyl silane (TCVS).<sup>20</sup> The covalently tethered surface vinyl groups of TCVS react with the vinyl monomers used to form grafted PGMA and PAAm layers. Then, as shown in Fig. 9-1, the nano-adhesive layer was cured to complete the bonding of two inorganic substrates. With this procedures, strong bonding of many organic and inorganic materials pairs was achieved including Si wafer - Si wafer, Si wafer - glass, and Si wafer - PDMS. The observations shown above clearly demonstrate that the nano-adhesive pair of iCVD PGMA and PAAm layers can be

applicable to broad range of organic and inorganic substrate materials, which enables the broad application of many kinds of flexible pre-patterned substrates to microfluidics.

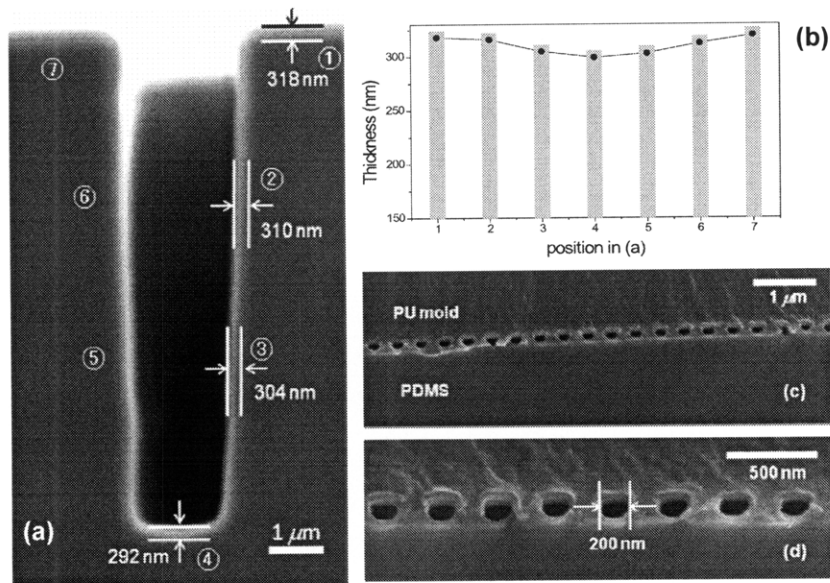


**Figure 9-3** Cross sectional SEM images of (a) a 318 nm thick PGMA film deposited conformally on standard trench ( $2 \mu\text{m} \times 8 \mu\text{m}$ ) and (b) the thickness variation of PGMA film with respect to the trench position in (a). Each numbers in x-axis corresponds to the numbers in (a). (c, d) a cured iCVD PGMA film on pre-patterned PDMS with a flat PET film coated with PAAm with different magnification. The cross sectional SEM image of (c) and (d) clearly shows that 200 nm-channels at the interface between PDMS and PU film are retained.

### 9.3.2 Conformal coverage and fabrication of nano-channel

Trenches ( $8 \mu\text{m}$  deep  $\times$   $2 \mu\text{m}$  wide) in silicon were used to examine the conformal coverage of iCVD PGMA. Fig. 9-3a and b demonstrate the cross-sectional SEM images of C-PEDOT (a) and the thickness variation of PGMA film (b) on these standard trenches

with respect to the position in the trench. The lowest thickness of PGMA at the bottom of trench was 91 % of the thickness at the trench mouth, which clearly demonstrates that PGMA film can conformally cover the trench structure. This conformal coverage is unique properties of CVD process, which is very difficult to achieve in other liquid phase based methods.<sup>21</sup>

Fig. 9-3c and d show the cross sectional SEM images of sealed substrates with 200 nm nano-channels. The thickness of PGMA and PAAm layers were 50 nm and 20 nm respectively, and the shape of the resulting nanochannel is essentially unchanged by the curing processes, suggesting that the viscous flow of both PGMA and PAAm is negligible as the movement of the grafted nanolayers is highly restricted.

### 9.3.3 Bond strength of sealed microfluidic devices

The adhesion strength of nano-adhesive must be sufficient for microfluidic device application.<sup>5, 11, 15, 17, 19</sup> Thus, microfluidic devices were fabricated via the nano-adhesives bonding procedure (Fig. 9-1) and tested for leakage with flowing water as the pressure in the microchannel was increased.<sup>15</sup> The PDMS pre-patterned replica was paired with a variety of organic and inorganic flat substrates (Table 9-1) and in all cases no leakage was observed at the maximum channel pressure achievable by the infusion syringe pump set-up, 50 psia. This value is sufficient for many microfluidic applications<sup>3, 6</sup> and compares to the top end of the 30 ~ 50 psia range generally obtainable from PDMS bonding with gaseous plasma treatment.<sup>1, 4, 15</sup> The film thickness of PGMA was varied from 50 nm to 300 nm maintaining the the thickness of PAAm to

50 nm, and the adhesion strength was practically identical. To test stability of the adhesive functional groups (Fig. 9-1a and 1b) grafted to surfaces of a PDMS replicate and PET flat substrates were stored for three months before performing the curing step. The resulting channel was leak-free at pressure of 50 psia. Thus, the nanoadhesive bonding method renders the immediate sealing unnecessary, which is in sharp contrast to the requirements for the well-established gaseous plasma method.<sup>15</sup> The stability of sealed device itself was also monitored. The bond strength of the test device exceeded 50 psia after three months of storage.

PDMS bonded with...	At 50 psia of channel pressure,
Si wafer	No leakage
PTFE	No leakage
PS Petri dish	No leakage
PC film	No leakage
PET film	No leakage

**Table 9-1** Summary of leakage test of microfluidic devices with PDMS and various kinds of substrate materials at the channel pressure of 50 psia.

#### 9.4 Conclusion

A novel nano-adhesive bonding process was demonstrated for creating microfluidic channels capable of withstanding pressures of higher than 50 psia. The nano-adhesive film showed strong and conformal adhesion on the substrates of complex geometries. The

thickness of nano-adhesive layer was sufficiently thin ( $<200$  nm) so as limit its infiltration into the microfluidic channel. Channels were successfully fabricated with this nano-adhesive film from many different organic and inorganic substrates including Si wafers, glass, quartz, PET, PC, PS, and PTFE, which clearly demonstrates that the method is fully compatible with various flexible substrates. To achieve these results, grafted iCVD PGMA was conformally coated on prepatterned trenches and plasma deposited PAAm was applied to the flat surfaces. These individual surfaces could be stored for at least two weeks before sealing. Sealing was achieved by placing the coated pieces face to face and then curing at  $70^{\circ}\text{C}$ . No blockage of the microfluidic channels by the adhesive was observed after the curing process. Hence, channels as small as  $200$  nm in width could be fabricated. High bonding strength of the fabricated channels was validated for at least three months. Moreover, the leftover amine and epoxide functionalities inside of channel wall can also be utilized for further independent functionalization.<sup>31</sup> Epoxy groups from sidewall of channels can be conjugated with amine compounds and amine groups at the flat side can also be separately functionalized with NHS-tethered compounds. Therefore, the inside of channel can be independently modified, which potentially enables selective functionalization of channel wall. Hence, other active moieties, such as sensing molecules, electrophoretic buffers, and other active species can also be bound to the walls for specific applications.

## **Acknowledgements**

This research was supported by the U.S. Army through the Institute for Soldier Nanotechnologies, under Contract DAAD-19-02-D-0002 with the U.S. Army Research Office.

## References

1. McDonald, J.C.; Duffy, D.C.; Anderson, J.R.; Chiu, D.T.; Wu, H.K.; Schueller, O.J.A.; Whitesides, G.M. Fabrication of microfluidic systems in poly(dimethylsiloxane). *Electrophoresis* **2000** *21*, 27-40.
2. Quake, S.R.; Scherer, A. From micro- to nanofabrication with soft materials. *Science* **2000** *290*, 1536-1540.
3. Unger, M.A.; Chou, H.P.; Thorsen, T.; Scherer, A.; Quake, S.R. Monolithic microfabricated valves and pumps by multilayer soft lithography. *Science* **2000** *288*, 113-116.
4. Duffy, D.C.; McDonald, J.C.; Schueller, O.J.A.; Whitesides, G.M. Rapid prototyping of microfluidic systems in poly(dimethylsiloxane). *Analytical Chemistry* **1998** *70*, 4974-4984.
5. Gu, J.; Gupta, R.; Chou, C.F.; Wei, Q.H.; Zenhausern, F. A simple polysilsesquioxane sealing of nanofluidic channels below 10 nm at room temperature. *Lab on a Chip* **2007** *7*, 1198-1201.
6. Gervais, T.; El-Ali, J.; Gunther, A.; Jensen, K.F. Flow-induced deformation of shallow microfluidic channels. *Lab on a Chip* **2006** *6*, 500-507.



7. Bubendorfer, A.; Liu, X.M.; Ellis, A.V. Microfabrication of PDMS microchannels using SU-8/PMMA moldings and their sealing to polystyrene substrates. *Smart Materials & Structures* **2007** *16*, 367-371.
8. Kim, P.; Jeong, H.E.; Khademhosseini, A.; Suh, K.Y. Fabrication of non-biofouling polyethylene glycol micro- and nanochannels by ultraviolet-assisted irreversible sealing. *Lab on a Chip* **2006** *6*, 1432-1437.
9. Paul, D.; Pallandre, A.; Miserere, S.; Weber, J.; Viovy, J.L. Lamination-based rapid prototyping of microfluidic devices using flexible thermoplastic substrates. *Electrophoresis* **2007** *28*, 1115-1122.
10. Abgrall, P.; Low, L.N.; Nguyen, N.T. Fabrication of planar nanofluidic channels in a thermoplastic by hot-embossing and thermal bonding. *Lab on a Chip* **2007** *7*, 520-522.
11. Wu, H.K.; Huang, B.; Zare, R.N. Construction of microfluidic chips using polydimethylsiloxane for adhesive bonding. *Lab on a Chip* **2005** *5*, 1393-1398.
12. Stjernstrom, M.; Roeraade, J. Method for fabrication of microfluidic systems in glass. *Journal of Micromechanics and Microengineering* **1998** *8*, 33-38.
13. Mao, P.; Han, J.Y. Fabrication and characterization of 20 nm planar nanofluidic channels by glass-glass and glass-silicon bonding. *Lab on a Chip* **2005** *5*, 837-844.
14. Yang, Z.; Matsumoto, S.; Goto, H.; Matsumoto, M.; Maeda, R. Ultrasonic micromixer for microfluidic systems. *Sensors and Actuators a-Physical* **2001** *93*, 266-272.

15. Patrino, N.; McLachlan, J.M.; Faria, S.N.; Chan, J.; Norton, P.R. A novel metal-protected plasma treatment for the robust bonding of polydimethylsiloxane. *Lab on a Chip* **2007** *7*, 1813-1818.
16. Bakajin, O.; Duke, T.A.J.; Tegenfeldt, J.; Chou, C.F.; Chan, S.S.; Austin, R.H.; Cox, E.C. Separation of 100-kilobase DNA molecules in 10 seconds. *Analytical Chemistry* **2001** *73*, 6053-6056.
17. Jia, Z.J.; Fang, Q.; Fang, Z.L. Bonding of glass microfluidic chips at room temperatures. *Analytical Chemistry* **2004** *76*, 5597-5602.
18. Liu, Y.J.; Rauch, C.B.; Stevens, R.L.; Lenigk, R.; Yang, J.N.; Rhine, D.B.; Grodzinski, P. DNA amplification and hybridization assays in integrated plastic monolithic devices. *Analytical Chemistry* **2002** *74*, 3063-3070.
19. Becker, H.; Gartner, C. Polymer microfabrication methods for microfluidic analytical applications. *Electrophoresis* **2000** *21*, 12-26.
20. Tenhaeff, W.T.; Gleason, K.K. Initiated and Oxidative Chemical Vapor Deposition of Polymeric Thin Films: iCVD and oCVD *Advanced Functional Materials* **2008** *18*, 969-1140.
21. Gates, S.M. Surface Chemistry in the Chemical Vapor Deposition of Electronic Materials. *Chemical Reviews* **1996** *96*, 1519-1532.
22. Lau, K.K.S.; Gleason, K.K. Particle surface design using an all-dry encapsulation method. *Advanced Materials* **2006** *18*, 1972-+.

23. Ma, M.L.; Mao, Y.; Gupta, M.; Gleason, K.K.; Rutledge, G.C. Superhydrophobic fabrics produced by electrospinning and chemical vapor deposition. *Macromolecules* **2005** *38*, 9742-9748.
24. Lau, K.K.S.; Bico, J.; Teo, K.B.K.; Chhowalla, M.; Amaratunga, G.A.J.; Milne, W.I.; McKinley, G.H.; Gleason, K.K. Superhydrophobic carbon nanotube forests. *Nano Letters* **2003** *3*, 1701-1705.
25. Mao, Y.; Gleason, K.K. Hot filament chemical vapor deposition of poly(glycidyl methacrylate) thin films using tert-butyl peroxide as an initiator. *Langmuir* **2004** *20*, 2484-2488.
26. Lau, K.K.S.; Gleason, K.K. Initiated chemical vapor deposition (iCVD) of poly(alkyl acrylates): An experimental study. *Macromolecules* **2006** *39*, 3688-3694.
27. Slocik, J.M.; Beckel, E.R.; Jiang, H.; Enlow, J.O.; Zabinski, J.S.; Bunning, T.J.; Naik, R.R. Site-specific patterning of biomolecules and quantum dots on functionalized surfaces generated by plasma-enhanced chemical vapor deposition. *Advanced Materials* **2006** *18*, 2095-+.
28. Carlisle, E.S.; Mariappan, M.R.; Nelson, K.D.; Thomes, B.E.; Timmons, R.B.; Constantinescu, A.; Eberhart, R.C.; Bankey, P.E. Enhancing hepatocyte adhesion by pulsed plasma deposition and polyethylene glycol coupling. *Tissue Engineering* **2000** *6*, 45-52.
29. Kang, E.T.; Zhang, Y. Surface modification of fluoropolymers via molecular design. *Advanced Materials* **2000** *12*, 1481-1494.

30. Zhao, J.Y.; Shang, Z.P.; Gao, L.X. Bonding quartz wafers by the atom transfer radical polymerization of the glycidyl methacrylate at mild temperature. *Sensors and Actuators a-Physical* **2007** *135*, 257-261.
31. Chen, H.Y.; McClelland, A.A.; Chen, Z.; Lahann, J. Solventless adhesive bonding using reactive polymer coatings. *Analytical Chemistry* **2008** *80*, 4119-4124.
32. Stone, F.W.; Stratta, J.J. *Encyclopedia of Polymer Science and Technology*; Union Carbide Corp., 2002;pp. 103~145.

# **Chapter Ten**

## CONCLUSIONS AND FUTURE WORK

## 10.1 Conclusions

### 10.1.1 Oxidative Chemical Vapor Deposition of Conducting Polymer Films

This thesis has demonstrated the oCVD of PEDOT films and their electronic, chemical, and morphological properties were investigated. By controlling the parameters in oCVD process, all of properties were systemically controllable. Moreover, two bio-functionalizable polymeric surfaces of PPMA and PGMA films were introduced and their functionalizability, conformality, and patternability were illustrated.

The substrate temperature of the oCVD process is a critical parameter which permits control over the conductivity of PEDOT films over a range of more than five orders of magnitude. From FTIR and Raman spectroscopy, the chemical nature giving rise to the systematic variation in the level conduction of the PEDOT film was elucidated. Specifically, the substrate temperature controls the conjugation length of the oCVD PEDOT. Additionally, the optical absorption spectra demonstrate that the combination of lack of doping and short conjugation length lead to low values of conductivity in films deposited at low substrate temperature. From the oCVD polymerization process, single apparent activation energy of  $28.1 \pm 1.1$  kcal/mol is observed for conductivity with respect to substrate temperature. We have also demonstrated with XPS that the surface of oCVD PEDOT consist purely of PEDOT doped with  $\text{Cl}^-$  ions. Uniform composition was maintained uniformly throughout the entire thickness of bulk film and its surface. The EDX demonstrates that the oCVD film forms an abrupt interface with the substrate. The maximum conductivity for current series of oCVD was about 1000 S/cm. In addition, the dopant concentration of oCVD films can be systemically controlled from 16 atomic % to

33 atomic % by changing only substrate temperature employed for film growth, and thus the work function of the final material can also be precisely tuned over the range 5.1 eV to 5.4 eV. Tuning the work function over this range is anticipated to facilitate the formation of ohmic contacts in organic device. A new nanostructured PEDOT film was also obtained via oCVD process by introducing new oxidant of  $\text{CuCl}_2$ . The pore size and porosity could be systematically tuned by modulating substrate temperature. Conformal coverage on standard trench in Si and on paper fiber mats was clearly visible in the SEM images with retention of the complex surface structure. The regularly nanostructured, hierarchical nanostructure has great potential for a variety of applications. For instance, highly hydrophilic conductive PEDOT film can be used for advanced electrochemical applications, such as bio-sensors. Moreover, grafting of conducting polymer films on aromatic organic substrates was successfully obtained via a linker-free one-step oCVD process. This grafting scheme relies on the ability of the Friedel-Craft catalyst to form radical cations on the substrate under the conditions oCVD conducting polymer growth. The grafted film exhibited a dramatic increase in adhesion strength. With directly grafted PEDOT, 60 nm features sizes were obtained on flexible and transparent polymeric substrates. In particular, the ability to graft conducting polymers on common substrates has the potential to revolutionize the fabrication of integrated circuitry for flexible electronics. This easy, one-step grafting process offers a wide process window and versatility in applications to various flexible substrates. In particular, this linker-free technique eliminates the tedious additional processes for grafting and opens up the possibility of mass-production of grafted flexible conducting layers at low cost. Finally, oCVD PEDOT was successfully applied to efficient

oPV cells. Although the oCVD cell device showed low shunt resistance and non-ideal J-V behavior, the decreased series resistance in oCVD cell leads the comparable device PCE of 5.2% under the green light illumination with respect to the control cell.

### **1.1.2 Initiated Chemical Vapor Deposition of Biofunctionalizable Polymer Films**

For bio-functionalizable surfaces, a new rapid synthetic pathway for depositing the click chemistry active polymer coating of PPMA was obtained via a one-step vapor-phase iCVD process utilizing a commercially available monomer. The pendent acetylene groups in PPMA were clearly observed in FTIR and XPS spectra. The well-defined acetylene surface functionality enables click chemistry through selective reactivity with azides. PPMA film demonstrated sensitivity to e-beam irradiation, which enabled clickable substrates having nanometer scale patterns without requiring the use of an additional e-beam resist. Direct e-beam exposure of this multifunctional iCVD layer, a 200 nm pattern, and QD particles were selectively conjugated on the substrates via click chemistry. Furthermore, we have demonstrated a dual functional nano-patterned platform with a minimum feature size of 110 nm. The fabrication process utilized sequential solventless CVD processes of iCVD PPMA and PECVD PAAM and patterned by a CFL process. By applying one-pot, biocompatible functionalization, the conjugate fluorescent dyes were assembled onto the pattern in a self-sorted fashion. Considering the ease of fabrication and the versatility and orthogonality of the utilized functional groups, we believe this platform can be a powerful tool for bio-device applications in high throughput, multi-component systems. Finally, a



novel nano-adhesive bonding process was demonstrated for creating microfluidic channels capable of withstanding pressures of higher than 50 psia. The nano-adhesive film composed of iCVD PGMA and PECVD PAAm showed strong and conformal adhesion on the substrates of complex geometries. Channels were successfully fabricated with this nano-adhesive film from many different organic and inorganic substrates, which clearly demonstrates that the method is fully compatible with various flexible substrates. These individual surfaces could be stored for at least two weeks before sealing. Sealing was achieved by placing the coated pieces face to face and then curing at 70°C. No blockage of the microfluidic channels by the adhesive was observed after the curing process. Hence, channels as small as 200 nm in width could be fabricated. High bonding strength of the fabricated channels was validated for at least three months.

## **10.2 Future Works**

### **10.2.1 Oxidative Chemical Vapor Deposition of Conducting Polymer Films**

The thesis has demonstrated that the oCVD process can produce well-defined conducting polymer film with high conductivity, systematic controllability of electrical, chemical and morphological properties, and initial organic electronic device applications. However, further process optimization via either application of new materials or tuning process parameters is required to answer for the limitation of current status of oCVD process technique can achieve.

To achieve complete vapor phase process, a volatile oxidant is highly desirable. Current oCVD process utilizes either  $\text{FeCl}_3$  or  $\text{CuCl}_2$  and both oxidants are solid in ambient pressure. Although vaporization of oxidant can easily be achieved by resistive heating in oCVD chamber, it is very difficult to control the flow rate of vaporized oxidant. Moreover, the oCVD deposited conducting polymer films contain residue oxidant which must be removed by solution process such as rinsing step. However, this rinsing step significantly limits the advantages that general CVD process can offer such as high purity, low interfacial damage, and conformal coverage. So far, many attempts have been applied for finding volatile oxidants but none of them were successful because of either too high or too low electrochemical potential, or either too high or too low vapor pressure of oxidant, or side reactions by the oxidant used. A proper, volatile oxidant can offer many kinds of advantages in oCVD process in that the process is really all-dry process, deposition rate and thickness can be systematically controllable by using iCVD type process, and chamber and film corrosion due to the leftover oxidant can be significantly reduced.

Regardless of the volatility of oxidants, it is still highly essential to find other kinds of oxidants for further optimization of electrical properties of conducting polymer films. For example, it is generally accepted that PEDOT film with  $\text{Fe(III)}$  tosylate shows higher conductivity than with  $\text{FeCl}_3$  because of too strong electronegativity of Cl anion that results in stronger electrostatic charge confinement and lower degree of charge delocalization. We have tried to use  $\text{Fe(III)}$  tosylate to evaporate in oCVD chamber, which was not successful because  $\text{Fe(III)}$  tosylate was decomposed at high crucible temperature. We already have demonstrated that morphology of PEDOT film could be systemically controlled by

changing Fe cation to Cu cation. We have not yet fully searched the availability of various kinds of anion as a dopant ion in oCVD conducting polymer films and different way of tuning electrical properties of conducting polymer is expected by introducing new oxidant.

For better extendability of oCVD process, many different types of monomers are needed to be tried. Currently we have demonstrated that oCVD process can deposit poly pyrrole and copolymer of EDOT-thiophene acetic acid, but the properties of deposited conducting polymer films are not yet reliable and repeatable and the conductivity of poly pyrrole is far lower than solution processed poly pyrrole layers. This is due to the undesirable 3-recombination which significantly reduces the electrical conductivity. The oCVD process uses stepwise reaction mechanism that cannot distinguish 2-recombination from undesirable 3-recombination. In case of PEDOT, EDOT monomer is end-capped in 3- and 4- positions, which significantly reduce the possibility of 3-recombination. However, many different kinds of conducting polymers such as poly pyrrole, poly aniline, and 3-alkyl thiophene are open to this 3-recombination. For this reason, it is highly expected to optimize the oCVD process to be selective to the recombination sites. Many different types of conducting polymers have a variety of their property-specific applications. For example, poly pyrrole is known to be biocompatible and biosensor application is being widely investigated. Poly (3-hexylthiophene) is currently used for channel layers in oTFTs and donor materials for oPV cells. Especially, the regioselectivity is proven to be critical for device performance. Compared with EDOT monomers, pyrrole and aniline monomers are much cheaper starting materials and that is an industrial request for commercialization of oCVD process.

Finally, we have demonstrated a primary organic electronic device application of oPV cell. However, it is critical to optimize the organic device performance using oCVD polymers. Although the initial result of device performance is very promising, the properties of oCVD devices are still worse than, if not, at most comparable to that with conventional PEDOT:PSS system. For further optimization should be focused to better performance, new application of oCVD conducting polymer films, and utilizing advantageous properties of oCVD conducting polymer films. For example, oCVD PEDOT can be used for electrode materials as source/drain in oTFTs and buffer layers for oLEDs, organic memory devices, and active layers for electrochromic devices and chemical/biochemical sensors. Since oCVD PEDOT is relatively hydrophobic and these properties can be used for better compatibility with following hydrophobic conjugated molecules – almost all of conjugated molecules are hydrophobic unless they are functionalized with hydrophilic functionalities. Especially, since oCVD PEDOT can be easily grafted on various aromatic polymer substrates, oCVD PEDOT can contribute a unique role to flexible electronics.

### **10.2.2 Initiated Chemical Vapor Deposition of Biofunctionalizable Polymer Films**

The thesis has demonstrated that functionalizable functionalities are successfully obtained by using iCVD process. The functionalities are shown to be orthogonal to each other, highly mechanically and chemically stable by using crosslinking agents and grafting agents. In addition to this stability, nanometer scale patterns were also illustrated for further

site-selective functionalization using various kinds of patterning tools such as e-beam writing lithography, CFL stamping lithography, and conventional photolithography. However, the applications of these advantageous films are not yet fully investigated and the future research should be focused to the application of this functional polymer films. First of all, the biocompatibility of each functionalities is necessary to investigate for further bio-applications. Due to its nonspecific physical binding of biomaterials such as DNAs and proteins, the area-selective and functionality-selective sorting of biomaterials are still demanding and this nanopatterned orthogonal functional surfaces can be highly advantageous for these applications such as multicomponent sensors, DNA chips and protein chips. Moreover, it can be a template for bio-mimicking environment that consists of thousands of mixture of bio-elements. As a starting point, proving biocompatibility of this functional surface can open up for further biodevice application.

Nano-adhesive layers have a potential for wide application to the microfluidic devices and substrates bonding procedures. In the thesis, the properties of nano-adhesive are focused but no application study was performed. Since the adhesion scheme utilizes an ideal chemically covalent bonding, the strong adhesion can be used for microfluidic devices where requires very high overhead pressure during the operations. Moreover, the leftover functionalities on the inside wall of the channel can be further utilized to immobilize the bio-functionalities. Coupled with the patterning technique applied on functionalizable surfaces mentioned above, we can selectively tether bio-entities inside of channel wall in microfluidic devices. In addition to this, this new concept nano-adhesive can realize the nanometer scale nanofluidic devices which have been impossible due to low modulus of

PDMS. Since the nano-adhesive is applicable generally to various kinds of organic/inorganic substrates with high modulus, nanofluidic channels can be easily fabricated. Moreover, the microfluidic device applications have been confined so far to aqueous system because PDMS is extremely swellable in organic solvents. However, the nano-adhesive layers can be applied to the substrates resistive to organic solvents and this combination can open up another possibility of microfluidic devices with organic solvents. This is very important step for further applications for lab on chips since many kinds of organic synthesis involves in organic solvents. Further iCVD process and sealing process optimization can realize this goal with ease.

## **Appendix A**

NEW ICVD/OCVD SYSTEM INTEGRATED  
INTO A ORGANIC ELECTRONIC DEVICE  
FABRICATION LINE

## **A.1 Motivation**

CVD polymers can be one of the best fit for further organic electronic device application in that the polymer films can be deposited onto any kinds of surfaces free of solvent-originated interfacial defects, the purity of polymer can be maximized, and the electronic properties are easily tunable. Both iCVD and oCVD process can offer a conductor and insulator films of which many types of organic devices can be made. However, for organic electronic device fabrication, it is critical to keep the device fabrication process apart from the ambient for high performance organic devices. For this reason, many kinds of organic electronic device fabrication lines are composed of series and parallel connections of vacuum chambers. To achieve the compatibility of organic electronic device fabrication step with iCVD and oCVD process, a new chamber was designed, installed and attached to main organic electronic device fabrication line in Professor Vladimir Bulović's lab.

## **A.2. Design**

### **A.2.1 Location**

The chamber is located in Professor Vladimir Bulović's lab. The iCVD/oCVD system is attached onto the transfer line chamber in organic electronic device fabrication line. Thoroughly cleaned substrates are introduced into the chamber through the Dry nitrogen glovebox. The substrates are put into the loadlock chamber connected with the glovebox and evacuated for substrate transfer. Afterward, all the sample transfer between the process vacuum chambers can be achieved *in vacuo*.



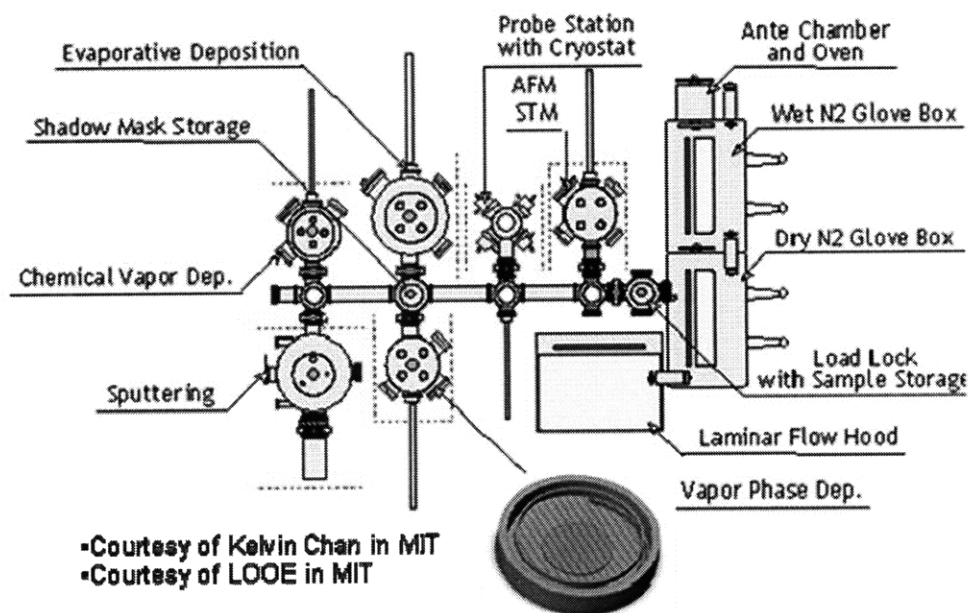


Figure A-1. Location of iCVD/oCVD system in organic electronic device fabrication line

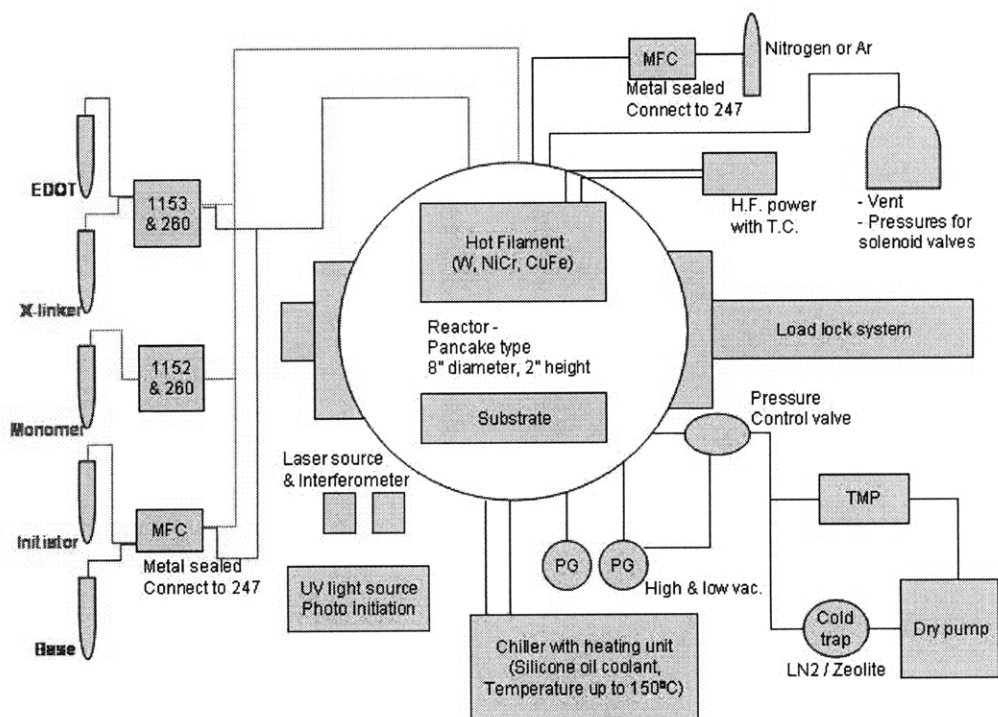


Figure A-2. Schematic diagram of iCVD/oCVD system in organic electronic device fabrication line

## A.2.2 Chamber configuration

### A.2.2.1 Introduction of Reactants into the iCVD/oCVD system

Various types of monomers, crosslinkers, and initiators can be introduced into the process chamber and the flow rates are controlled by mass flow controllers. For dilution of reactant partial pressure, nitrogen carrier gas line was also attached to the chamber. To maintain the vapor phase of reactants, the reactant introduction line is heated by resistive heating tapes. The temperature of heating tapes is PID controlled by solid-state relay valve.

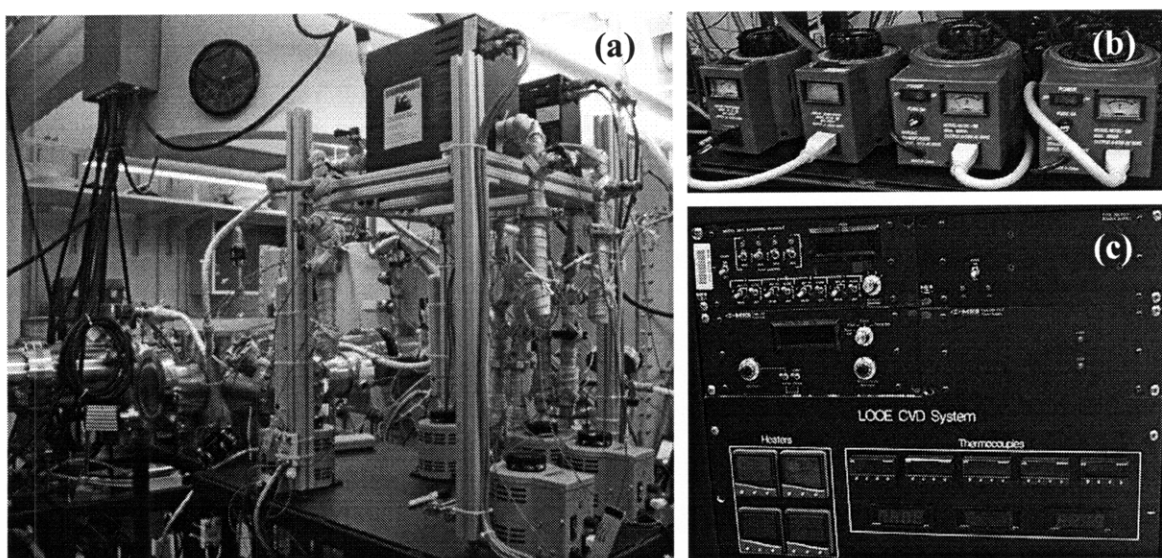


Figure A-3. Digital camera images of (a) reactants introduction line configuration, (b) power supply of heating tape, and (c) MFC controller and heating tape temperature controller in electrical rack.

### A.2.2.2 Chamber configuration of iCVD/oCVD system

The iCVD/oCVD system consists of two-stage system – upper part is for iCVD and lower part for oCVD process. Between the upper and lower part, a stage is located and used for sample stage. The stage temperature can be controlled by cooling water and IR-lamp heating.

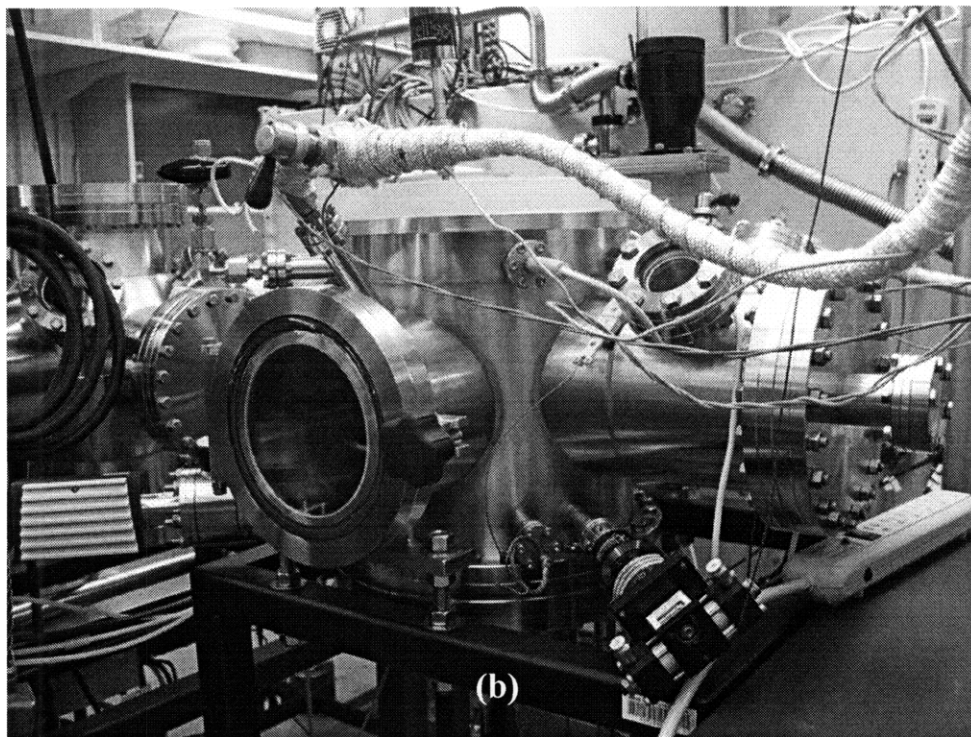
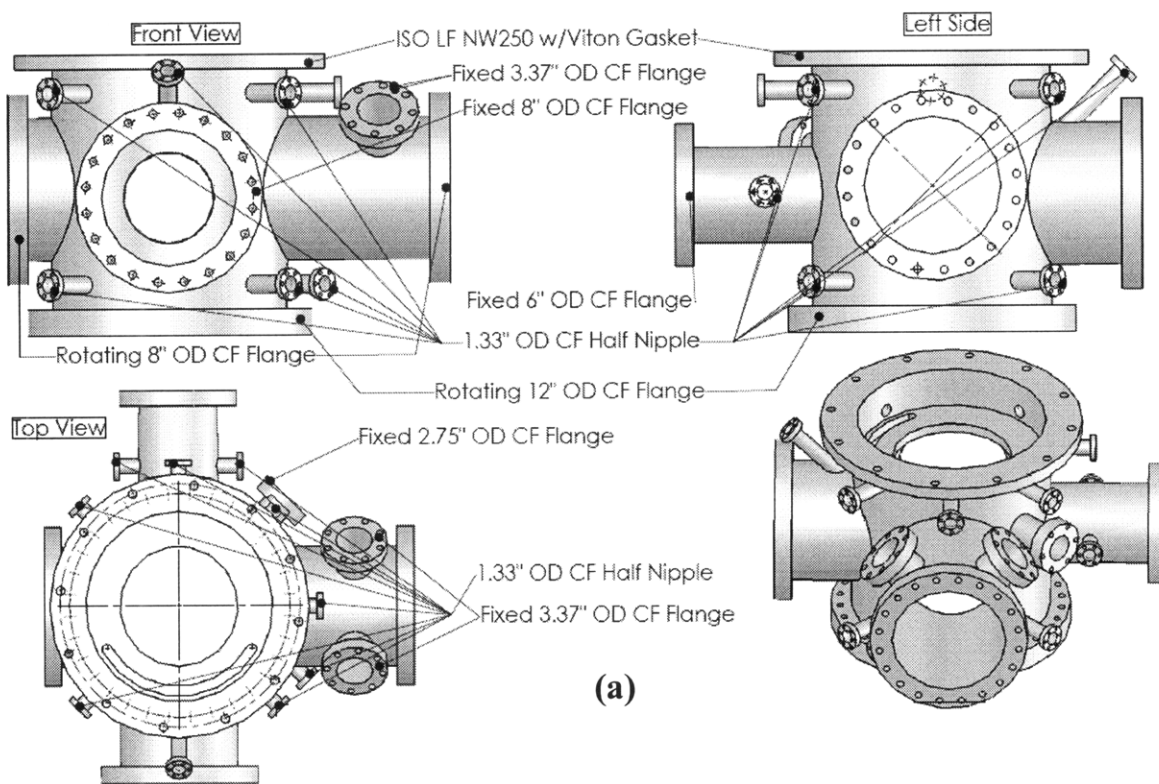


Figure A-4. (a) Schematic drawing and (b) digital camera image of iCVD/oCVD system

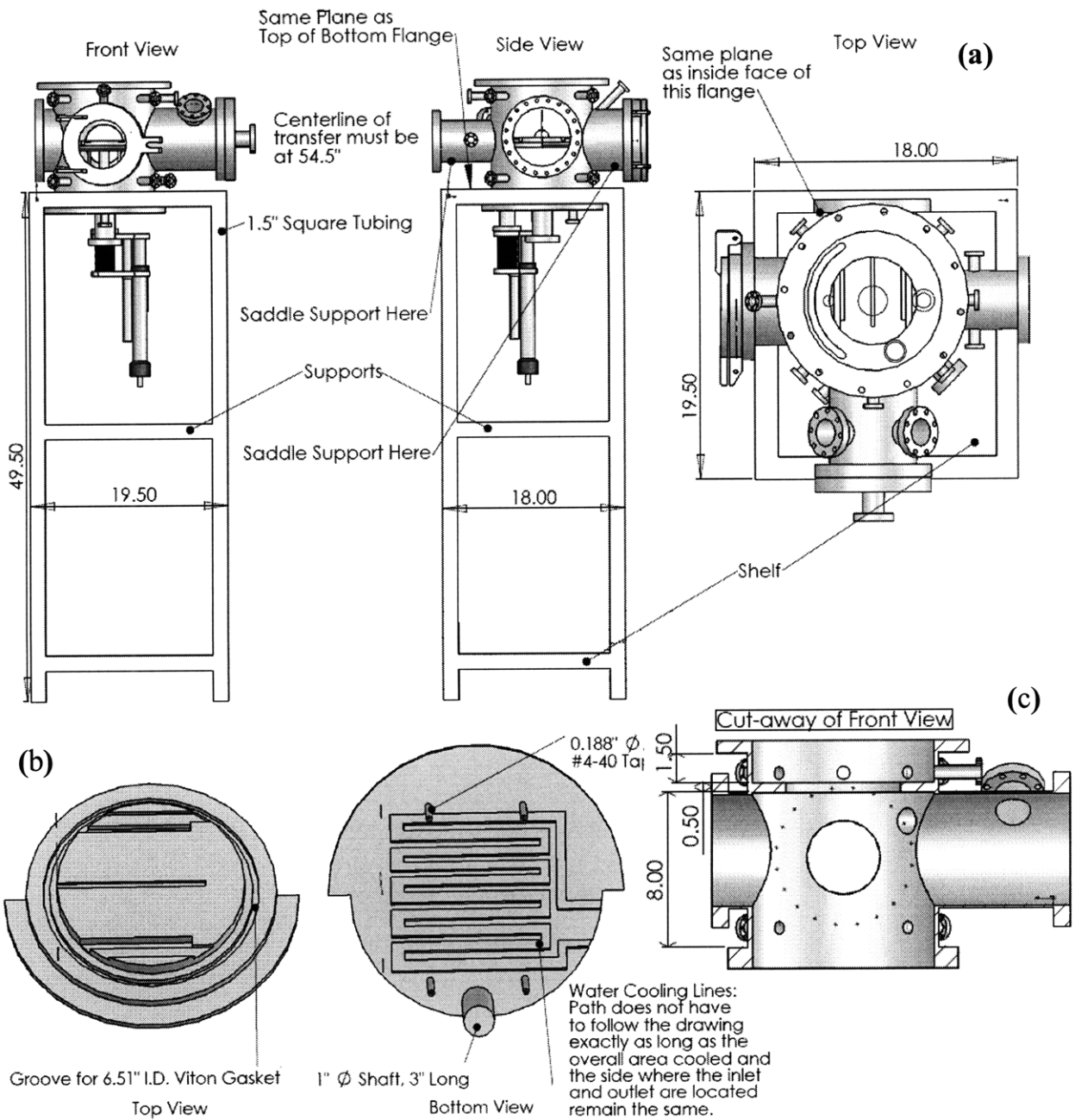


Figure A-5. Schematic drawing of (a) base, (b) stage, (c) cross-section of iCVD/oCVD system. A z-stage motor is attached at the bottom flange of iCVD/oCVD system.

### A.2.2.3 Transfer line and sample holder-stage alignment

Once the sample holder is transferred from main transfer chamber into the iCVD/oCVD system chamber, the sample holder can be flipped up for iCVD and down for oCVD process. The pin-and-hole alignment is used for transfer line alignment between transfer line cart and loadlock transfer arm. The transferred sample holder can be located onto the stage along with the guide trench on the stage and fixed on the stage. The stage can be escalated up and down by z-stage motor control to completely isolate iCVD/oCVD process chamber during the CVD process.

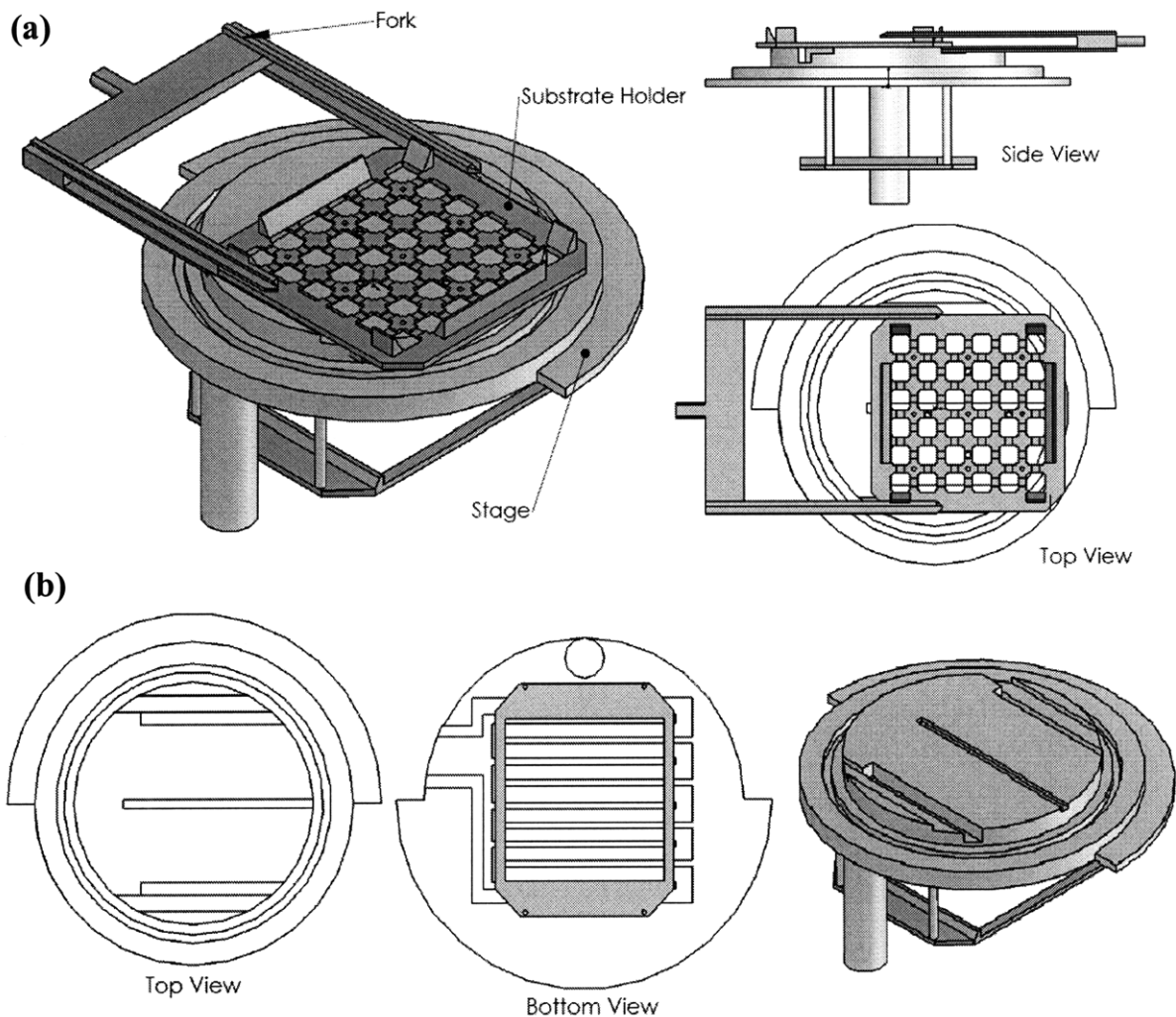


Figure A-6. Schematic drawing of sample holder alignment onto the stage: (a) upper part and (b) bottom part of iCVD/oCVD system.

#### A.2.2.4 Pumping system in iCVD/oCVD system

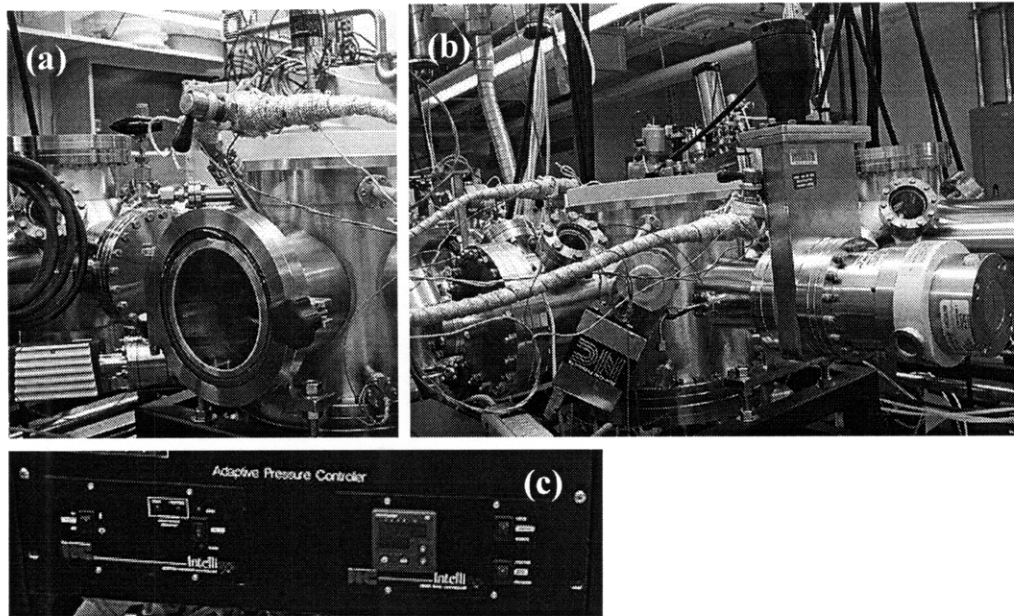


Figure A-7. Digital camera image of (a) vacuum gauges for high vacuum (red circle at bottom left) and low vacuum (red circle at upper right), (b) turbomolecular pump, PID controllable butterfly valve, and gate valve for turbomolecular pump connection, and (c) PID controllable butterfly valve control readout in electrical rack.

For iCVD and oCVD process, only primary dry pump is necessary and the process pressure is ranged from 20 to 2000 mTorr and Edwards iQDP 40 dry pump is installed on the iCVD/oCVD system. However, an ultra high vacuum is required for sample holder transfer system. For this purpose, Pfeiffer TPU240 turbomolecular pump is installed. The base pressure was  $1.2 \times 10^{-7}$  torr which meets for the requirement of sample transfer system. A gate valve is used for the conversion between the turbomolecular pump and dry pump. To check base pressure, Pfeiffer PBR 260 vacuum gauge was used, which allows measuring ultra high vacuum. For iCVD/oCVD process, process pressure needs to be controlled, which can be achieved by PID controllable butterfly valve (247D, Nor-Cal) coupled with low vacuum gauge. The controllable

process pressure is from 20 ~ 1500 mTorr which is nicely fit to the process pressure of iCVD/oCVD process.

#### A.2.2.5 iCVD process in iCVD/oCVD system

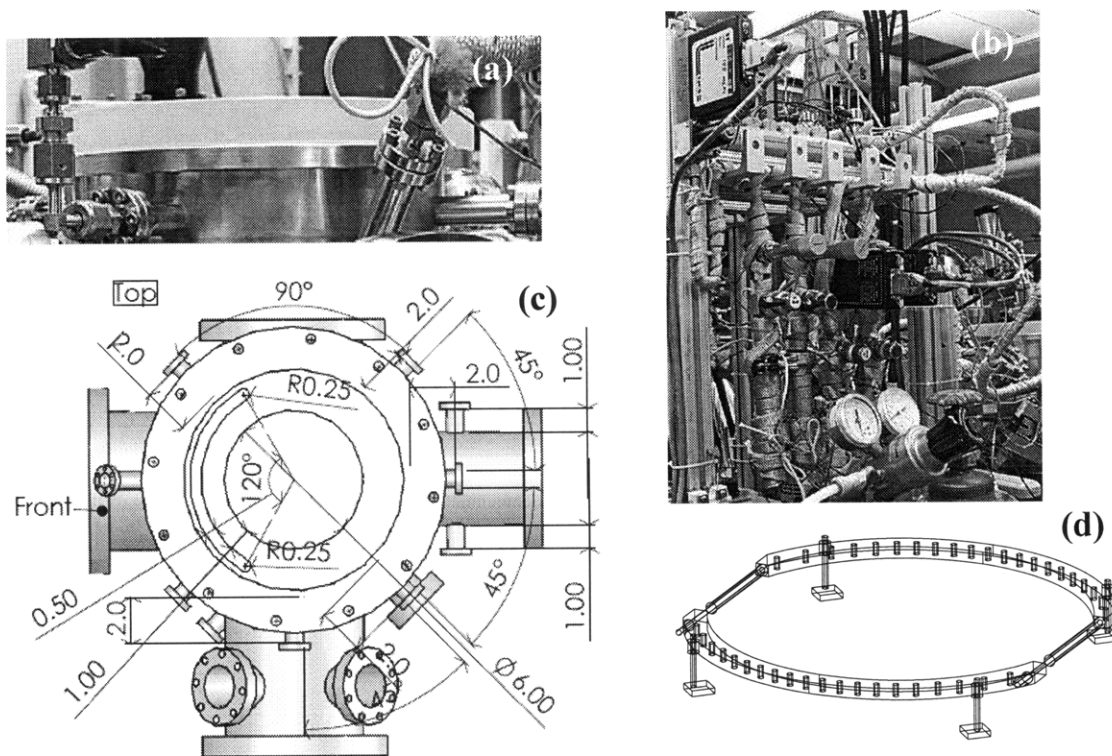


Figure A-8. Digital camera images of (a) upper part of iCVD/oCVD system for iCVD process and (b) source jar setup. Schematic diagram of (c) top view of iCVD/oCVD system for iCVD process and (d) filament chuck configuration.

Four source jars are installed which can be used for two monomer, crosslinker, and initiator, which enables the copolymerization, alternating polymer deposition, and crosslinked polymer deposition. All the source transfer line is merged into one inlet port to the iCVD/oCVD system. The filament to substrate distance was designed to 2 cm which is slightly larger than standard iCVD process – about 1.5 cm – due to sample holder alignment. Quartz upper lid is

used and the system can use both thermal and photo initiation of iCVD process. The configuration of filament is exactly same as that of iCVD chambers in Gleason's group. The stage has coolant line which can control the substrate temperature from  $-30 \sim 150$  °C by using silicone oil coolant. Interferometer system is installed for *in situ* thickness monitoring. The process pressure can be controlled by PID controllable butterfly valve. Temperature of source jars, transfer line, filament, and the substrate is also PID controllable by solid-state relay. Up to 150 mm diameter of sample is applicable.

#### A.2.2.6 oCVD process in iCVD/oCVD system

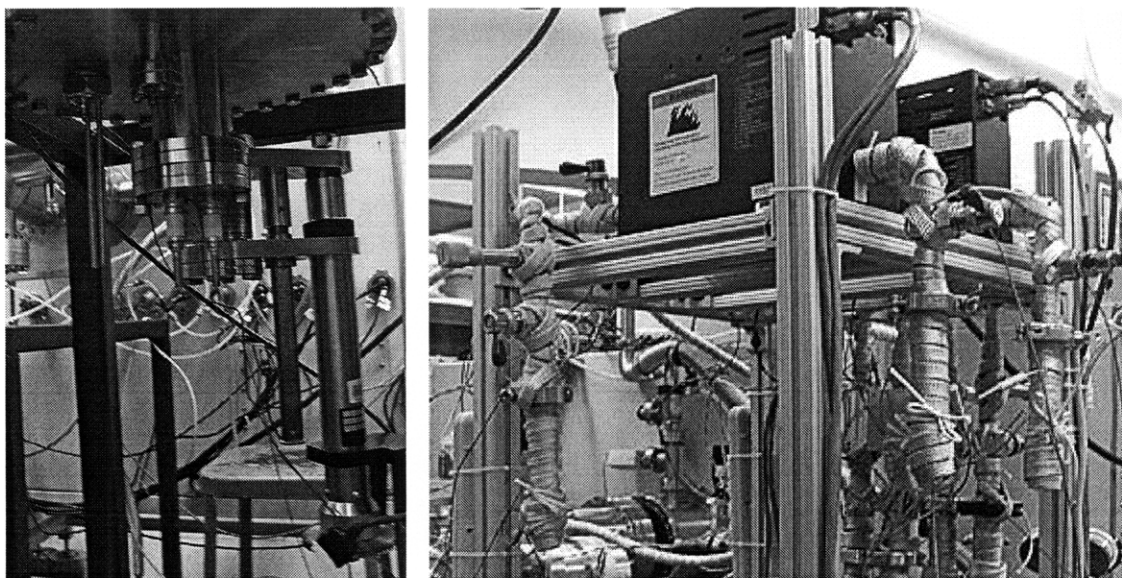


Figure A-9. Digital camera images of (a) bottom part of iCVD/oCVD system for iCVD process and (b) source jar setup. z-stage motor, thickness monitor, and resistive heating unit for oxidant evaporation is shown in (a).

Three source jars are installed which can be used for two monomer including EDOT and pyrrole, and additives such as base to control the conductivity of conducting polymer films. All the source transfer line is merged into one inlet port to the iCVD/oCVD system. Oxidant is evaporated by using resistive heating unit whose heating temperature is controlled by PID



controllable power source (Luxell, RADAK cell). Shutter is installed at the oxidant side to start/stop the oCVD process. Quartz crystal thickness monitor (QCM) is installed to monitor the thickness of oCVD conducting polymer thickness and the deposition rate can also be controlled by monitoring the deposition rate by QCM. The substrate temperature can be controlled from ambient ~ 150 °C by using IR heater irradiation. The process pressure can be controlled by PID controllable butterfly valve. Temperature of source jars, transfer line, and the substrate is also PID controllable by solid-state relay. Up to 150 mm diameter of sample is applicable.